University of South-Eastern Norway
Faculty of Technology, Natural Sciences and Maritime Studies

Doctoral dissertation no. 10
2018

Khim Chhantyal

Sensor Data Fusion based Modelling of Drilling Fluid Return Flow through Open Channels

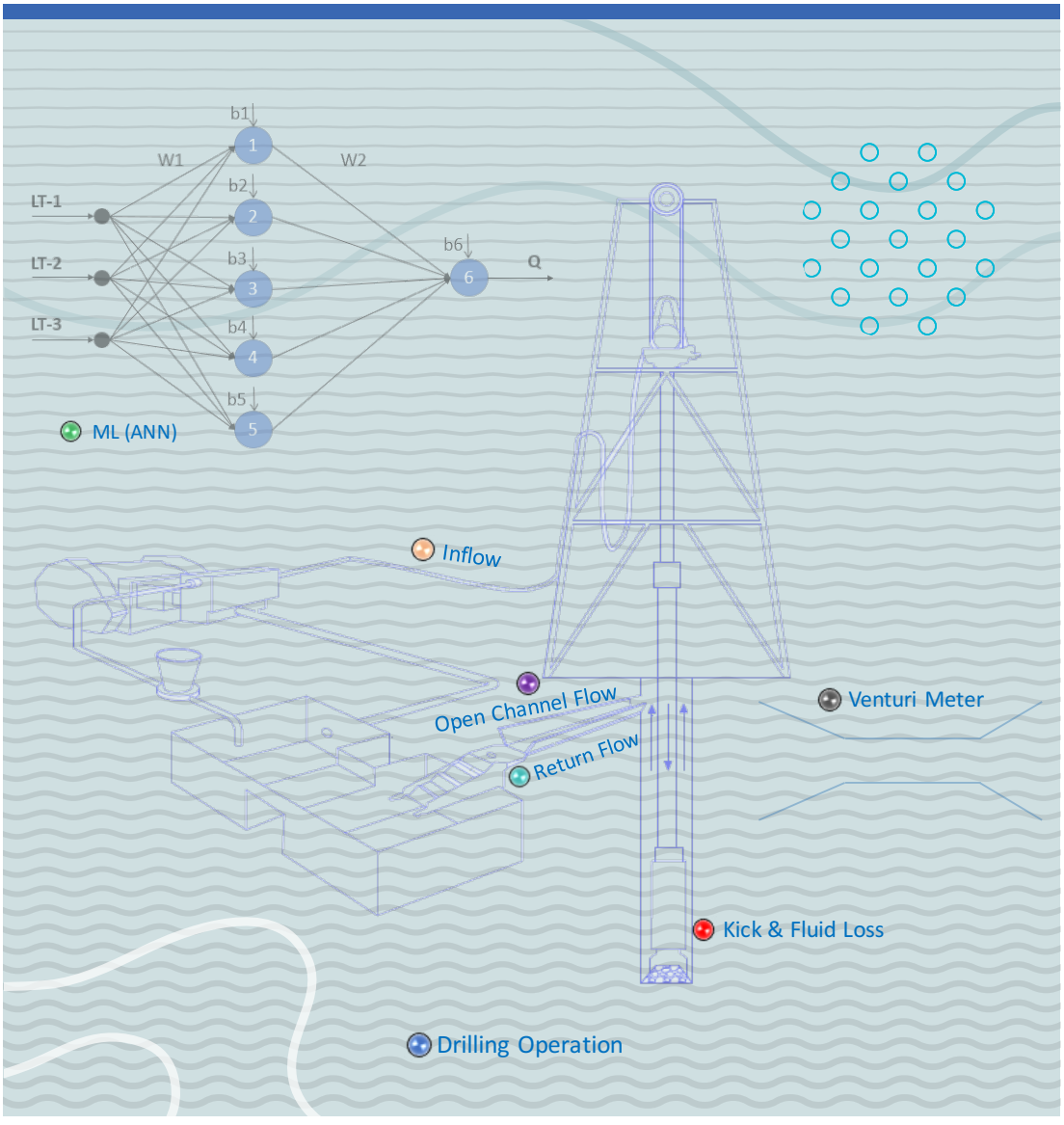

Khim Chhantyal

Sensor Data Fusion based Modelling of Drilling Fluid Return Flow through Open Channels

A PhD dissertation in
Process, Energy and Automation Engineering

Faculty of Technology, Natural Sciences and Maritime Studies
University of South-Eastern Norway
Porsgrunn, 2018

Doctoral dissertations at the University of South-Eastern Norway no. 10

ISSN: 2535-5244 (print)
ISSN: 2535-5252 (online)

ISBN: 978-82-7206-483-8 (print)
ISBN: 978-82-7206-484-5 (online)

Print: University of South-Eastern Norway

Dedicated to my parents, to my wife, to all my family members and friends

Preface

This thesis is submitted to University of South-Eastern Norway (USN) for the degree of Doctor of Philosophy to the Department of Electrical Engineering, Information Technology, and Cybernetics under the Faculty of Technology, Natural Sciences, and Maritime Sciences. The research work is funded by the Ministry of Education and Research of the Norwegian Government, for four years with 25% teaching duties and starting from September 2014.

The work is mainly related to flow measurement in the return line of drilling fluid circulation while drilling. In any drilling operations, wellbore stability is the primary objective for safe and efficient drilling. The study focuses on the usage of the delta flow measurement (i.e., the difference between inflow and return flow) for maintaining the wellbore stability. An accurate return flow measurement is a comparatively challenging task, which is investigated in this study.

For the return flow measurement, a simple and accurate flow measurement system using Venturi constriction is presented that may replace an existing uniform open channel. For the study, three different types of existing flow models are investigated. Different machine learning based flow models are developed. The models are tested in a flow loop available at USN, Campus Porsgrunn using synthetic drilling fluids with rheological properties that are comparable with water-based drilling mud. The experimental results show that the models are applicable for non-Newtonian fluid flow measurements. I hope the models will be of use in the real drilling operations for both inflow and outflow measurements.

Acknowledgement

I would like to express my sincere gratitude towards my supervisor Saba Mylvaganam for his help and support in this work. I would also like to thank my co-supervisor Håkon Viumdal for his valuable contribution. We three together as a team has successfully managed to complete this work in time. My sincere thanks also go to my co-supervisor Gerhard Nygaard for sharing his expert knowledge on drilling operations during the early period of the work.

I am grateful to the University of South-Eastern Norway and the Ministry of Education and Research of the Norwegian Government for funding the work. I would like to thank Equinor ASA for providing and commissioning the flow loop with various types of sensors and control systems dedicated to flow studies. The economic support from the Research Council of Norway and Equinor ASA through project no. 255348/E30 "Sensors and models for improved kick/loss detection in drilling (Semi-kidd)" is gratefully acknowledged. I greatly appreciate and acknowledge the expert advice on drilling operations by Dr. Geir Elseth of Equinor.

I thank my colleagues and friends; Rajan Kumar Thapa, Morten Hansen Jondahl, Sharamnsha Bhandari, Navraj Gyawali, Minh Hoang, Amir Seterkesh, and Sudeep Parajuli for their support and help.

Finally, I would like to thank my parents, Gamman Chhantyal and Man Maya Chhantyal. They always taught me to dream and motivated me to live the dream. I owe thanks to my wife, Geeta Chhantyal, who was always by my side; for long working days, for sleepless nights, working weekends, and working vacations. She has helped me technically, non-technically, and spiritually. Without her companion, this journey would have never been successful.

Summary

In drilling oil & gas wells, pressure control is essential for several reasons, but primarily for safety. The wellbore pressure should be maintained within the pressure window to avoid the kick and fluid loss while drilling. During drilling, wellbore pressure can be measured in real-time, but it is a challenge to determine the pressure window. One possible way to monitor wellbore pressure is the delta flow method, where the difference between inflow and return flow is utilized to indicate the kick or the fluid loss. For delta flow method, inflow measurement is comparatively easy as the inflowing fluid is a single phase fluid with known rheological parameters. The returning fluid is a multiphase fluid contaminated with rock cuttings, sand, formation fluids/gases, etc. and is a challenge to measure.

The primary objective of this PhD work is to develop models or sensor systems to estimate the return flow through an open channel in drilling circulation loops. During the work, different flow measurement systems are analysed, modified, and developed. The performance of the measurement systems is evaluated based on the standard requirements needed for a suitable flowmeter. All the experimental works are performed using a flow loop available at University of South-Eastern Norway, Campus Porsgrunn. The flow loop consists of an open channel with Venturi constriction for flow measurement. For the study, drilling fluids with different rheological properties are used.

The analysis performed using an already existing flow measurement systems for an open channel with uniform geometry shows that these measurement systems are limited by the fluid rheology and accuracy. Three different flow models (i.e., upstream-throat levels based, upstream level based and critical level based) for the fluid flow through an open channel with Venturi constrictions are analysed. All of the three models are accurate and meet the standard requirements in a favourable condition. Upstream-throat levels based flow model (with mean absolute percentage error (MAPE) of 2.33%) and upstream level based flow model (with MAPE of 2.92%) need a proper tuning of a kinetic energy correction factor depending on the type of flow regime. The flow regime depends on the rheological parameters of a fluid and the rheological parameters of return flow changes in each circulation while drilling. Due to this reason, these two flow models are not reliable for return flow measurement without a proper tuning of the correction factor. The critical level based flow model (with MAPE of 5.81%) is comparatively less affected by the correction factor. The limitation of this model is to locate a critical level position within the throat section along the Venturi constriction. In this study, instead of performing a direct critical level measurement, it is estimated based on the fuzzy logic regulator and fixed position upstream level measurement. The modifications in the critical level based flow model give improved estimates of the flow.

One possible problem using the Venturi constriction can be an accumulation of solid particles within the conversing section of the constriction. In this case, return flow through an inclined open channel can be a simple solution, which accelerates the accumulated sediments. The flow study using an inclined open channel shows

that the model is reliable up to the inclination angle of 0.4 [deg]. The results are valid for the geometry of the open channel used in the experiments.

Due to the limitation of these flow models with the need for a proper selection of the correction factor, different machine learning based flow models are developed. Volumetric flow based machine learning models are highly accurate with MAPE up to 2.05 % and are applicable for fluids with different rheological parameters. These models are based on level measurements without cumbersome tuning of various parameters and hence useful in open channel return flow measurements of any fluids.

Contents

List of Figures

List of Tables

List of Abbreviations

ADP	**A**nnular **D**ischarge **P**ressure
AI	**A**rtificial **I**ntelligence
ANFIS	**A**daptive **N**euro-**F**uzzy **I**nference **S**ystem
ANN	**A**rtificial **N**eural **N**etwork
BR	**B**ayesian **R**egularization
CFD	**C**omputational **F**luid **D**ynamics
CG	**C**onnection **G**as
FLR	**F**uzzy **L**ogic based **R**egulator
FLC	**F**uzzy **L**ogic **C**ontroller
H	**H**igh
HH	**H**igh **H**igh
L	**L**ow
LL	**L**ow **L**ow
LT	**L**evel **T**ransmitter
MAPE	**M**ean **A**bsolute **P**ercentage **E**rror
MSER	**M**aximum **S**pecific **E**nergy based **R**egulator
ML	**M**achine **L**earning
MPD	**M**anaged **P**ressure **D**rilling
MSE	**M**ean **S**quared **E**rror
NB	**N**egative **B**ig
NS	**N**egative **S**mall
OK	**O**k
PB	**P**ositive **B**ig
P&ID	**P**iping and **I**nstrumentation **D**iagram
PLR	**P**olynomial **L**inear **R**egression
POG	**P**ump **O**ff **G**as
PS	**P**ositive **S**mall
RBF	**R**adial **B**asis **F**unction
ROP	**R**ate **O**f **P**enetration
RTRL	**R**eal **T**ime **R**ecurrent **L**earning
SLR	**S**imple **L**inear **R**egression
SPP	**S**tand**P**ipe **P**ressure
SVR	**S**upport **V**ector **R**egression
TG	**T**otal **G**as
USN	**U**niversity of **S**outh-Eastern **N**orway
ZO	**Z**ero

List of Symbols

A	Cross-sectional area	$[m^2]$
b	Bottom width	$[m]$
c_1	Shape factor constant	$[-]$
c_2	Shape factor constant	$[-]$
C_{Chezy}	Chezy coefficient	$[m^{1/2}/s]$
C_d	Coefficient of discharge	$[-]$
C_s	Shape coefficient	$[-]$
C_v	Coefficient of velocity	$[-]$
E_s	Specific energy	$[m]$
f	Unknown target function	$[-]$
f_h	Final hypothesis	$[-]$
g	Gravitational acceleration	$[m/s^2]$
k	Consistency index	$[cP]$
K	Numerical constant dependent on channel shape	$[-]$
h	Fluid level	$[m]$
h_c	Critical level	$[m]$
n	Flow behavior index	$[-]$
$n_{Manning}$	Manning's number	$[s/m^3]$
P_b	Wellbore pressure	$[Pa]$
P_f	Formation pore pressure	$[Pa]$
P_{ff}	Formation fracture pressure	$[Pa]$
Q_v	Volumetric flow rate	$[l/s]$
R_h	Hydraulic radius	$[m]$
R_H	Haldenwang's Reynolds number	$[-]$
V	Fluid velocity	$[m/s]$
x	Level input	$[m]$
y	Estimated flow rates	$[l/s]$
z	Height from a datum line	$[m]$
ρ	Fluid density	$[kg/m^3]$
α	Kinetic energy correction factor	$[-]$
θ	Slant angle	$[deg]$
Θ	Channel angle	$[deg]$
τ	Shear stress	$[Pa]$
τ_w	Average wall shear stress	$[Pa]$
τ_y	Yield stress	$[Pa]$
γ	Shear rate	$[1/s]$

Part I

Overview

Chapter 1

Introduction

1.1 Background

In extracting oil and gas, one important phase is the drilling operation, where the reservoir is connected to the surface through a drill pipe. In drilling operations, drilling fluid (often termed as 'drilling mud') is circulated in a closed loop. A typical drilling fluid circulation loop is shown in Figure 1.1. The drilling fluid is continuously pumped down, from the mud tank to wellbore through the drill pipe, and is circulated through the annulus back to the surface. The returning fluid comes to the fluid treatment system, where drill cuttings are filtered, and appropriate additives are added to the fluid to make sure its properties stay within the specifications. The circulation is continued until the desired depth is reached. The drilling fluids are non-Newtonian, which helps:

- to remove rock-cuttings from the downhole due to their high viscous nature with a high yield point,
- to lubricate the drill bit, and
- to keep the wellbore pressure within the pressure window limits to prevent kicks and their losses, (Bourgoyne et al., 1986; Caenn, Darley, and Gray, 2011a).

This PhD work is related to monitoring and controlling of wellbore pressure for ensuring wellbore stability. For any reservoir, there exist pressure limits (often termed as 'pressure window') where the drilling operations can be performed safely. A simple example of pressure window diagram is shown in Figure 1.2. In a typical pressure window diagram, a lower bound is a formation pore pressure (P_f) and an upper bound is a formation fracture pressure (P_{ff}). These variables are only roughly known, based on e.g. seismic analysis, and varies with depth and geological properties of the formation. However, for safe and efficient drilling, the wellbore pressure (P_b) should be within the pressure limits. The major component contributing to the wellbore pressure is the hydrostatic pressure exerted due to the fluid in the annulus, (Bourgoyne et al., 1986).

Two main problems (fluid loss and kick) might occur in the case of reservoir failure as shown in Figure 1.3a. If the wellbore pressure is greater than the formation pore pressure (i.e., $P_b > P_f$), the high-pressure drilling fluid displaces the low-pressure formation fluids and enters into formation pores resulting in a fluid loss. If the wellbore pressure further increases and exceeds the formation fracture pressure (i.e., $P_b > P_{ff}$), the drilling fluids will fracture the formation and the fluid loss increases. This is a state of fluid loss while drilling. In the case of wellbore pressure lower than the formation pore pressure (i.e., $P_b < P_f$), the high-pressure formation fluids and gases influx into and displace low-pressure drilling fluids. It is a state of kick while drilling. The kick should be detected as early as possible, as it can lead to

wellbore stability problems and in extreme case, it can result in the blowout of the whole rig, for example, the Deepwater Horizon explosion, (Hauge and Øien, 2012).

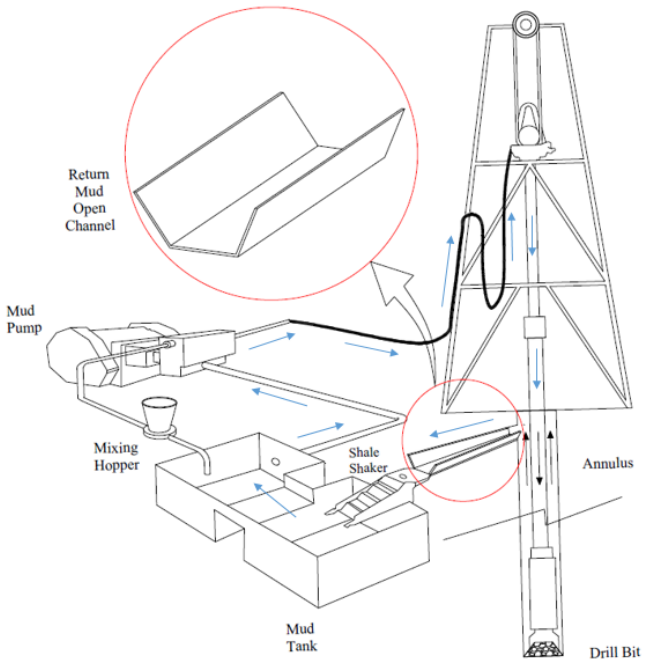

FIGURE 1.1: The circulation of drilling fluid while drilling an oil well. The open channel in the return flow is highlighted. Arrows indicate flow direction. Adapted from (Jack, 2018).

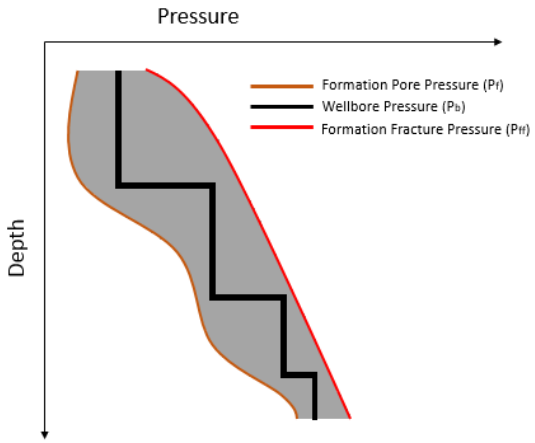

FIGURE 1.2: A typical pressure window showing the wellbore pressure, and the lower and upper pressure limits. Adapted from (Bourgoyne et al., 1986).

1.2 Early Kick/Loss Detection

Early detection of these unwanted conditions (i.e., kick and loss) can lead to less fluid loss, less formation damage, lower drilling cost, and increased safety. Kick and loss can be detected in real-time either by using different surface measurements or by using downhole measurements. Different types of kick/loss detection methods

used in both conventional drilling and managed pressure drilling (MPD) are presented in (Cayeux and Daireaux, 2013; Johnson et al., 2014; Ayesha, Venkatesan, and Khan, 2016). However, the focus of the study is on early kick/loss detection for conventional drilling operations.

1.2.1 Mud log Data Method

Early kick detection using a real-time mud logging data is still the first choice method in conventional drilling operations. Mud logging is a continuous recording and analysing of a real-time well site information. The mud log data consist of pit gain, return flow rate, rate of penetration (ROP), drop in pump pressure, total gas (TG), pump off gas (POG), and connection gas (CG). In this method, a state of kick is suspected with the increase in pit gain, return flow rate, ROP, and gas contents. Hence, there is a need for human interpretation to continuously analyse and monitor the logged data for decisive actions against the unwanted conditions. (Anfinsen and Rommetveit, 1992; Ahmed, Hegab, and Sabry, 2016)

1.2.2 Mud Tank Volume Method

An early indication of kick and fluid loss can be detected by monitoring the volume of drilling fluid in the mud tank, highlighted in (Anfinsen and Rommetveit, 1992). It is a straightforward way to monitor kick/loss but is not always reliable as discussed in (Cayeux and Daireaux, 2013). Interpreting the active mud tank volume may be difficult if a significant amount of the circulating mud is buffered in the return flow lines, shale shakers and other transfer tanks. The direct addition of base water/oil and fluid additives may be interpreted as gain, and the transfer of drilling mud from the active mud tank to another tank may look like a loss.

1.2.3 Delta Flow Method

Delta flow method is one of the simplest methods of detecting kick and loss, which was first introduced in (Speers and Gehrig, 1987) and later discussed in (Orban, Zanner, and Orban, 1987; Orban and Zanker, 1988; Lloyd et al., 1990; Schafer et al., 1991; Haeusler, Makohl, and Harris, 1995). Delta flow method uses the difference between the inflow of drilling fluid into the wellbore and the return flow of drilling fluid from the wellbore to detect unusual conditions as shown in Figure 1.3b. The case of inflow > return flow, is an indication of a fluid loss and the case of inflow < return flow, is an indication of a kick.

1.2.4 Other Methods

Standpipe and annular discharge pressures method presented in (Reitsma, 2010; Reitsma, 2011; Mills et al., 2012) can be used for early detection of kick and loss. In this method, the pressure drops are measured in the inflow section (i.e., standpipe pressure (SPP)) and return flow section (i.e., annular discharge pressure (ADP)) to identify the abnormal conditions. An early kick/loss detection based on the downhole annular pressure measurements are discussed in (Hutchinson and Rezmer-Cooper, 1998; Ayesha, Venkatesan, and Khan, 2014; Ayesha, Venkatesan, and Khan, 2016). The usage of the travel time of pressure waves through the drill string and annulus to identify kick/loss is presented in (Codazzi et al., 1992; Stokka et al., 1993). (Hargreaves, Jardine, and Jeffryes, 2001; Kamyab et al., 2010; Cayeux and Daireaux, 2013)

presented different numerical methods for kick/loss detections. Compared to conventional drilling, MPD provides significantly better kick detection. For example, the kick volumes detected using MPD kick detection system can be much smaller compared to kick detection system of conventional drilling as discussed in (Nas, 2011; Grayson and Gans, 2012). MPDs using delta flow method uses Coriolis mass flow meter for flow measurements, and the Coriolis meter readings are not reliable in the presence of excessive gas. (Patel, Cooper, and Billings, 2013) presented an advanced gas extraction and analysis system, which can be used downstream of MPD choke and before the Coriolis meter. The gas extraction system removes most of the gas ahead of the flow measurement.

Typically, drilling operations in oil & gas wells have real-time data of the wellbore pressure and are monitored in the drilling fluid circulation system on the platform, (Bourgoyne et al., 1986). However, the pressures of the formation being drilled are challenging to estimate and difficult to measure. Therefore, this PhD work focuses on the delta flow method for the early kick/loss detection.

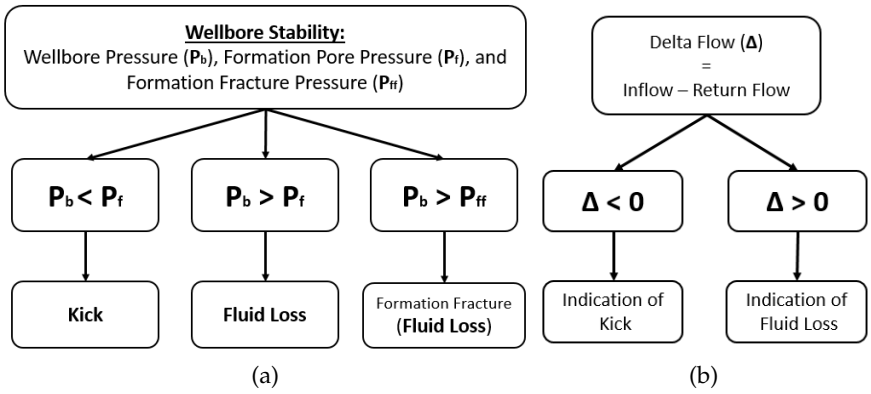

FIGURE 1.3: a) Block diagram of wellbore instability scenario, highlighting a state of kick or fluid loss. b) Block diagram of delta flow method, indicating an early detection of kick or fluid loss.

1.3 Inflow/Return Flow Meters

For inflow and return flow measurements, several flow measurement systems are discussed in the literature, (Speers and Gehrig, 1987; Orban, Zanner, and Orban, 1987; Orban and Zanker, 1988; Johnsen et al., 1988; Orban, Zanker, and Orban, 1988; Schafer et al., 1991; Loeppke et al., 1992). For inflow measurements, Coriolis mass flow meter, conventional pump stroke counter, electromagnetic flow meter, and pump rotary speed transducer can be used. For return flow measurement, standard paddle meter, electromagnetic flow meter, ultrasonic flow system, and Venturi flow meter can be used. Table 1.1 shows the detailed specifications of these return flow measurement systems. All of these flow measurements systems are tested and being used in the drilling operations. For any flow meter to be applicable for drilling fluid flow measurement, (Orban, Zanner, and Orban, 1987) has given several requirements for a suitable flow meter as:

- The reliability and the accuracy of measurements should be guaranteed over the full range of flow.

- An accuracy of 1.5 - 3 [l/s] for the flow rates up to 75 [l/s] in a common drilling operation environment.
- For any fluid with a viscosity range of 1 - 200 [cP] and density range of 1000 - 2160 [kg/m^3], the accuracy should be maintained.

The inflow drilling fluid is relatively clean, pure, and has known rheological parameters. Therefore, the inflow rate can be measured using accurate flow meter like Coriolis mass flow meter. The return flow drilling fluid is multi-phase fluid mixed with rock cuttings, formation fluids, and gases. It is a challenging task to measure return flow rate. In this PhD work, the focus is on using a Venturi constriction in the open channel (as marked in Figure 1.1) for the return flow measurement. By modifying the existing open channel, the aim is to find a simple and cheap alternative way of measuring return flow using non-intrusive level measurements.

1.4 Objectives

The primary objective of this PhD work is to investigate different flow measurement system for the return flow measurement. For the study, the objective is divided into two main tasks:

- Study and analyse existing open channel flow measurement systems
- Data fusion based modelling of open channel flow

1.5 Structure of Thesis

There are two parts in the thesis. Part I gives an overview of the work and is further divided into separate chapters. Different types of flow measurement systems used in a uniform geometry open channel or an open channel with Venturi constriction are discussed in Chapter 2. An overview of the experimental set-up used in this work is given in Chapter 3. Different flow measurement systems are analysed in Chapter 4. In Chapter 5, an overview of different machine learning (ML)[1] algorithms and their performance are presented. Conclusion and future recommendation are discussed in Chapter 6. Part II presents some of the selected articles related to the work.

1.6 Main Contributions

To meet the main objective of the PhD work, contributions are made in several aspects of the work. The summary of the work is given in Figure 1.4. The following are the main contributions to the work:

- Three different existing open channel flow models are tested in the flow loop as presented in Chapter 4. Experiments are performed using the fluids with different rheological properties. Based on the analysis, a suitable modification is implemented in one of the flow model (critical level based model), which improved the performance of the model as discussed in Section 4.2.2 and Paper A.

[1] Henceforth, Machine Learning is represented by ML.

- Different ML based flow models are developed, which can accurately estimate flow based on only level measurements as presented in Chapter 5, Paper B and Paper C. All the ML algorithms are developed in MATLAB, and the models are successfully implemented in LabVIEW software program for the experimental study.
- The LabVIEW software program used to run the flow loop is upgraded continuously.
- Different drilling fluids with different rheological parameters are prepared to circulate in the flow loop for flow studies. The recipe for preparing the fluids and their rheological behaviours are presented in Section 3.3.3.

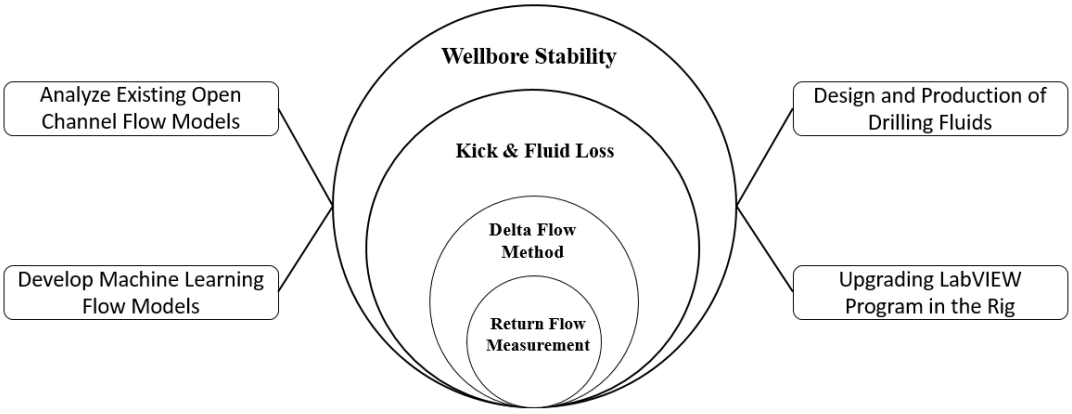

FIGURE 1.4: The structure of the thesis with the main elements – modelling and data fusion.

TABLE 1.1: Comparison of different return flow measurement systems.

Flowmeters	**Implementation**	**Measurement principle**	**Accuracy**[a]	**Limitations**
Paddle flow meter	paddle in contact with the fluid	deflection of a paddle	poor	poor accuracy
Electromagnetic flow meter	needs U-shaped tube, where the flow meter is placed	perturbations in a magnetic field	0.5 %	limited to conductive fluids
Doppler ultrasonic flow meter	a non-intrusive transducer clamped on the outside surface of the pipe	Doppler effect	1 %	sonic attenuation
Weir and Venturi meter	channel is restricted	fluid level before the restriction	2 - 5 %	dependent on fluid rheology

[a]These accuracies are based on Newtonian fluids given in (Orban, Zanner, and Orban, 1987)

Chapter 2

Open Channel Flow Measurement

A flow of a fluid in a conduit with a free surface is an open channel flow. For example rivers, canals and irrigation ditches, storm and sanitary sewer systems, sewage treatment plants, industrial waste applications, transportation of non-Newtonian slurries, etc. The flow measurement is important for most of these applications. In this chapter, different types of open channel flow measurement systems are discussed.

2.1 Flow Measurement in Open Channels with Uniform Cross-section

In the past years, there are several methods developed for flow measurement through a uniform geometry open channel. Some of the selected methods are discussed in this section.

2.1.1 Chezy and Manning Equations

Back in 1768, Chezy developed an empirical equation for turbulent flow through an open channel, which is given in Equation 2.1, (Chanson, 2004).

$$V = C_{Chezy}\sqrt{R_h \sin\Theta} \tag{2.1}$$

where V is average velocity of the fluid, C_{Chezy} is a coefficient to be adjusted based on the roughness of the channel, R_h is a hydraulic radius, and Θ is a channel slope.

Similar to Chezy equation, an alternative flow equation is developed by Robert Manning in 1889, which is given in Equation 2.2, (Chanson, 2004).

$$V = \frac{1}{n_{Manning}} (R_h)^{2/3} \sqrt{\sin\Theta} \tag{2.2}$$

where $n_{Manning}$ is a coefficient that represents the roughness of the channel.

The applications of these models are limited as they need a proper tuning of the coefficients (i.e., C_{Chezy} and $n_{Manning}$) and are applicable only for Newtonian fluids, (Alderman and Haldenwang, 2007). Other similar models are discussed in (Alderman and Haldenwang, 2007).

2.1.2 Rainer Haldenwang's Equation

There are several flow models used for non-Newtonian fluid flow starting with (Kozicki and Tiu, 1967), (Coussot, 1994), and other different flow models are discussed in (Alderman and Haldenwang, 2007). Haldenwang et al. have been developing a reliable flow model for non-Newtonian fluid flow through a uniform geometry open

channel, (Haldenwang, 2003; Burger, 2014; Burger, Haldenwang, and Alderman, 2010a; Burger, Haldenwang, and Alderman, 2014). In (Burger, Haldenwang, and Alderman, 2014), open channel flow models applicable to all types of non-Newtonian fluids (Bingham-plastic, power-law, or Herschel-Bulkley fluid) are presented. Equation 2.3 and Equation 2.4 are the models used to estimate average velocity of the fluid in laminar and turbulent flow respectively.

$$V = \frac{R_h}{2}\left[\frac{(16/K)\tau_w - \tau_y}{k}\right]^{1/n} \tag{2.3}$$

$$\begin{aligned} V &= \sqrt{\frac{2\tau_w}{\rho c_1 (R_H)^{c_2}}} \\ \textit{where,} \quad R_H &= \frac{8\rho V^2}{\tau_y + K\left(\frac{2V}{R_h}\right)^n} \end{aligned} \tag{2.4}$$

where K is the constant dependent on the geometry of the channel (for example K is 17.6 for a trapezoidal channel, which is experimentally found in (Burger, Haldenwang, and Alderman, 2010b)). τ_w is average wall shear stress, τ_y is a yield stress, k is consistency index, n is flow behavior index, ρ is density, c_1 and c_2 are empirical constants based on the geometry of the channel (for example $c_1 = 0.0851$ and $c_2 = -0.2655$ for a trapezoidal channel, (Burger, Haldenwang, and Alderman, 2010b)), and R_H is Haldenwang's Reynolds number.

The flow models given in Equations 2.3 and 2.4 depend on the rheological properties of the fluid. In drilling fluid circulations, the returning fluids have different rheological properties in each circulation, and it is a challenge to perform real-time rheology measurements. Hence, these models are not applicable for measuring the return flow of drilling fluid while drilling.

2.1.3 Paddlemeter and Rolling Float Meter

In drilling operations, conventional flow meters like paddle meter and rolling float meter are used for return flow measurements. In paddle meter, a spring-mounted plate or paddle is placed in the return flow line, and the deflection of the paddle is correlated with the average velocity of the fluid flow. The rolling float meter has a wheel floating over the surface of the fluid. The height of the floating wheel is closely related to the depth of the fluid and the flow rate. Some of the rolling float meters consist of the magnetic rotary sensor on the wheel, which measures the spin rate and thus flow rate. (Schafer et al., 1991)

These types of flow meters are used for return flow measurement in mud log data method for detecting kick/loss but are not accurate enough for the delta flow measurement as discussed in (Orban, Zanner, and Orban, 1987).

2.2 Flow Measurement in Open Channels with Venturi Constriction

2.2.1 Venturi Meter

A basic Venturi meter has a converging section, a throat, and a diverging section as shown in Figure 2.1. The converging section of the Venturi region causes a local increase in the flow velocity. The local gain in kinetic energy due to the increased

velocity creates a local decrease in pressure (in a pipe flow) or local decrease in fluid level (in an open channel flow). This effect is what Giovanni Battista Venturi in 1797 named the "Venturi Effect". Later in 1888, Clemens Herschel became the first person to introduce commercial Venturi tubes, (Herschel, 1888).

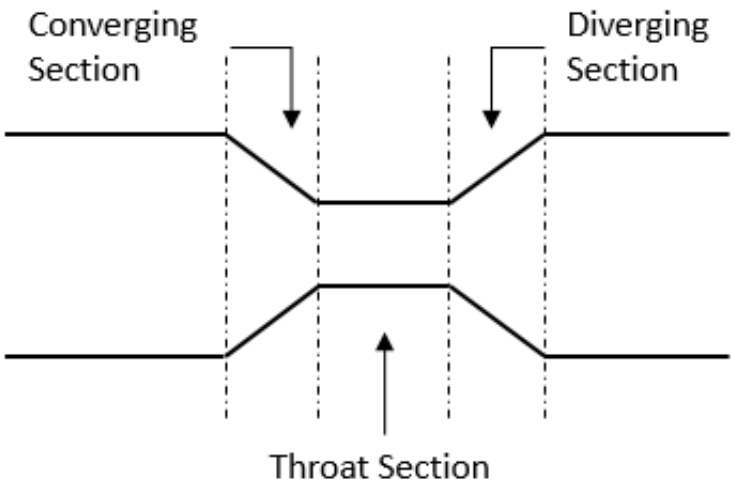

FIGURE 2.1: A Venturi meter with a converging section, a throat section and a diverging section.

The pressure drop (or the change in fluid levels) within the Venturi region can be used to measure the flow rate of the fluid. In the special case of steady and incompressible fluids, Bernoulli's equation can be used to derive pressure drop (or change in fluid levels) and volumetric flow relation.

For a pipe flow, other measurement devices (like orifice plates, flow nozzles and Venturi nozzles) can be used to create similar change in kinetic energy in a flowing fluid. However, the Venturi meters are capable of handling large flow volumes with very low permanent pressure loss in the system compared to other measuring devices, (Tompkins, 1974; Evans, 2007).

For an open channel flow, weir (like V-notch weir) can be used to measure flow. Basically, a weir has an obstruction in the flow path, which causes an increase in the fluid level. The increased fluid level above the top of the weir is correlated to the flow rate. As the fluid flow is obstructed in a weir, Venturi flumes are preferred for fluid flow application with suspensions, like the return drilling fluid flow. (Bengtson, 2010)

For a basic Venturi flowmeter to be accurate, the fluid flow in the Venturi channel has to be laminar, (Tompkins, 1974). Turbulent flow introduces factors which complicate the measurement, e.g. non-linear frictional effects and three-dimensional velocity vectors, (Tompkins, 1974). Therefore, a long upstream section that can assure a laminar flow or a minimized fluctuation flow is required for reliable Venturi flow measurements, (Tompkins, 1974).

Three different types of flow models based on the Venturi principle are introduced in this section. The performance of these models is discussed in Chapter 4. For these models, there should exist a critical flow within the throat section of the channel. In the critical flow condition, there exists a hydraulic jump, which flows backward and creates a sub-critical flow in the upstream[1] section of the channel.

[1]Upstream and downstream sections are with respect to the critical point, which lies within the throat section. Sections before and after the critical point are the upstream section and the downstream section respectively.

The computational fluid dynamics (CFD) simulations of backward propagation of the hydraulic jump are studied in (Malagalage et al., 2013) and is shown in Figure 2.2. If the hydraulic jump does not propagate back to the start of the channel, there exists a supercritical flow in the upstream. In this case, there is no critical flow within the Venturi constriction, and hence the flow estimations of these models are not reliable as presented in Chapter 4. Figure 2.3 shows a typical fluid level profile through the open Venturi channel in the critical flow condition. There is a sub-critical flow in the upstream section. Experimental level measurement shows that the upstream level slowly reduces towards the start of the channel as the energy in the backward propagating fluid reduces. This results in slightly varying levels in the upstream section.

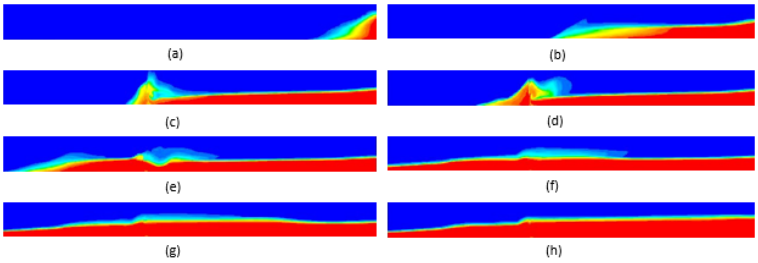

FIGURE 2.2: CFD simulation of water (shown red in figure) flowing through a Venturi flume. The flow direction is from right to left. a) Starting of the flow. b) Water flows through the open channel. c) Flowing water meets the Venturi constriction and experiences a hydraulic jump. d) The hydraulic jump leads to the back propagation (reflected pressure wave) of the water. e) With sufficient increase in potential energy, water starts to flow again. f)g)h) The back propagation (reflected pressure wave) of water gradually reaches to the start of the open channel, giving a steady level in the upstream section. (Malagalage et al., 2013)

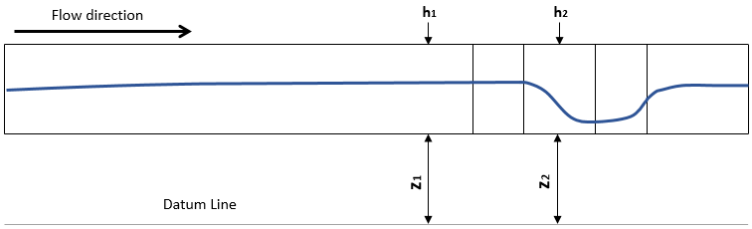

FIGURE 2.3: A typical level profile of fluid flowing through the open channel with Venturi constriction. The flow is sub-critical in the upstream section due to a hydraulic jump in the throat section.

2.2.2 Upstream-Throat Levels based Flow Measurement

This flow model estimates the volumetric flow based on the upstream and throat level measurements, henceforth referred as upstream-throat levels based flow model. Based on the fundamental Bernoulli principle, a flow model for an open channel with Venturi constriction is given in Equation 2.5, (Ganji and Wheeler, 2010).

$$Q_v = C_d A_1 A_2 \left\{ 2g \left\{ \frac{(h_2 - h_1) + (z_2 - z_1)}{\alpha_2 A_1^2 - \alpha_1 A_2^2} \right\} \right\}^{1/2} \tag{2.5}$$

where Q_v is volumetric flow rate, C_d is coefficient of discharge, A is a cross-sectional area, g is gravitational acceleration, h is fluid level, z is elevation with respect to the datum, and α is kinetic energy correction factor or Coriolis coefficient. Subscripts 1 and 2 represent the variables and parameters at upstream and at throat section respectively as shown in Figure 2.3.

2.2.3 Upstream Level based Flow Measurement

This flow model estimates the volumetric flow based on a single upstream level measurement, henceforth referred as upstream level based flow model. A volumetric flow rate through a trapezoidal open channel with Venturi constriction can be estimated using a single upstream level as given in Equation 2.6, (ISO-4359, 2013).

$$Q_v = C_d C_s C_v \left(\frac{2}{3}\right)^{3/2} \left(\frac{g}{\alpha_1}\right)^{1/2} b_2 h_1^{3/2} \tag{2.6}$$

where C_s is shape coefficient, C_v is coefficient of velocity, and b is the bottom width of the channel.

2.2.4 Critical Level based Flow Measurement

In the case of critical flow, the volumetric flow rate can be estimated using a critical level measurement within the throat section as given in Equation 2.7. For a trapezoidal cross-section geometry, the mathematical details are given in Paper A.

This flow model requires the knowledge about the location of the critical level, which is varying with the flow rate. A real-time positioning of a level sensor is not a feasible task, and hence a study on critical level correction is performed under Section 4.2.2. This flow model estimates the volumetric flow based on a critical level measurements, henceforth referred as critical level based flow model.

$$Q_v = \left\{ \frac{\left(\frac{g}{\alpha_2}\right) h_c^3 (b_2 + h_c \cot\theta)^3}{b_2 + 2h_c \cot\theta} \right\}^{1/2} \tag{2.7}$$

where h_c is a critical level and θ is a channel slope angle.

Other similar flow measurement techniques are discussed in (Boiten, 2002; Yeung, 2007; Berg et al., 2015; Agu et al., 2017).

Chapter 3

Experimental Set-up, Drilling Fluids and Sensors

All the experimental works are performed using a flow loop available at University of South-Eastern Norway (USN). A short overview of the flow loop, open Venturi channel, drilling fluids, and sensor systems are given in this chapter.

3.1 Flow Loop

For the study of the return flow measurement using a Venturi constriction in an open channel, a flow loop is available at USN, Porsgrunn Campus. The flow loop is provided by Equinor ASA. The flow loop consists of a fluid tank, a fluid pump, an open channel with Venturi constriction, Coriolis mass flow meters, a blender for mixing, and other different sensors and sensor systems. Figure 3.1 shows a P&ID of the flow loop. A fluid pump is used to pump the fluid from the tank, through the pipelines, to the open channel, and back to the tank, completing a circulation loop similar to the drilling mud circulation. The picture of the flow loop is shown in Figure 1 in Paper B. The open channel consists of a Venturi constriction and three ultrasonic level sensors (LT-1, LT-2, and LT-3), which are used to estimate flow rates. Coriolis mass flow meter (FT-1) is used as a reference flow meter.

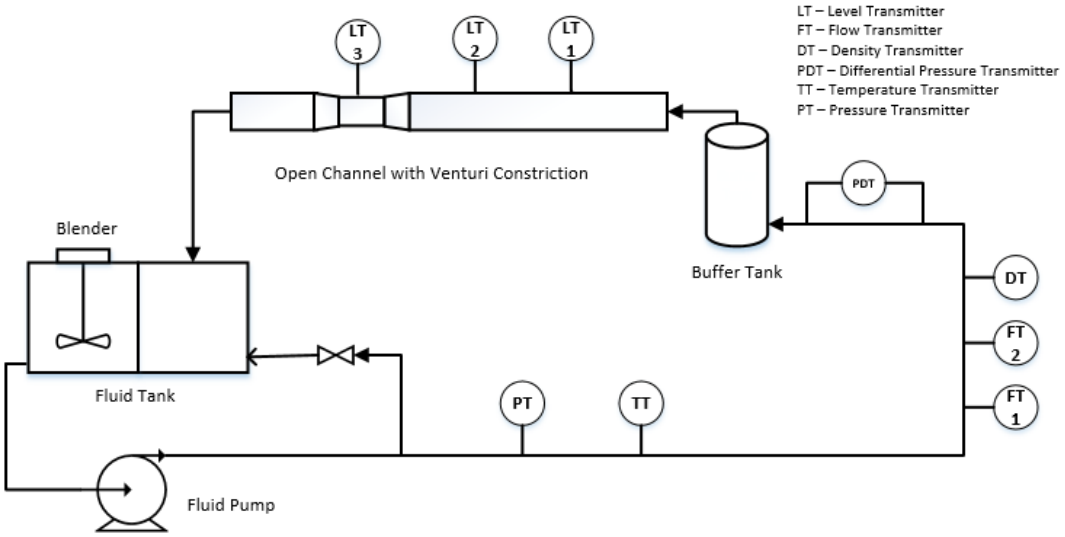

FIGURE 3.1: P&ID of the flow loop available at University of South-Eastern Norway, Porsgrunn Campus.

3.2 Open Venturi Channel

The flow loop consists of an open channel with Venturi constriction. The geometry of the open channel is based on the standard geometry provided by (Bamo, 2009), which can measure a flow rate up to 69 $[l/s]$. The CFD simulations studied in (Malagalage et al., 2013) (i.e., Figure 2.2 in Chapter 2) are based on the same geometry. In the field, the range of flow can be increased by appropriately changing the geometry of the channel. In (Bamo, 2009), dimensions and geometries needed for a flow rate up to 695 $[l/s]$ are given. Figure 3.2a shows a top view of the open channel. The upstream of the channel is long enough to ensure the critical flow through the channel. Figure 3.2b shows a trapezoidal cross-sectional view of the channel. Further, the channel is tiltable to an angle of ± 2 degrees to the horizontal.

Figure 3.3 shows a 3D view of the open Venturi channel with three ultrasonic level sensors. The positions of these three level sensors are easily adjustable and can be used to scan a level profile in the channel. With reference to the flow models presented in Chapter 2, usually, two level measurements (one at the upstream section and another at the throat section) are used.

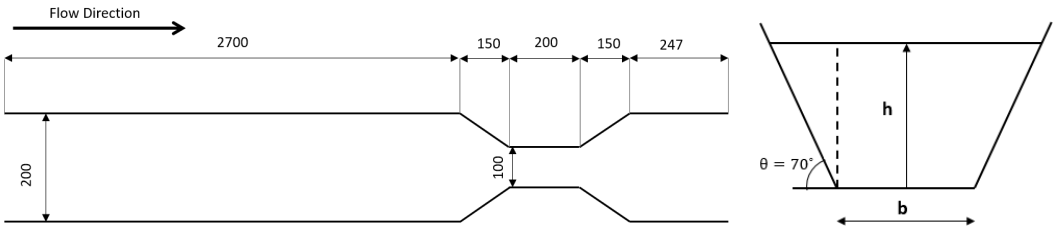

FIGURE 3.2: .
]Geometry of the open Venturi channel. a) Top View sketch. b) Cross-sectional view sketch. All the dimensions are in [mm]. The information on dimensions is taken from (Glittum et al., 2015).

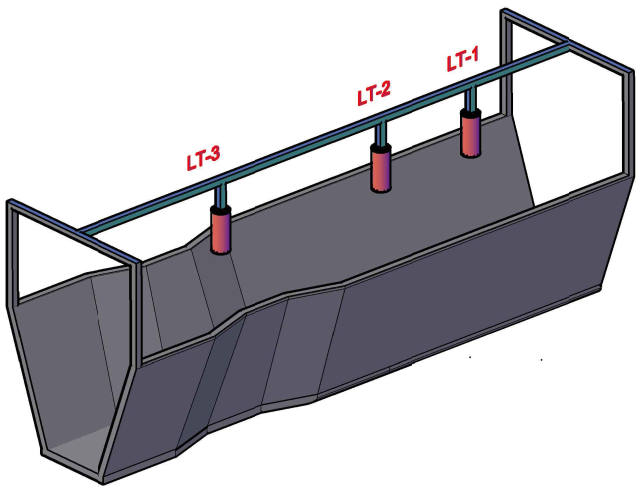

FIGURE 3.3: An open channel with Venturi constriction and three ultrasonic level sensors. (Chhantyal, Viumdal, and Mylvaganam, 2017a)

3.3 Drilling Fluids

3.3.1 Background on Rheology of Drilling Fluids

Based on the rheological behaviour, fluids can be classified into Newtonian and non-Newtonian fluids. Viscosity is defined as the ratio of shear stress to shear rate. For Newtonian fluids, viscosity remains constant with changing shear rate (for example water), whereas the viscosity of non-Newtonian fluids changes with shear rate (for example drilling fluids). Non-Newtonian fluids exhibit mainly shear-thinning or shear-thickening behaviours. (Caenn, Darley, and Gray, 2011b)

- Shear-thinning fluids: the viscosity of the fluids decreases with increasing shear rate. Shear-thinning fluids can be pseudoplastic or viscoplastic in nature. Pseudoplastic fluids flow as soon as shearing force or pressure is applied, whereas viscoplastic fluids flow after certain yield stress as shown in Figure 3.4.
- Shear-thickening or dilatant fluids: the viscosity of the fluids increases with increasing shear rate.

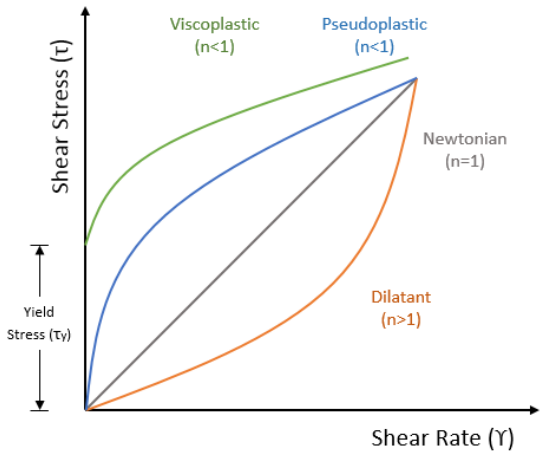

FIGURE 3.4: Shear stress vs. shear rate curve for both Newtonian and non-Newtonian fluids. Adapted from (Caenn, Darley, and Gray, 2011b).

3.3.2 Shear-thinning Drilling Fluids

Drilling fluids should be preferably shear-thinning in nature as these fluids become thick in a low-velocity flow and thin in a high-velocity flow. For the same volumetric flow rate, the velocity of circulation fluid is high through the drill pipe and low through the annulus due to the different cross-sectional area. As the velocity is high through the drill pipe, the thickness of the fluid reduces and requires less pumping energy. At the same time, the low velocity through the annulus increases the thickness of the fluid, which will avoid the settling of rock cuttings. (Caenn, Darley, and Gray, 2011b)

Drilling fluid behaviour can be described using two standard rheological models, i.e., Power Law model and Herschel-Bulkley model (often termed as modified Power Law model). The models are defined in Equation 3.1. (Caenn, Darley, and

Gray, 2011b)

$$\begin{aligned} \tau &= k\gamma^n, \quad \text{(Power Law Model)} \\ \tau &= \tau_y + k\gamma^n, \quad \text{(Herschel-Bulkley Model)} \end{aligned} \tag{3.1}$$

where τ is shear stress, τ_y is yield stress, γ is shear rate, k is consistency index, and n is flow behaviour index (n=1 for Newtonian fluids, n<1 for shear-thinning fluids, and n>1 for shear-thickening fluids).

3.3.3 Design and Production of Non-Newtonian Fluids

To study the flow measurement using Venturi channel, several non-Newtonian fluids with rheology similar to real drilling muds are used. The drilling fluid used emulating the properties of the drilling muds used in the field are water-based fluids with potassium carbonate as densifying agent and xanthan gum as viscosifier.

A drilling mud with a high pH value is desirable to control corrosion rate and hydrogen embrittlement, (Bourgoyne et al., 1986). In addition, the high pH is a favourable environment for most of the viscosity control additives, (Bourgoyne et al., 1986). Hence, Potassium carbonate is used, which is a white salt with the density of 2420 $[kg/m^3]$, soluble in water (solubility of 112 $[g]/100$ $[ml]$ water at 20°C) and forms strongly alkaline solution. The Equation 3.2 shows the exothermic dissolution reaction while blending the fluid.

$$K_2CO_{3(s)} + H_2O_{(l)} \rightarrow 2KOH_{(aq)} + CO_{2(g)} \tag{3.2}$$

Xanthan gum is a polysaccharide secreted by the bacterium Xanthomonas Campestris that are mostly used as a food additive and a rheology modifier. Xanthan gum is highly pseudoplastic in nature. The hydrogen bond and polymer entanglement make the structure of xanthan gum compact. When shear force is applied, the polymers are de-aggregated, and the viscosity is reduced. The xanthan gum rapidly retains its original viscosity after the shear force is removed. (Keltrol, 2007)

The amount of xanthan gum required to have a thicker fluid is about $0.1 - 0.5\%$ of a total volume of the solvent as suggested in (Logsdon, 2013). Excessive use of xanthan gum not only increases the viscosity of the fluid but also increases the foam and bubble size. A large amount of foams and air bubbles are unwanted features as they affect the ultrasonic level measurements and the Coriolis readings.

Table 3.1 shows the chemical composition of different fluids used in the study. All the fluids are non-Newtonian fluids with shear thinning nature as shown in Figure 3.5. Fluid-1 is water mixed with some residual fluids while changing the fluids in the flow loop.

3.4 Sensors used in Experiments

In this work, three ultrasonic level sensors placed over the open Venturi channel and the Coriolis mass flow meter are used. Coriolis mass flow meter is used a reference flow meter. Figure 3.6 and Table 3.2 show the pictures of the measurement devices and their technical specifications respectively.

When drilling fluid is circulated through the flow loop, a significant amount of foams/air bubbles are observed. The amount of foam increases with increasing flow rate. The ultrasonic level sensors are very sensitive to foams and air bubbles present in the fluid. Therefore, it is important to either filter the foams before the level measurements or implement some on-line signal filtering after the measurements.

TABLE 3.1: Different fluids used in the study along with the corresponding chemical compositions. Fluid 1 is a mixture of water with residual fluids in the tank during the process of changing drilling fluid in the flow loop.

Fluids	Potassium Carbonate [%weight]	Xanthan Gum [%weight]	Density $[kg/m^3]$	Flow Index (n)	Consistency Index (k)
Fluid-1	-	-	1015	0.97	0.01
Fluid-2	18	0.07	1145	0.63	0.05
Fluid-3	21	0.07	1190	0.64	0.04
Fluid-4	29	0.21	1240	0.47	0.23
Fluid-5	73	0.22	1340	0.82	0.03

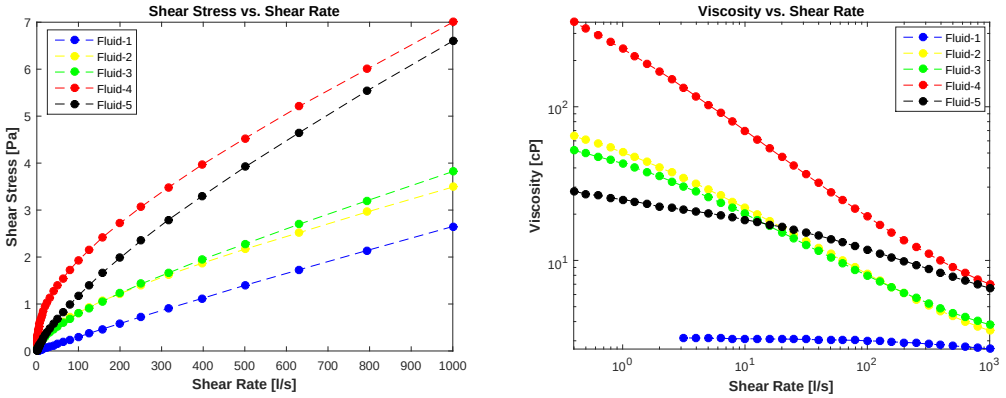

(a) (b)

FIGURE 3.5: a) Shear stress vs. shear rate curves for all the types of non-Newtonian fluids used in the study. b) Viscosity curves at different values of shear rates for the all the fluids. The rheological parameters are measured using Anton Paar Viscometer in Equinor ASA laboratory. (Chhantyal et al., 2018)

(a) (b)

FIGURE 3.6: a) Rosemount-3107 ultrasonic level sensor, (Emerson, 2014). b) Endress+Hauser Promass 63F Coriolis mass flow meter, (Endress+Hauser, 2013).

To mechanically filter the foams before the level measurements, a simple filter net is used in the open channel without disturbing the flow. Figure 3.7 shows the filtration of foams using the filter net. The foams/air bubbles present in the circulating fluids are highly reduced using the filter net.

Further, the signals from three ultrasonic sensors and Coriolis mass flow meter

TABLE 3.2: Technical specifications of the ultrasonic level sensor and Coriolis mass flow meter. Based on information from the vendors.

Measurement Devices	**Vendor (Model)**	**Range**	**Uncertainty**
Ultrasonic level sensors	Rosemount (3107)	$< 1\ [m]$	$\pm 2.5\ [mm]$
Coriolis mass flow meter	Endress + Hauser (Promass 63F)	$0 - 1000\ [l/min]$	$\pm 0.10\ \%$

are passed through a moving average filter (MAF) with 10 previous observations. The filtered signals are comparatively less noisy as shown in Figure 3.8. The filtered ultrasonic level measurements will result in further stable flow rate estimations. In general, Coriolis readings are stable and accurate as shown in Figure 3.8d. However, Coriolis mass flow readings are not reliable in the presence of excessive amount of foams/air bubbles. A detailed discussion on the performance of Coriolis mass flow meter in the presence of foams/air bubbles is presented in Chapter 4.

(a) (b) (c) (d)

FIGURE 3.7: a) Drilling fluid (Fluid-5 is used) flowing through the open Venturi channel. b) A simple filter net designed to filter foams. c)d) The filter net is effectively filtering foams during the fluid circulation.

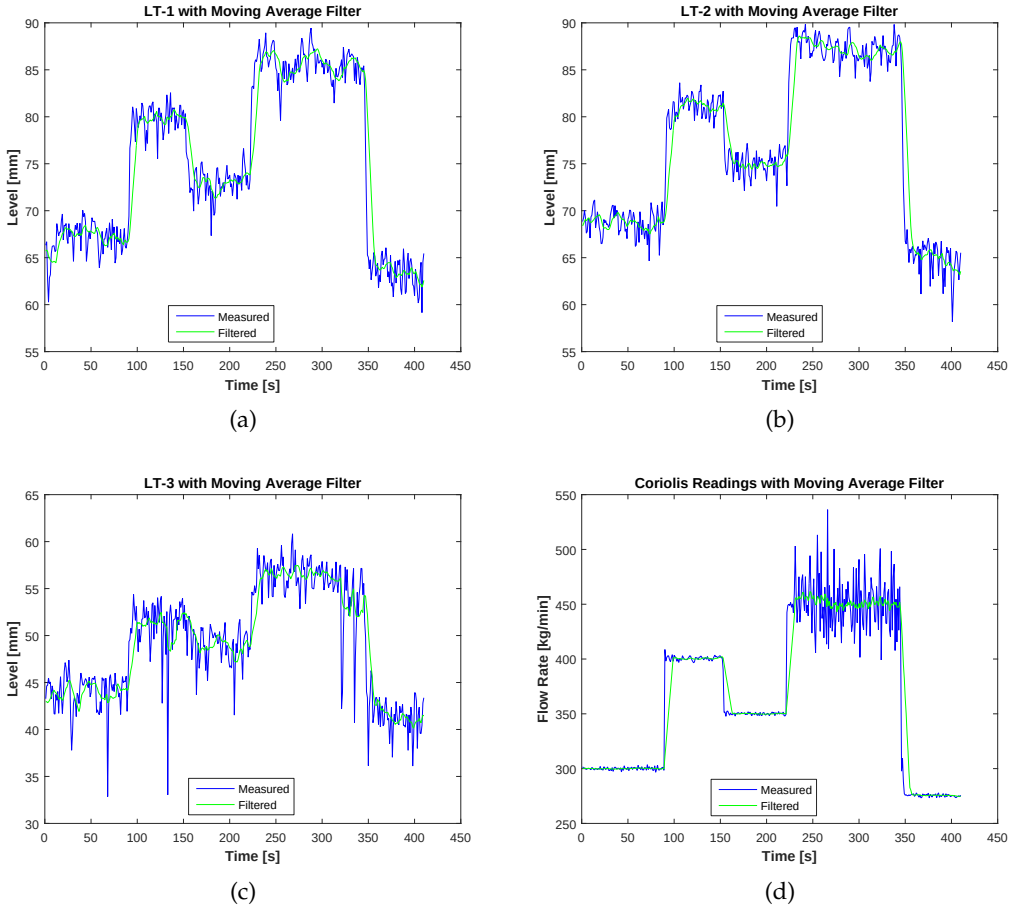

FIGURE 3.8: The level measurements using three ultrasonic level sensors and the Coriolis mass flow meter readings are filtered using moving averaged filter with 10 previous observations. The level sensor LT-1 is placed near to the start of the open channel.

Chapter 4

Flow Measurement Techniques with some aspects of Modelling

In this chapter, different flow measurement systems for open channels with Venturi constriction are analysed. Mean absolute percentage error (MAPE) is used for comparing and evaluating the performance of the measurement systems.

4.1 Coriolis Mass Flow Meter

A Coriolis mass flow meter can measure a fluid flow with high accuracy under favourable conditions. Figure 4.1a shows the comparison of Coriolis mass flow readings with the reference set-points for highly viscous fluid (here, Fluid-5 is used). Experimentally, it can be seen that the amount of air bubbles increases in the circulating fluid as the flow rate increases. Further, the rate of increase in air bubbles is high for high viscous fluids. Due to the increase in air bubbles, the Coriolis readings are affected at high flow rates as shown in Figure 4.1a. The observations indicate that the Coriolis readings are highly sensitive to air bubbles.

For the further verification, additional air bubbles are generated in the circulating fluid using a blender, available in the flow loop. Figure 4.1b shows the Coriolis mass flow meter readings with the set-points after using a blender. It can be observed that the Coriolis readings are not reliable at all. With the running blender, there is a large amount of air bubbles, even in the low flow rates resulting in a high fluctuation of Coriolis readings.

The Coriolis mass flow meter tested with the drilling fluid consisting of a large amount of air bubbles, mimicking the presence of formation gases while drilling shows that the flow meter is not suitable for return flow measurements. However, it can be used for inflow measurements where drilling fluids contain no impurities.

4.2 Open Channel Flow Models

The open channel flow models (i.e., upstream-throat levels based, upstream level based, and critical level based) presented in Section 2.2 can measure fluid flow through an open channel with Venturi constriction, both in the presence of excess air bubbles or without air bubbles. Figure 4.2 shows the comparison of flow estimations using two flow models (i.e., upstream-throat levels based and upstream level based) while circulating the drilling fluid having excessive air bubbles. A similar discussion is presented in Paper C.

The performance of the models in Figure 4.2 shows that the flow estimations of these models are comparatively not affected by the air bubbles with regards to

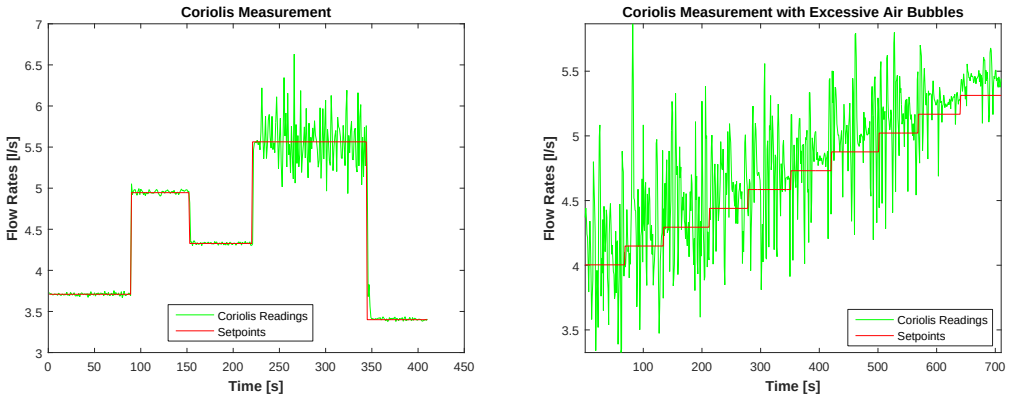

(a) (b)

FIGURE 4.1: a) Coriolis mass flow meter readings are reliable in the presence of low air bubbles and the readings are affected as the amount of air bubbles increases. b) Coriolis mass flow meter readings in the presence of excessive air bubbles are not reliable, (Chhantyal et al., 2018).

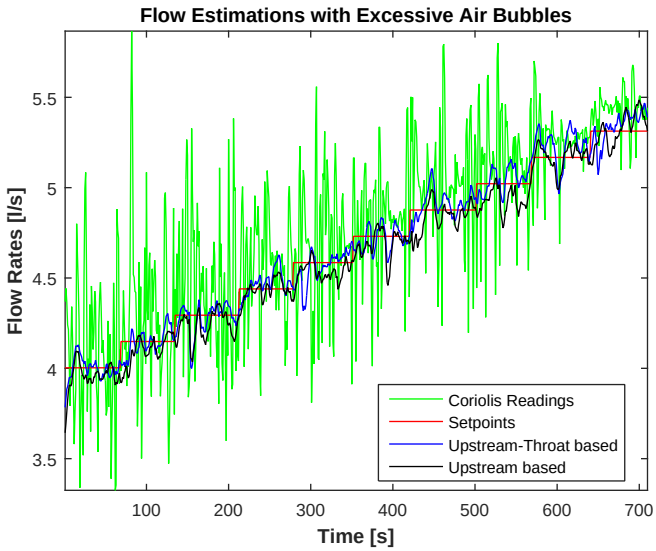

FIGURE 4.2: The flow models are capable of estimating reliable flow rates in the case of excessive presence of air bubbles. (Chhantyal et al., 2018)

Coriolis mass flow meter. However, excessive presence of air bubbles affect the ultrasonic level measurements, which will directly affects the flow rate estimations of these models. There is a need for some filtering algorithms to improve the level measurements. To further reduce the noise caused by the foam formation, ultrasonic transducers might be replaced by the radar sensor, (Thapa et al., 2017).

Figure 4.3 shows the flow estimations of three different flow models with reference to randomly varying set-points. The performance of these models is evaluated using MAPE as shown in Table 4.1. The comparison shows that both upstream-throat levels based flow model and upstream level based flow model have highly accurate flow estimations with MAPE of 2.33% and 2.92% respectively. The critical level based flow model has the highest MAPE of 5.81%. It is due to the fact that a

critical level position changes with the change in the flow rate[1]. In this comparison study, flow estimations are based on the critical level position of 4.3 $[l/s]$. Due to this reason, the ultrasonic level sensor is measuring the true critical level only for 4.3 $[l/s]$. Hence, the flow rate estimations are accurate for 4.3 $[l/s]$ and nearby flow rates.

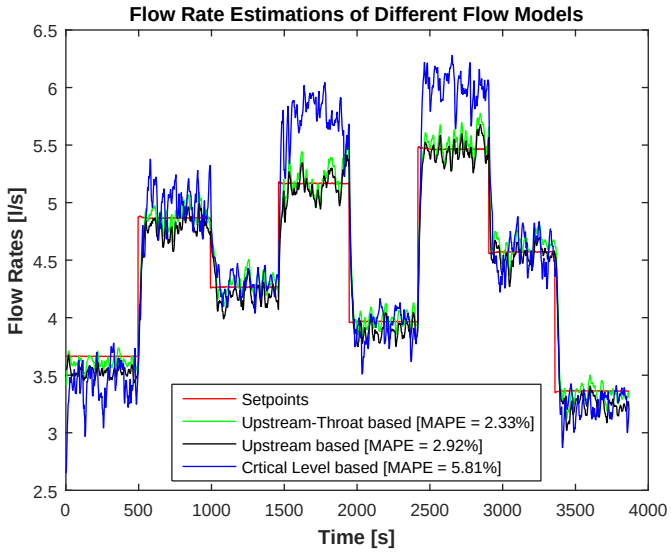

FIGURE 4.3: The comparison plot of flow rate estimations of three different flow models. Fluid-5 is used.

TABLE 4.1: The comparison of the performance of three different flow models based on Mean Absolute Percentage Error (MAPE).

Flow Models	**MAPE** [%]
Upstream-throat levels based	2.33 %
Upstream level based	2.92 %
Critical level based	5.81 %

4.2.1 Tuning of Correction Factor

One of the limitations of these flow models is a need for tuning a kinetic energy correction factor (α) (in Equations 2.5, 2.6 and 2.7). The correction factor is introduced to compensate for an error in average velocity consideration. A flow profile is different for laminar and turbulent flow. In the laminar flow profile, the velocity of flow is high on the surface and slows down towards the bed of the channel, in an open channel flow. In the case of turbulent flow profile, the flow velocities are randomly distributed. Therefore, the average velocity consideration is applicable only for turbulent flow regime and hence, the correction factor is assumed to be '1' for turbulent flow and '2' for laminar flow, (USYD, 2005). The selection of the correction factor depends on the type of flow regime and the rheology of the fluid. The correction factor should be tuned for different flow rates of the same fluid or for different fluids. Based on the experimental results, the correction factor in the upstream section is tuned between $\alpha_1 = 1.2$ to 1.4 for the fluids available in the flow loop. Figure 4.4

[1] The change in a critical level position with respect to the change in the flow rate is shown in Figure 7b of Paper A.

shows the upstream level based flow model fitted to a data using different values of the correction factor. The best fitted upstream level based flow model is achieved with the correction factor of $\alpha_1 = 1.4$. Further details are discussed in Paper C.

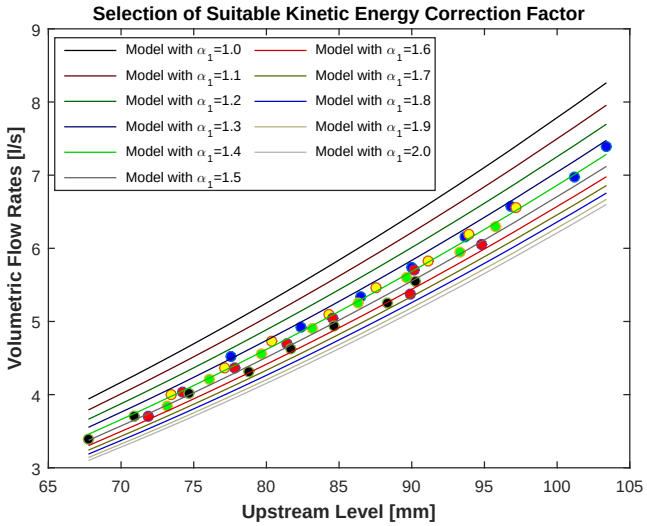

FIGURE 4.4: Tuning of the kinetic energy correction factor (α_1) in the upstream section. (Chhantyal et al., 2018)

4.2.2 Corrected Critical Level based Flow Measurement

Experimentally, it can be observed that the flow through the throat section is usually turbulent. Hence, there is no need to tune the correction factor in the throat section (i.e., $\alpha_2 = 1$). Hence, two flow models (i.e., upstream-throat levels based and upstream level based) are mainly affected by the selection of correction factor. The critical level based flow model is comparatively less or not affected. However, the limitation of this model is to identify a critical level for a given flow rate. Due to the fact that the position of critical level changes with the flow rate, positioning a level sensor within the throat section for critical level measurement is a challenging task as illustrated in Paper A.

Instead of measuring a critical level directly, two critical level correction algorithms are studied. They are a Fuzzy Logic based regulator and maximum specific energy based regulator. These regulators estimate critical level based on throat level measurement. Figure 4.5 shows an overview of the critical level correction algorithms.

Fuzzy Logic based Regulator (FLR)

The correction of the critical level based flow rate estimations needs a suitable type of regulator. To identify a regulator for our case, experiments were performed at different flow rates. The detailed experimental procedure is presented in Paper A. Figure 4.6 is the specific energy diagram showing the relation between specific energy and fluid level at different flow rates. The asterisk sign at different curves indicates the minimum specific energy point, which corresponds to the critical level for the given flow rate. An artificial neural network (ANN) fit is made for the different critical levels, which shows a linear increase in the critical level with increasing flow rate. This linear relationship confirms a need for a proportional (P-type) regulator.

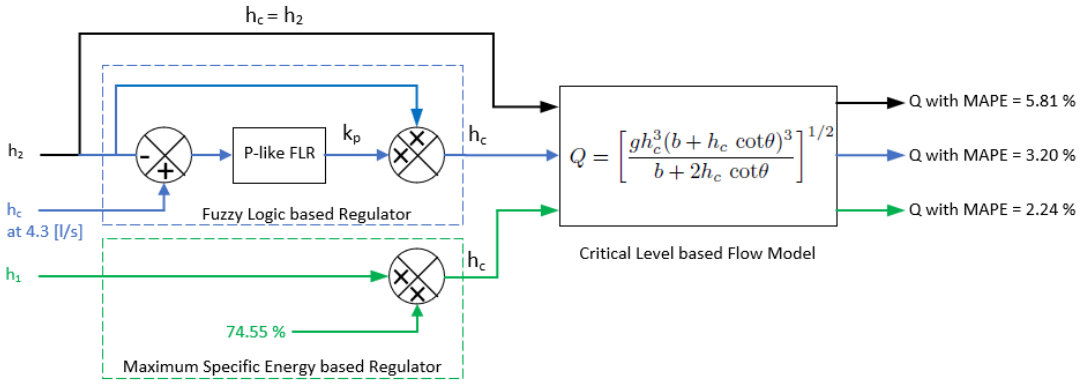

FIGURE 4.5: Overview of the critical level correction algorithms. h_1, h_2 and h_c are upstream level at 147 $[cm]$ position, throat level at 156 $[cm]$ position and critical level respectively.

The highlighted coordinate in Figure 4.6 shows a critical level of 53.72 $[mm]$ for the flow rate of 4.3 $[l/s]$, which is the reference critical level considered for our study. The reference critical level is measured using an ultrasonic level sensor at 156.2 $[cm]$ position[2] in the throat section. The ultrasonic sensor is fixed in this position (at 156.2 $[cm]$) for further measurements. Figure 4.7 shows different level profiles within the Venturi constriction for different flow rates. The deviation (i.e., the critical level (h_c) at 4.3 $[l/s]$ - ultrasonic throat level measurements (h_2 at 156.2 $[cm]$) at any flow rates) is used as an input to Proportional (P) like Fuzzy Logic Controller (FLC), and output is a proportional gain k_p. Thus, obtained k_p is used to correct the ultrasonic throat level measurements, which eventually corrects the flow estimations. The block diagram of the FLR correction algorithm is presented in blue color in Figure 4.5.

The membership functions and rules of the Proportional (P) like FLC are shown in Figure 4.8 and Table 4.2 respectively. The input fuzzy variables NB, NS, ZO, PS, and PB represent Negative Big, Negative Small, Zero, Positive Small, and Positive Big respectively. The output fuzzy variables LL, L, OK, H, and HH represent Low Low, Low, OK, High, and High High respectively.

TABLE 4.2: If-Then Rule Matrix of the P-like Fuzzy Logic Controller.

Deviation	**Proportional Gain** (k_p)
NB	LL
NS	L
ZO	OK
PS	H
PB	HH

Understanding the Rules of the P-like Fuzzy Logic Controller

- deviation $\approx$ zero: In this case, the flow rate is closer to the reference flow rate (4.3 $[l/s]$) and the throat level measurement (h_2 at 156.2 $[cm]$) is closer to the reference critical level (53.72 $[mm]$). Hence, the proportional gain (k_p) is set closer to 1, which makes no or fine adjustments in the throat level measurement.

[2]The position scale is given in Figure 2 of Paper A.

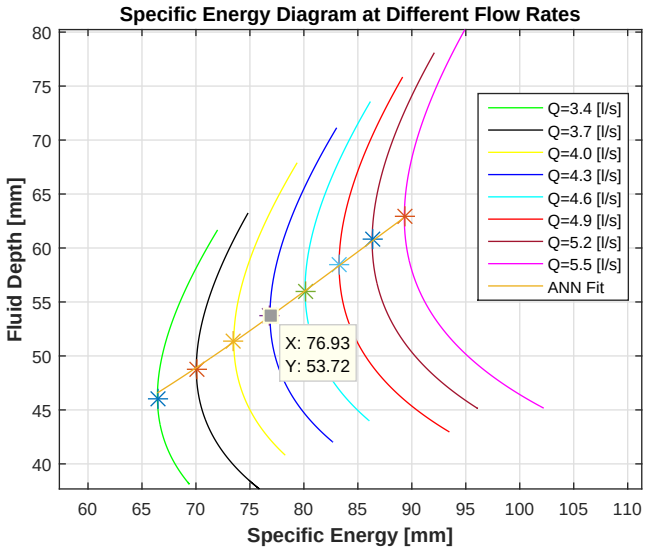

FIGURE 4.6: The specific energy diagram showing the relationship between specific energy and fluid level at different flow rates. The asterisk sign at each curve represents the point of minimum specific energy and the corresponding critical level. Fluid-5 is used.

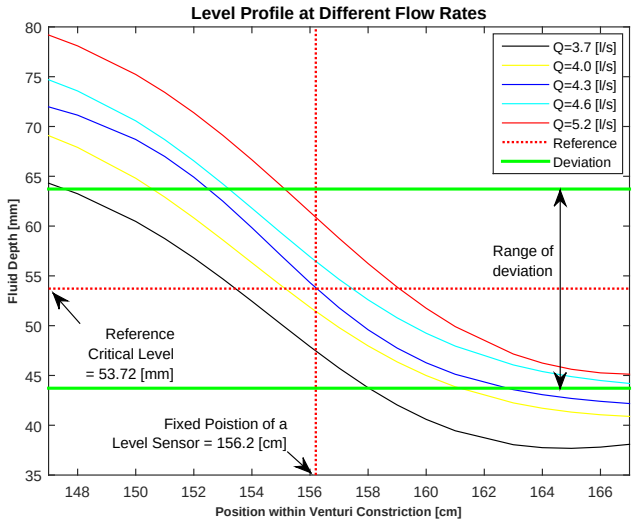

FIGURE 4.7: Fluid level profiles within the Venturi constriction at different flow rates. For the reference flow rate of 4.3 $[l/s]$, the reference critical level is 53.72 $[mm]$ and the fixed position of the ultrasonic level sensor is at 156.2 $[cm]$ position. Fluid-5 is used.

- deviation is positive: In this case, the flow rate is lower than the reference flow rate and the critical level position will shift towards the left (i.e., upstream) of 156.2 $[cm]$ position. As the upstream level is always greater than the downstream level, the proportional gain (k_p) is set higher than 1 to increase the throat level measurement.

- deviation is negative: In this case, the flow rate is higher than the reference flow rate and the critical level position will shift towards the right (i.e., downstream) of 156.2 $[cm]$ position. As the downstream level is always lower than

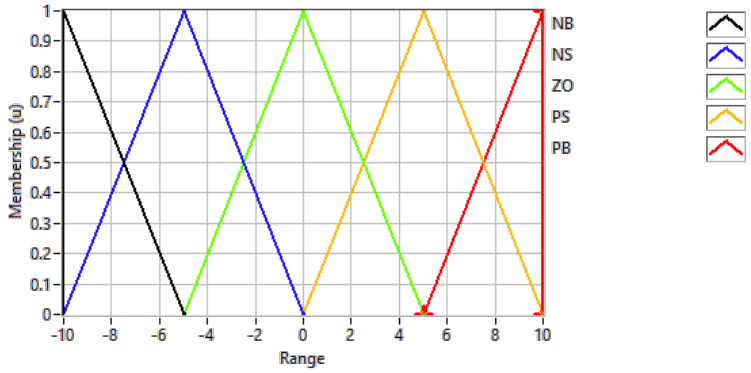

(a) Input Variable 'deviation'

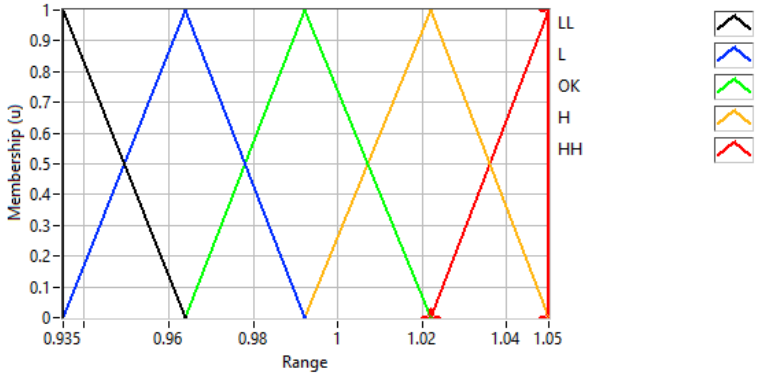

(b) Output Variable 'kp'

FIGURE 4.8: a) Input Variable "deviation" membership function. b) Output Variable "Proportional Gain (k_p)" membership function. Membership functions generated using Fuzzy Logic Toolbox in LabVIEW.

the upstream level, the proportional gain (k_p) is set less than 1 to decrease the throat level measurement.

Figure 4.9 shows the comparison of critical level based flow estimations before and after the correction. The implementation of the regulator improved the error percentage from 5.81% to 3.20%. However, the regulator is based on a single fluid and needs to be recalibrated for other fluids.

Maximum Specific Energy based Regulator (MSER)

The Bernoulli flow principle gives the energy equation of flow for a steady and incompressible fluid. The energy equation can be transformed into specific energy equation using specific weight resulting in Equation 4.1. The mathematical details are given in Paper A.

$$E_s = h + \frac{(Q_v/A)^2}{2g} \tag{4.1}$$

where E_s is specific energy.

Figure 4.10a shows specific energy profile of fluid flow along the Venturi flume at different flow rates (plotted using Equation 4.1). These profiles show that the minimum specific energy point changes with the flow rate. However, there exists

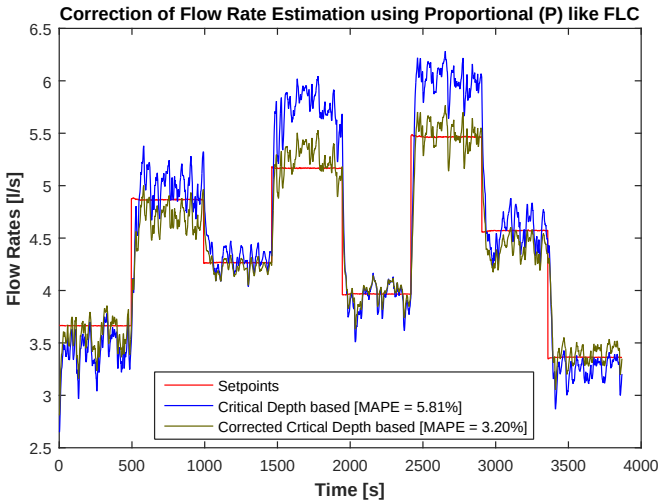

FIGURE 4.9: The comparison of critical level based flow estimations before and after the correction using the Proportional (P) like Fuzzy Logic Controller. Fluid-5 is used.

a maximum specific energy point at the start of throat section (i.e., position = 147 $[cm]$), which does not change with the flow rate. The idea of MSER is to utilize the measurement at this fixed position of maximum specific energy to estimate the critical level.

For Fluid-4, the levels at maximum and minimum specific energies for seven different flow rates are taken. Figure 4.10b shows a linear regression fit between the levels at maximum and minimum specific energies. Along the x-axis, the upstream level denotes the level at maximum specific energy, which is level measurements at 147 $[cm]$ position along the channel. Along the y-axis, the critical level denotes the level at minimum specific energy, which is experimentally identified using specific energy diagrams. The linear relation shows that a critical level is 0.7455 times the upstream level for the fluid under consideration (i.e., Fluid-4).

$$h_c^{estimated} = 74.55\% \times h_{upstream}^{measured} \tag{4.2}$$

where $h_{upstream}^{measured}$ and $h_c^{estimated}$ are the measured upstream level at 147 $[cm]$ position along the channel and estimated critical level respectively. Further, the obtained linear relation is also validated for Fluid-3 and Fluid-5 as shown in Figure 4.11a and Figure 4.11b respectively. Similar to Fluid-4, actual critical levels for Fluid-3 and Fluid-5 are obtained from corresponding specific energy diagrams. The predicted critical levels are 74.55% of upstream level measurements at 147 $[cm]$ position for both fluids. The validation results show that the linear relation still holds for these two fluids with MAPE of 1.20% and 0.61% for Fluid-3 and Fluid-5 respectively.

To evaluate the performance of the MSER correction algorithm, Fluid-5 is circulated in the flow loop with varying flow rates. Two ultrasonic level sensors are placed at the horizontal position of 147 $[cm]$ and 156.2 $[cm]$ to measure the level at maximum specific energy and the level at minimum specific energy for 4.3 $[l/s]$ flow rate respectively. Figure 4.12a shows different level measurements including level at 147 $[cm]$ position (i.e. upstream level), level at 156.2 $[cm]$ position, and estimated critical level (i.e. 74.55% of level at 147 $[cm]$).

Figure 4.12b shows the comparison of flow rate estimations based on the level at

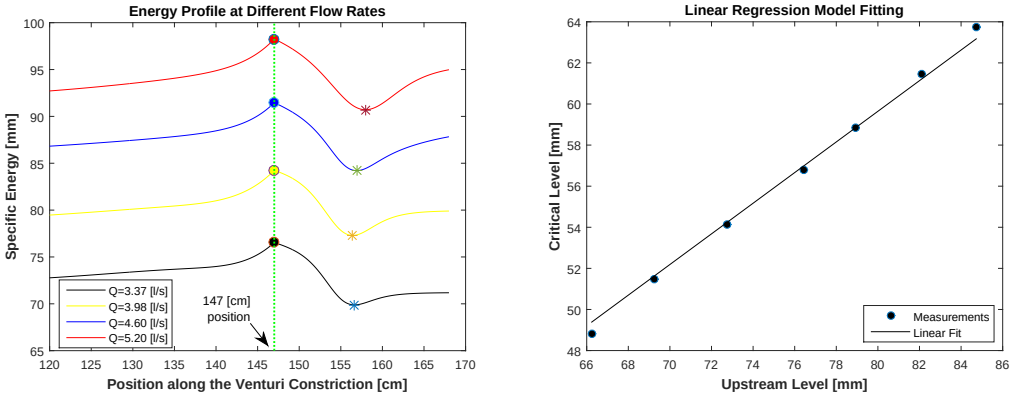

(a) (b)

FIGURE 4.10: (a) Specific energy profiles at different flow rates for Fluid-4. For all the flow rates, the maximum specific energy is found at the start of the throat section. (b) Linear relationship between upstream level measurements at the maximum specific energy point and critical level measurements at the minimum specific energy point.

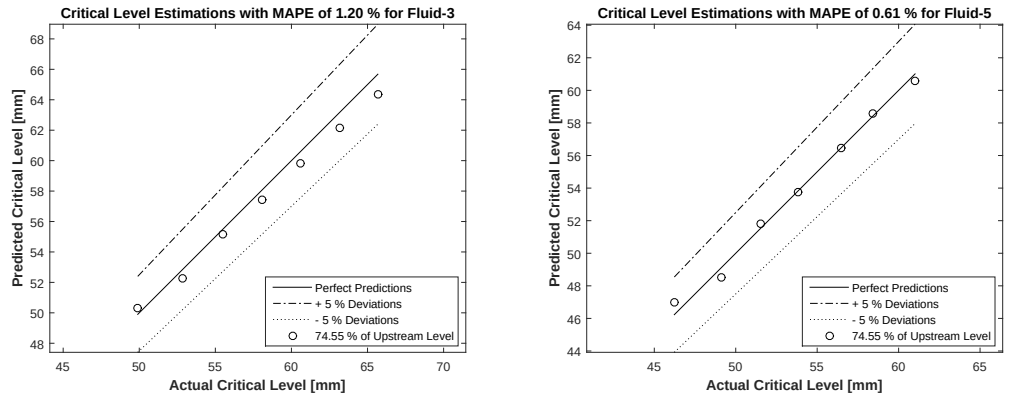

(a) (b)

FIGURE 4.11: Testing the linear relationship with other fluids. (a) The linear relationship holds for Fluid-3 with mean absolute percentage error (MAPE) of 1.20%. (b) The linear relationship holds for Fluid-5 with MAPE of 0.61%.

156.2 $[cm]$ position and estimated critical level. As expected, the flow rate estimations using level at 156.2 $[cm]$ position are accurate for flow rates closer to 4.3 $[l/s]$ and are not reliable for flow rates away from 4.3 $[l/s]$ with MAPE of 5.81%. However, the flow rate estimations based on estimated critical are capable of estimating randomly varying flow rates with MAPE of 2.24%. The block diagram of MSER correction algorithm is shown in green color in Figure 4.5.

Table 4.3 shows the comparison of flow rate estimations using critical level based flow model before and after corrections using FLR and MSER.

Similarly, critical level can be estimated using an upstream level (i.e., steady fluid level before the constriction).

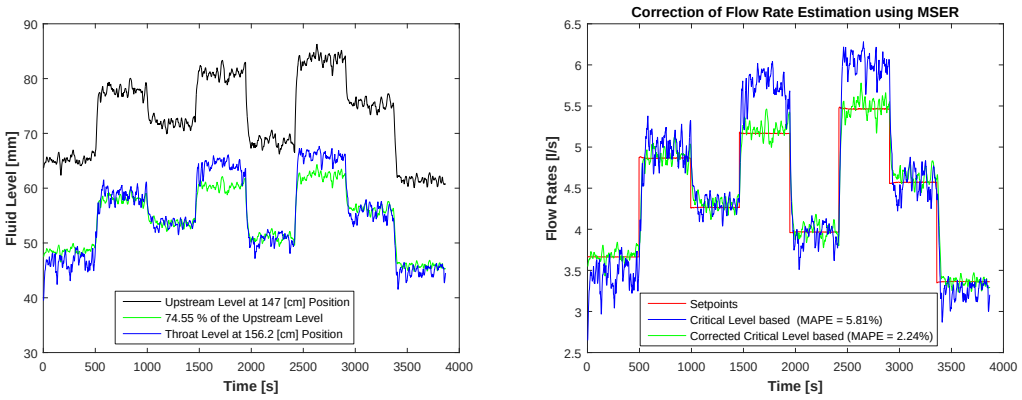

(a) (b)

FIGURE 4.12: (a) Different level measurements including upstream level at 147 $[cm]$ position, estimated critical level (i.e. 74.55% of upstream level), and level at 156.2 $[cm]$ position (i.e. critical level for the flow rate of 4.3 $[l/s]$). (b) Comparison of flow rate estimations based on level at 156 $[cm]$ position and estimated critical level. Fluid-5 is used.

TABLE 4.3: The performance of critical level based flow model is improved using FLR and MSER.

Flow Models	**MAPE** [%]
Critical level based	5.81 %
Correction with FLR	3.20 %
Correction with MSER	2.24 %

4.2.3 Flow Measurement with an Inclined Channel

The results so far show that the Venturi flow meter is capable of measuring flow with acceptable accuracy. However, in the application of fluid flow with solid materials may encounter challenges regarding the accumulation of sediments within the bottom surface of the Venturi flow meter. In the case of non-Newtonian drilling fluid flow containing rock cuttings, there is a high risk of accumulation of sediments. One simple way to decrease this risk is by inclining the open channel at an angle downwards in the direction of flow. Hence, this section presents the study of flow measurement using inclined Venturi channel.

The flow loop used in this work has the possibility of inclining the Venturi channel up to 2 degrees downwards. From Chapter 2, the upstream-throat levels based flow model defined by Equation (2.5) can handle different angles of inclination. The term "$z_2 - z_1$" takes into account the angle of inclination. Figure 4.13 shows the comparison of flow rate estimates using upstream-throat levels based flow model at four different angles (0, 0.2, 0.5, and 0.7 degrees). The results show that the model estimations are only acceptable for lower inclination angles (less than 0.5 degrees).

Figure 4.14 shows the variations in three different ultrasonic level measurements (LT-1, LT-2, and LT-3) for 300 $[kg/min]$ fluid flow at different angles of inclination. The level measurements used in the analysis are the averaged values of level measurements for each angle. The flow estimates using the upstream-throat levels based model are not reliable, if there is no critical flow or if the downstream level measurement is over 80% (also mentioned in (Bamo, 2009)) of upstream level measurement.

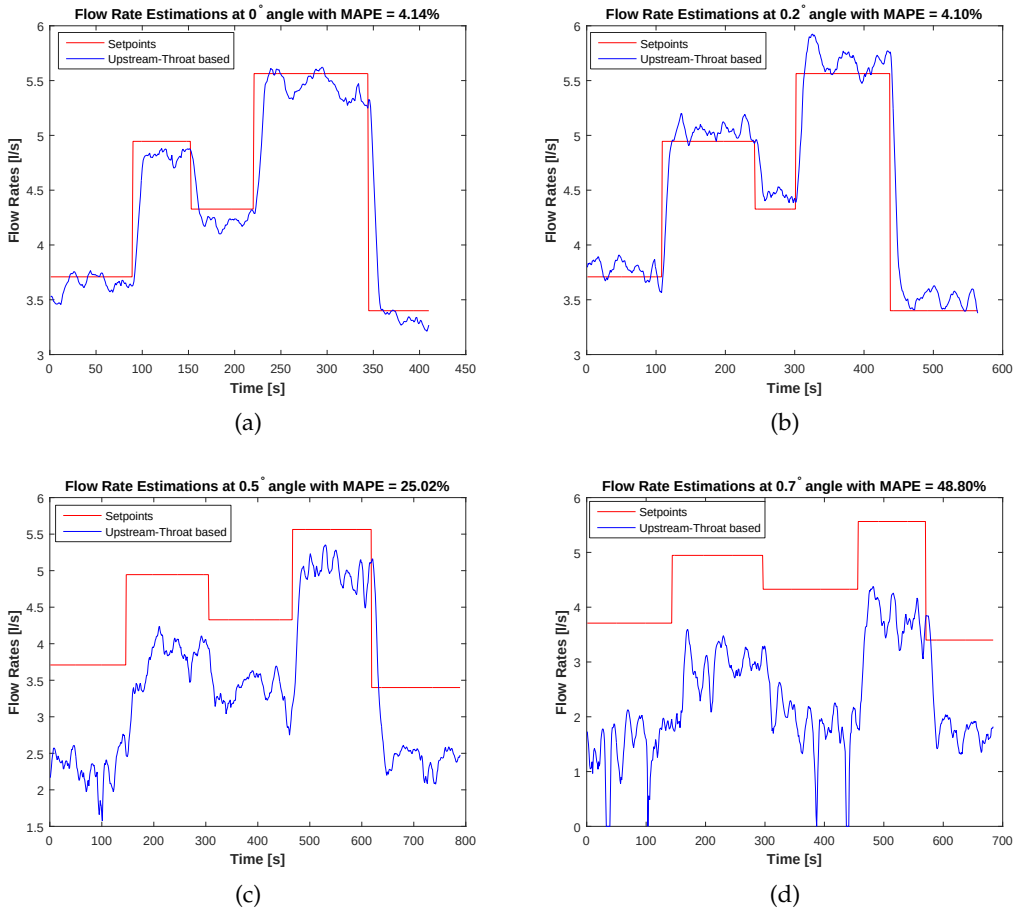

FIGURE 4.13: The flow estimation of upstream-throat levels based flow model at different angles of inclination. Fluid-5 is used.

In this analysis, LT-2 is upstream level measurement and LT-3 is a level measurement at the throat. The locations of the three ultrasonic level sensors are shown in Figure 3.3. For angles 0 to 0.4 degrees, the LT-3 level measurements are less than 80% of LT-2 level measurements. For this range of angles, the flow estimates using the model are reliable. From the angle of 0.5 degrees, the downstream level is over 80% of the upstream level, and thus the flow estimates are not reliable. The LT-2 level measurements are decreasing with an increase in angle of inclination as shown in Figure 4.14. After a certain angle of inclination, the downstream level measurements are higher than the upstream level measurements, which indicates the absence of critical flow. Similar studies are carried for other flow rates. Experimentally, it is seen that the critical flow does not exist when the angle exceeds 0.9 degrees for the Venturi channel used in this work.

In Figure 4.14, the variation in the measurements of another upstream level sensor (LT-1) with varying angles of inclination is also shown. The possibility of using the estimates of the model with different angles of inclination is further limited if the upstream level is measured using LT-1. From Figuree 4.14, it can be seen that the LT-1 upstream level measurement is lower than the LT-3 downstream level measurement after 0.2 degrees angle. It shows that the flow rate estimation using the level measurements of LT-1 and LT-3 are reliable only with an angle of inclination from 0 to 0.1 degrees. The study shows that the position of upstream level measurement determines the possible inclination angle that the model can handle.

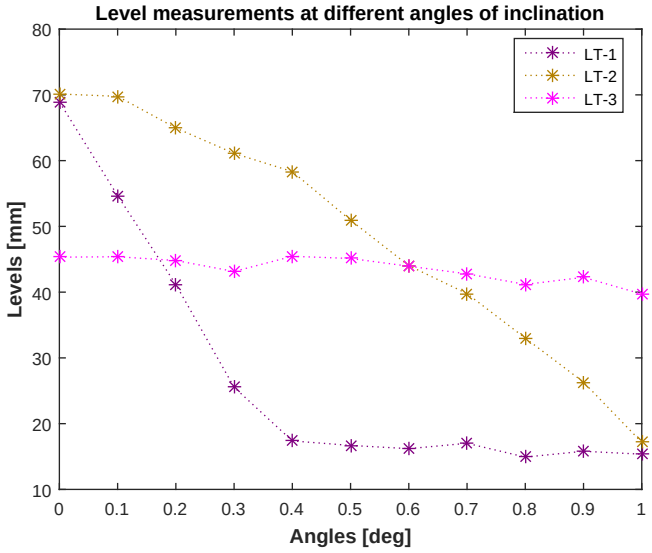

FIGURE 4.14: Variation in three different ultrasonic level measurements at different angles of inclination for 300 $[kg/min]$ fluid flow. The three different levels are indicated by the arrows in Figure 4.15.

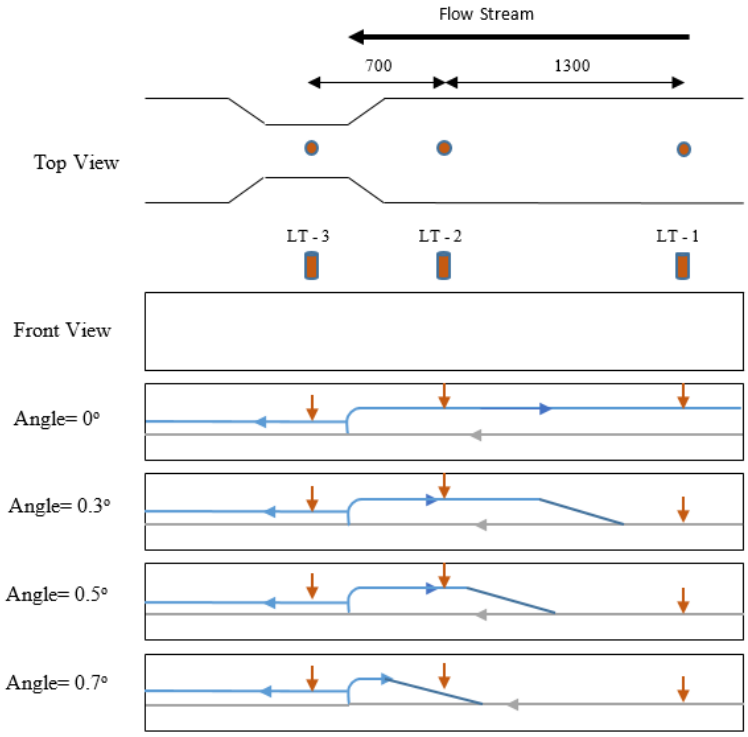

FIGURE 4.15: The schematic visualization of critical flow regime showing the reverse flow of fluids depending on the angles of inclination of the open Venturi channel. Arrows indicate the levels given by the ultrasonic sensors.

Figure 4.15 schematically shows the reason for the critical flow regime in the Venturi channel, which is similar to the CFD simulation results presented in Figure 2.2 in Chapter 2. The freely flowing fluid experiences a critical depth in the throat of the Venturi channel, which results in the reverse movement of waves. The increased upstream level measurements are used to estimate the flow rate through the channel.

The traversing distance of reverse flow depends on the angle of inclination. For a high value of inclination angle, there is either short and turbulent reverse flow or no critical flow at all. In the case of using LT-2 and LT-3 for the flow rate estimation, the level measurements are reliable up to 0.3 degrees. At an angle of 0.5 degrees, the LT-2 ultrasonic level measurement is exposed to the turbulence of reverse flow waves, resulting in unreliable flow estimates despite critical flow conditions. For higher angles of inclination, LT-2 upstream level measurements are apparent level measurements. Hence, the corresponding flow rate estimates are not accurate. Based on the Figure 4.15, using LT-1 in combination with LT-3 leads to reliable flow rate estimates only when the channel is horizontal.

Chapter 5

ML Models for Flow Measurement

Machine Learning is a branch of Artificial Intelligence (AI), where "Machine" refers to "programming algorithm" and "Learning" refers to "calibrating or training" the algorithm. Hence, ML is a science of getting computer or software algorithms to learn from data without being explicitly programmed, (Andrew, 2016).

Figure 5.1 shows a ML process. A data set is *randomly* divided into three different sets; training set , validation set, and test set. The ML models are trained using the training set. Figure 5.2 illustrates how ML models are trained, (Abu-Mostafa, 2012). In the training process, the objective is to find an unknown target function (f) that maps input (x) and output (y) variables. The training data sets are passed into a learning algorithm, which will stepwise adjust some parameters of an initial model (hypothesis) to match the input-output dataset. By the end of the training, the final hypothesis (f_h) is considered as the closest match to the unknown target function (f).

Validation can be performed during or after the training. Hence, the validation data set is used to validate each hypothesis during the training or the final hypothesis after the training. Finally, the best obtained hypothesis is tested using the test set data. In this thesis, the developed ML model refers to the best obtained hypothesis.

5.1 Data Pre-processing

To generate data for ML studies, experiments are performed in the flow loop. Three ultrasonic level measurements above the open channel are used as input data and the Coriolis mass flow meter readings are used as an output data. Figure 5.3 shows

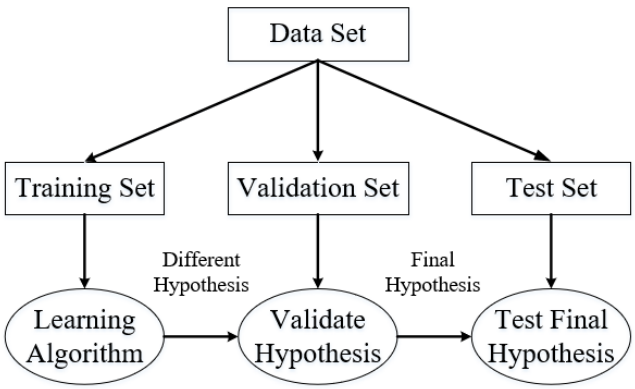

FIGURE 5.1: A flowchart showing the complete ML processes with training set, validation set, and testing set. (Chhantyal, Viumdal, and Mylvaganam, 2017a)

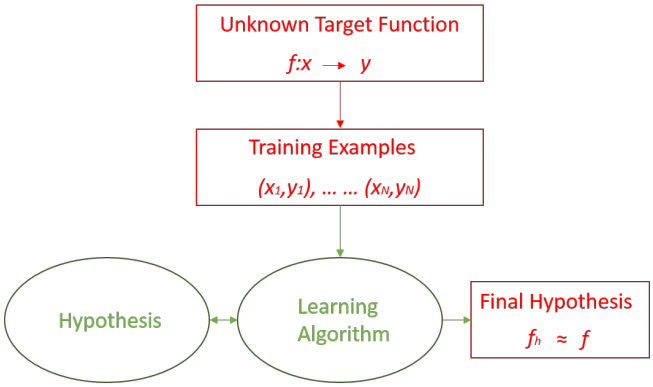

FIGURE 5.2: An overview of how ML algorithms are trained. (Abu-Mostafa, 2012)

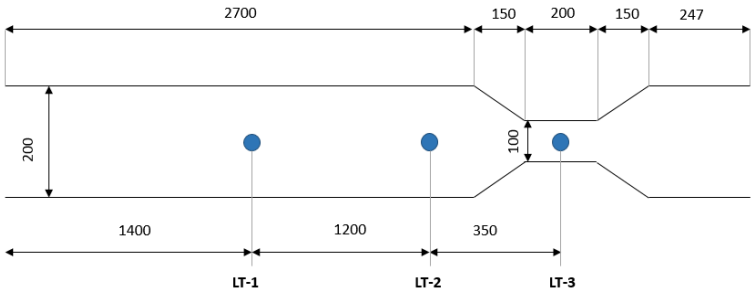

FIGURE 5.3: Top view of the open Venturi channel showing the location of three ultrasonic level sensors. These ultrasonic level measurements are used as input features for machine learning based flow models.

a top view of the open Venturi channel with the locations of ultrasonic level sensors. One, two, or all of these three level measurements are used as input feature(s) for ML based flow models. The experimental data set are scaled to [0,1] or [-1,1] range and are randomly divided into training, validation, and testing set.

5.2 ML Algorithms

The flow rate estimation based on the level measurements is a supervised regression problem in ML. Several linear and non-linear ML regression algorithms are investigated. All of these algorithms are written and trained in MATLAB. The developed flow models are used in LabVIEW software program of the flow loop for experimental studies.

5.2.1 Linear Models for Flow Estimations

A model represented by a linear combination of model parameters (often termed as coefficients or weights) is a linear model. In this work, following two linear regression models are used to estimate the flow rate based on level measurements.

1. Simple Linear Regression (SLR): In SLR, a linear model has a single or multiple features as input.

2. Polynomial Linear Regression (PLR): In PLR, features with different degrees of power are linearly combined.

The models are trained using gradient descent algorithm with a cost function of mean squared error (MSE).

5.2.2 Non-linear Models for Flow Estimations

To investigate a possible non-linear dependency between level and flow rate, different non-linear models are used in the study. Broadly, artificial neural network (ANN) and support vector regression (SVR) approaches are implemented.

1. Artificial Neural Network:
   ANN model is a non-linear model, which is trained to understand complex patterns in the given data. Analogous to the human brain, artificial neurons are connected to each other to make some decisions in ANN. The connection weights and the bias term of each neuron are the model parameters of ANN. In this study, several different types of ANN are used to estimate the flow rate based on the level measurements.

   (a) Feedforward ANN: is a static ANN that uses current inputs to estimate current outputs. Details on feedforward ANN with several learning algorithms are given in Paper B. In the paper, the presented results using feedforward ANN models are trained with Bayesian Regularization (BR) learning algorithm.

   (b) Feedback ANN: is a dynamic ANN that uses current inputs, and previous inputs and outputs to estimate current outputs. Details on feedback ANN are given in (Chhantyal et al., 2016b). In this thesis, the presented results using feedback ANN models are trained with Real-Time Recurrent Learning (RTRL) algorithm.

   (c) Adaptive Neuro-Fuzzy Inference System (ANFIS): is a combination of fuzzy logic system and artificial neural network. The model parameters (parameters of membership functions) and rules of fuzzy inference system are trained similar to ANN training. The ANFIS model for flow estimation is developed using Fuzzy Logic Toolbox in MATLAB and details are given in Paper B.

2. Support Vector Regression:
   SVR model is developed by transforming an original data in the input space into the higher dimensional feature space through non-linear mapping functions. In this study, ultrasonic level measurements are transformed into higher dimensional feature space using the Radial Basis Function (RBF). In this high dimensional feature space, an optimized linear regression model is developed to estimate the flow rate. Further details are given in Paper B.

5.3 Generalization of ML Models

A trained ML model should generalize a new data. Improper implementation of learning algorithm can lead to either under-fitted or over-fitted models. An under-fitted model cannot even justify training data. Hence the complexity of the model should be increased. An over-fitted model might perfectly fit the training data but has a large generalization error when tested with a new data set. In such cases, the trained model is only suitable for the training data, which is a state of data memorization. Therefore, a reliable ML model should be able to generalize a new data. All

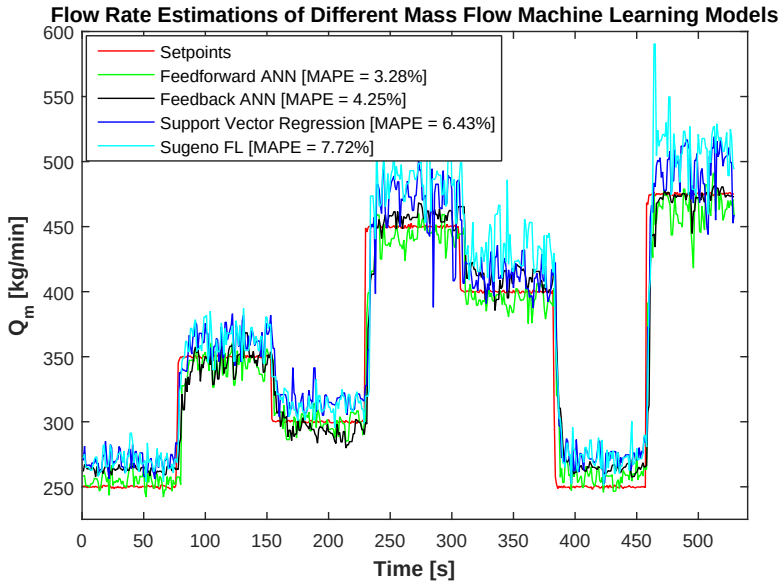

FIGURE 5.4: The comparison of flow rate estimations of different mass flow ML models.

the models developed in this work are validated and tested with several new data sets. Three different ways to avoid over-fitting problems are:

1. Large training data set:
   All the models are trained with a large number of training data.

2. Regularization:
   In feedforward ANN, a learning algorithm that can regularize (minimize) the model parameters to avoid over-fitting is implemented.

3. Proper tuning of hyper-parameter:
   To ensure an appropriate selection of hyper-parameters, a grid-search method with cross-validation is used.

5.4 Performance Evaluation of ML based Flow Models

Due to limitations with the existing open channel flow models as discussed in Chapter 4, different types of ML models are developed in this PhD work.

5.4.1 Mass Flow ML Models

As a start, ML models that can estimate mass flow rates based on the three ultrasonic level measurements as inputs are studied. The mass flow study is presented in several conference papers (Chhantyal et al., 2016c; Chhantyal et al., 2016d; Chhantyal, Viumdal, and Mylvaganam, 2017b) and a detailed study is presented in Paper B.

Figure 5.4 and Table 5.1 shows the comparison of flow estimations using different mass flow ML models. The estimations of these models are accurate for the considered range. But, these models are reliable only for the single fluid that is used in the calibration/training process. Typically to have the same mass flow, a low density fluid requires high volumetric flow and a high density fluid requires low volumetric flow. Hence, a mass flow model based on only level measurements

TABLE 5.1: The comparison of the performance of different mass flow ML models based on Mean Absolute Percentage Error (MAPE).

Mass Flow ML Models	**MAPE** [%]
Feedforward ANN	3.28 %
Feedback ANN	4.25 %
Support Vector Regression	6.43 %
Sugeno typed Fuzzy Logic	7.72 %

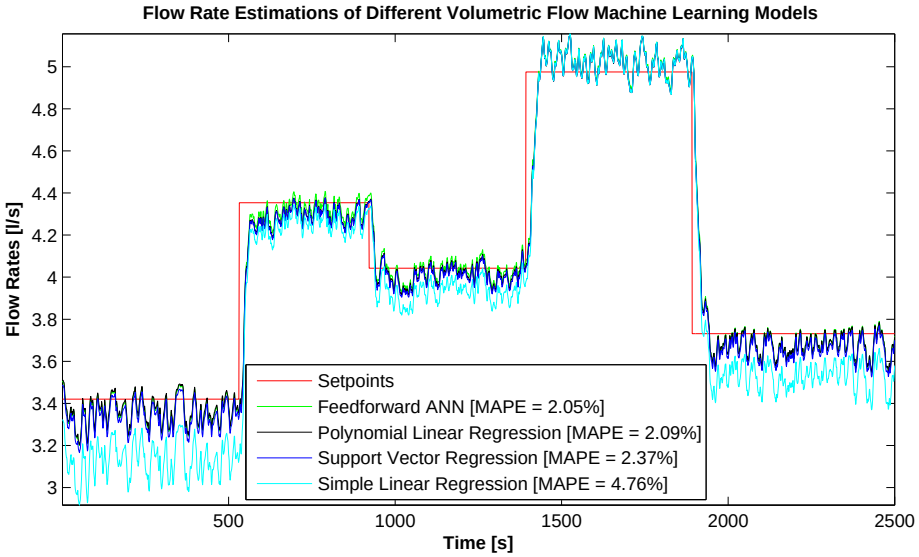

FIGURE 5.5: The comparison of flow rate estimations of different volumetric flow ML models.

are not reliable as the level can be different for a same mass flow rate of different fluids. One possible way to generalize the mass flow models is by introducing density as another input along with three level measurements. Experimental results presented in Paper C show that it is a possible solution. However, density measurement is performed manually in most of today's drilling platforms. This makes the approach not practical in a real-time flow measurement in the current scenario. In the context of non-Newtonian flow of drilling fluid monitoring and control, a patent of (Song and Dykstra, 2017) via the oil & gas company Halliburton deals with real-time monitoring of downhole drilling including general approaches for mud density and viscosity estimations. Specific details are left open in the patent.

5.4.2 Volumetric Flow ML Models

Due to the limitation in generalizing several fluids using the mass flow models, volumetric flow ML models are developed. Volumetric flow models presented in Paper C are based on single upstream level measurement and can generalize different fluids. The experimental data using all the drilling fluids available in the test loop show that the volumetric flow is highly correlated with upstream level. Hence, different linear and non-linear models are developed to correlate volumetric flow and fluid level. For the considered range (i.e., $3 - 7.5$ $[l/s]$), all the volumetric flow models are highly accurate as shown in Figure 5.5 and Table 5.2.

TABLE 5.2: The comparison of the performance of different volumetric flow ML models based on Mean Absolute Percentage Error (MAPE).

Volumetric Flow ML Models	**MAPE** [%]
Feedforward ANN	2.05 %
Polynomial Linear Regression	2.09 %
Support Vector Regression	2.37 %
Simple Linear Regression	4.76 %

To meet the flow range requirement (i.e., $0 - 75\ [l/s]$) given in Section 1.1 for a suitable flow meter, the developed models are extrapolated. For the comparison, the upstream level based flow model with $\alpha = 1.4$ is used as a reference. The extrapolation results show that the flow estimations using polynomial linear regression model and support vector regression model are very close to the reference estimations. Further, the results show that the simple linear regression and artificial neural networks are limited to the calibration data range. Detailed analysis is given in Paper C. For real implementations, all the ML models should be trained with datasets covering the whole range of flow rates.

5.4.3 Recalibration of ML based Flow Models

Volumetric flow ML models are better than mass flow ML models as volumetric models can be trained for different fluids. These models solely depend on the level measurements (i.e., $Q_{ML} = f(h)$) and do not consider the geometry of the channel. Hence, these empirical models need recalibration before using in any other open Venturi channel with different geometries. This is a limitation with ML based flow models. However, the flow models discussed in Chapter 2 consider a geometry (i.e., bottom width (b)) of the channel along with level measurements (i.e., $Q = f(h, b)$).

Chapter 6

Conclusions and Future Recommendations

In this chapter, main conclusions of the thesis and possible future works are discussed.

6.1 Conclusions

This PhD work presents the study of different flow measurement systems for a non-Newtonian fluid through an open channel. The primary focus is on measuring the return flow of drilling fluid to maintain the wellbore stability by using the delta flow method. In the first part of the work, several different types of flow measurements systems are evaluated. A highly accurate Coriolis mass flow meter is tested with the drilling fluid containing a large amount of air bubbles mimicking the entrained gas in real drilling mud. The experimental results show that the Coriolis flow meter readings fluctuate in the presence of excess air bubbles. Three different volumetric flow models for an open channel with a Venturi constriction have reliable flow estimations both in the presence of excess air bubbles or without air bubbles. However, these flow models need a proper tuning of a suitable correction factor for reliable flow estimations. Experimental results show that two models (i.e., upstream-throat levels based and upstream level based) are highly affected by the correction factor tuning. The third flow model (i.e., critical level based) is comparatively less affected by the correction factor but has a limitation of identifying a critical level position for flow estimation. The flow estimations of the critical level based model are improved using proportional (P) like fuzzy logic regulator and by using estimated critical level instead of measured critical level. Further, upstream-throat levels based flow model is used for estimating the fluid flow through an inclined open channel. The experimental results show that the flow estimations are reliable up to 0.4 [deg] angles for the channel geometry used in the study.

In the second part of the work, ML based flow models are developed for flow estimations based on level measurements. The presented mass flow rate based ML models give highly accurate flow estimations. However, these models are only applicable to the fluid used in the training/calibrating process. With a density as an additional input, the existing ML models are capable of estimating flow rates of different fluids used in the training process. Due to a limitation in a real-time density measurement in a drilling platform, this solution is currently not feasible. More generalized ML models based on volumetric flow are developed. These models are only based on the level measurements and are independent of any tuning parameters. Experimental results using these models show that the flow estimations are highly

accurate with an accuracy up to 2.05% and reliable for different fluids. The models are very simple and hence easily implemented in the return flow line of drilling mud.

6.2 Recommendations for Future Work

This PhD work is able to answer many challenging questions regarding non-Newtonian fluid flow measurement system through an open channel. Although the objective of the study is fulfilled, several other challenges and questions arose during the period.

6.2.1 Improving Level Measurements

In this study, the fluid level is measured using the ultrasonic level sensor. Ultrasonic level measurements are affected by the turbulence and the air bubbles present in the flowing fluid. Hence, the level measurements are noisy and unstable for high flow rates and the fluids with an excess of air bubbles. In the study, mechanical filter nets and signal filtering are used to improve the noisy level measurements. As the flow models solely depend on the level measurements, the estimation accuracy is highly correlated with the accurate level measurements. Therefore, the improvement in the level measurement set up can lead to better flow estimations. A preliminary test is carried out using radar sensor for level measurement. The test results show that the radar sensor is more stable and accurate compared to the ultrasonic level measurements. I would suggest replacing ultrasonic level sensors with radar level sensors in the flow loop. There have been some promising results in using Lamb waves with clamp-on excitation of ultrasonic waves for liquid flow metering, (Kippersund, Frøysa, and Lunde, 2012; Aanes et al., 2017; Xsens, 2018; Flexim, 2018). In case of a drilling fluid flow in closed conduits, some of the currently existing sensor modalities along with Lamb waves based ultrasonic flow metering can be used in developing ML based algorithms for estimating the return flow.

6.2.2 Possibility of Density and Viscosity Estimations

The fluid level profile and the location of critical level changes with respect to the change in flow rate, density and viscosity of the fluid. The varying level profile is proportional to the fluid flow and density of the fluid. As the fluid flow can be calculated using the proposed models, density can be estimated using the level and fluid flow information.

The viscosity of the shear thinning fluids decreases with increase in the flow rate. The decrease in the viscosity refers to the decrease in the resistance to flow, and hence the position of critical level shifts towards the end of the throat. The shifts are proportional to the flow rates and can be correlated with the viscosity of the fluid. In addition, a preliminary study on estimating viscosity of non-Newtonian fluids using ML algorithms is carried out in (Chhantyal et al., 2016a). The study was not continued due to lack of real-time rheological parameter measurements in the flow loop.

6.2.3 Study using Channels of Different Geometry

The current results are based on the channel geometry available in the flow loop at USN. The future study must be carried out using channels with different geometries.

The presented models and relationships should be validated with field installations. Tuning these models for different geometries and at site involves a long-term test with experimental planning. As a start, simulation study (for example CFD simulations) for estimating flow using different channel geometries can be performed.

Bibliography

Aanes, Magne et al. (2017). "Time-of-flight dependency on transducer separation distance in a reflective-path guided-wave ultrasonic flow meter at zero flow conditions". In: *The Journal of the Acoustical Society of America* 142.2, pp. 825–837.

Abu-Mostafa, Yaser (2012). *Introductory Machine Learning Online Course*. Caltech, Pasadena, California, USA. URL: http://work.caltech.edu/telecourse.html.

Agu, Cornelius E et al. (2017). "Algorithm with improved accuracy for real-time measurement of flow rate in open channel systems". In: *Flow Measurement and Instrumentation* 57, pp. 20–27. DOI: 10.1016/j.flowmeasinst.2017.08.008.

Ahmed, Mohammed A, Omar A Hegab, and Ahmed Sabry (2016). "Early detection enhancement of the kick and near-balance drilling using mud logging warning sign". In: *Egyptian Journal of Basic and Applied Sciences* 3.1, pp. 85–93. DOI: 10.1016/j.ejbas.2015.09.006.

Alderman, Neil J and Rainer Haldenwang (2007). "A review of Newtonian and non-Newtonian flow in rectangular open channels". In: *Hydrotransport 17 - The 17th International Conference on the Hydraulic Transport of Solids, Symposium series: South African Institute of Mining and Metallurgy* 46, pp. 87–106.

Andrew, Ng (2016). *Machine Learning*. Coursera, Online. URL: https://www.coursera.org/learn/machine-learning.

Anfinsen, BT, Rolv Rommetveit, et al. (1992). "Sensitivity of early kick detection parameters in full-scale gas kick experiments with oil-and water-based drilling muds". In: *SPE/IADC Drilling Conference*. Society of Petroleum Engineers. DOI: 10.2118/23934-MS.

Ayesha, Nayeem, Ramachandran Venkatesan, and Faisal Khan (2014). "Monitoring early kick indicators at the bottom hole for blowout prevention". In: *Oceans-St. John's, 2014*. IEEE, pp. 1–10. DOI: 10.1109/OCEANS.2014.7003206.

— (2016). "Monitoring of down-hole parameters for early kick detection". In: *Journal of Loss Prevention in the Process Industries* 40, pp. 43–54. DOI: 10.1016/j.jlp.2015.11.025.

Bamo, Measure (2009). *Flow rate measurement in open channel: DF 250 A Instructions manual*.

Bengtson, Harlan (2010). *Open Channel Flow Measurement*. URL: https://www.brighthubengineering.com/hydraulics-civil-engineering/51435-introduction-to-the-weir-and-flume/.

Berg, Christian et al. (2015). "Model-based drilling fluid flow rate estimation using Venturi flume". In: *IFAC-PapersOnLine* 48.6, pp. 171–176. DOI: 10.1016/j.ifacol.2015.08.027.

Boiten, Wubbo (2002). "Flow measurement structures". In: *Flow Measurement and Instrumentation* 13.5, pp. 203–207. DOI: 10.1016/S0955-5986(02)00057-2.

Bourgoyne, Adam T et al. (1986). *Applied drilling engineering*. Vol. 2. SPE textbook series. Richardson, TX: Society of Petroleum Engineers. ISBN: 1-55563-001-4.

Burger, Johannes H (2014). "Non-Newtonian open channel flow: the effect of shape". PhD Dissertation. Cape Town, 8000, South Africa: Faculty of Engineering, Cape Peninsula University of Technology.

Burger, Johannes H, Rainer Haldenwang, and Neil J Alderman (2010a). "Experimental database for non-Newtonian flow in four channel shapes". In: *Journal of Hydraulic Research* 48.3, pp. 363–370. DOI: 10.1080/00221686.2010.481849.

— (2010b). "Friction factor-Reynolds number relationship for laminar flow of non-Newtonian fluids in open channels of different cross-sectional shapes". In: *Chemical Engineering Science* 65.11, pp. 3549–3556. DOI: 10.1016/j.ces.2010.02.040.

— (2014). "Laminar and turbulent flow of non-newtonian fluids in open channels for different cross-sectional shapes". In: *Journal of Hydraulic Engineering* 141.4, p. 04014084. DOI: 10.1061/(ASCE)HY.1943-7900.0000968.

Caenn, Ryen, Henry CH Darley, and George R Gray (2011a). *Composition and properties of drilling and completion fluids*. Gulf professional publishing.

— (2011b). *Composition and properties of drilling and completion fluids*. Gulf professional publishing. Chap. 5, pp. 204–212,244–251.

Cayeux, Eric, Benoit Daireaux, et al. (2013). "Precise Gain and Loss Detection Using a Transient Hydraulic Model of the Return Flow to the Pit". In: *SPE/IADC Middle East Drilling Technology Conference & Exhibition*. Society of Petroleum Engineers. DOI: 10.2118/166801-MS.

Chanson, Hubert (2004). *Hydraulics of open channel flow*. Butterworth-Heinemann.

Chhantyal, Khim, Håkon Viumdal, and Saba Mylvaganam (2017a). "Soft Sensing of Non-Newtonian Fluid Flow in Open Venturi Channel Using an Array of Ultrasonic Level SensorsAI Models and Their Validations". In: *Sensors* 17.11, p. 2458. DOI: 10.3390/s17112458.

Chhantyal, Khim, Håkon Viumdal, and Saba Mylvaganam (2017b). "Ultrasonic level scanning for monitoring mass flow of complex fluids in open channels A novel sensor fusion approach using AI techniques". In: *Sensors, 2017 IEEE*. Glasgow, United Kingdom. DOI: 10.1109/ICSENS.2017.8234010.

Chhantyal, Khim et al. (2016a). "Estimating viscosity of non-Newtonian fluids using support vector regression method: Rheological parameters of drilling fluids using data fusion". In: *Sensors Applications Symposium (SAS), 2016 IEEE*. IEEE. DOI: 10.1109/SAS.2016.7479860.

Chhantyal, Khim et al. (2016b). "Flow rate estimation using dynamic Artificial Neural Network with ultrasonic level measurements". In: *The 9th Eurosim congress on modelling and simulation*. Oulu, Finland.

— (2016c). "Flow rate Estimation using Dynamic Artificial Neural Networks with Ultrasonic Level Measurements". In: *The 9th Eurosim congress on modelling and simulation*. Oulu, Finland.

Chhantyal, Khim et al. (2016d). "Ultrasonic level sensors for flowmetering of non-Newtonian fluids in open Venturi channels: Using data fusion based on Artificial Neural Network and Support Vector Machines". In: *Sensors Applications Symposium (SAS), 2016 IEEE*. IEEE, pp. 1–6. DOI: 10.1109/SAS.2016.7479829.

Chhantyal, Khim et al. (2018). "Ultrasonic Level Based Soft Sensing of Volumetric Flow of Non-Newtonian Fluids in Open Venturi Channels". In: *IEEE Sensors Journal* 18.12, pp. 5002–5013. DOI: 10.1109/JSEN.2018.2831445.

Codazzi, Daniel et al. (1992). "Rapid and reliable gas influx detection". In: *SPE/IADC Drilling Conference*. Society of Petroleum Engineers. DOI: 10.2118/23936-MS.

Coussot, Philippe (1994). "Steady, laminar, flow of concentrated mud suspensions in open channel". In: *Journal of Hydraulic Research* 32.4, pp. 535–559. DOI: 10.1080/00221689509498581.

Emerson (2014). *Rosemount Ultrasonic 3107 Level and 3108 Flow Transmitters*. URL: http://www.emerson.com/en-us/automation-solutions.

Endress+Hauser (2013). *Coriolis Mass Flow Measurement System Promass 63*. URL: https://www.endress.com/en/Field-instruments-overview/63F.

Evans, Russell N (2007). *Eccentric Venturi flow meter*. US Patent 7,299,707.

Flexim (2018). *Ultrasonic Flow Meter*. URL: https://www.flexim.com/en.

Ganji, Ahmed Reza and Anthony J Wheeler (2010). *Introduction to engineering experimentation, third edition, Chapter 10, 346-348*. Pearson Education, Upper Saddle River, New Jersey, 07458.

Glittum, Stian et al. (2015). *Expansion of test facility for flow measurement on drilling fluid*. Bachelor Thesis, University College of Southeast Norway.

Grayson, Brian, Anton Hubertus Gans, et al. (2012). "Closed loop circulating systems enhance well control and efficiency with precise wellbore monitoring and management capabilities". In: *SPE/IADC Managed Pressure Drilling and Underbalanced Operations Conference and Exhibition*. Society of Petroleum Engineers. DOI: 10.2118/156893-MS.

Haeusler, Detlef, Friedhelm Makohl, TWR Harris, et al. (1995). "Applications and field experience of an advanced delta flow kick detection system". In: *SPE/IADC Drilling Conference*. Society of Petroleum Engineers. DOI: 10.2118/29344-MS.

Haldenwang, Rainer (2003). "Flow of non-Newtonian fluids in open channels". PhD Dissertation. Cape Town, 8000, South Africa: Department of Civil Engineering, Cape Technikon.

Hargreaves, David, Stuart Jardine, Ben Jeffryes, et al. (2001). "Early kick detection for deepwater drilling: New probabilistic methods applied in the field". In: *SPE Annual Technical Conference and Exhibition*. Society of Petroleum Engineers. DOI: 10.2118/71369-MS.

Hauge, Stein and Knut Øien (2012). "Deepwater horizon: Lessons learned for the norwegian petroleum industry with focus on technical aspects". In: *Chemical Engineering* 26. DOI: 10.3303/CET1226104.

Herschel, Clemens (1888). *Apparatus for measuring the quantity of water flowing through a pipe*. US Patent 381,373.

Hutchinson, Mark, Iain Rezmer-Cooper, et al. (1998). "Using downhole annular pressure measurements to anticipate drilling problems". In: *SPE Annual Technical Conference and Exhibition*. Society of Petroleum Engineers. DOI: 10.2118/49114-MS.

ISO-4359 (2013). *Flow Measurement Structures Rectangular, Trapezoidal and U-shaped Flumes*.

Jack (2018). *Drilling rig circulating system*. URL: http://www.oilngasdrilling.com/drilling-rig-circulating-system.html.

Johnsen, HK et al. (1988). "Development and Field Testing of a High-Accuracy Full-Bore Return Flow Meter". In: *SPE/IADC Drilling Conference*. Society of Petroleum Engineers. DOI: 10.2118/17228-MS.

Johnson, Austin et al. (2014). "Advancing deepwater kick detection". In: *IADC/SPE Drilling Conference and Exhibition*. Society of Petroleum Engineers. DOI: 10.2118/167990-MS.

Kamyab, Mohammadreza et al. (2010). "Early kick detection using real time data analysis with dynamic neural network: a case study in Iranian oil fields". In: *Nigeria Annual International Conference and Exhibition*. Society of Petroleum Engineers. DOI: 10.2118/136995-MS.

Keltrol (2007). *Xanthan gum, eight edition*. USA: CP Kelco, a Hurber Company.

Kippersund, Remi Andre, Kjell Eivind Frøysa, and Per Lunde (2012). *Flow measuring apparatus*. US Patent 8,141,434.

Kozicki, William and Carlos Tiu (1967). "Non-newtonian flow through open channels". In: *The Canadian journal of chemical engineering* 45.3, pp. 127–134. DOI: 10.1002/cjce.5450450302.

Lloyd, GM et al. (1990). "Practical Application of Real-Time Expert System for Automatic Well Control". In: *SPE/IADC Drilling Conference*. Society of Petroleum Engineers. DOI: 10.2118/19919-MS.

Loeppke, Glenn E et al. (1992). *Development and evaluation of a meter for measuring return line fluid flow rates during drilling*. Tech. rep. Sandia National Labs., Albuquerque, NM (United States). DOI: 10.2172/5036200.

Logsdon, Jason (2013). *How to use xanthan gum*. URL: http://www.amazingfoodmadeeasy.com/info/modernist-ingredients/more/xanthan-gum.

Malagalage, Anjana et al. (2013). *Simulatioin of Open Channel Flow for Mass Flow Measurement*. Master Project, University College of Southeast Norway. URL: https://bibsys-almaprimo.hosted.exlibrisgroup.com:443/HIT:default_scope:BIBSYS_ILS71535399070002201.

Mills, Ian et al. (2012). "Simulator and the first field test results of an automated early kick detection system that uses standpipe pressure and annular discharge pressure". In: *SPE/IADC Managed Pressure Drilling and Underbalanced Operations Conference and Exhibition*. Society of Petroleum Engineers. DOI: 10.2118/156902-MS.

Nas, Steve (2011). "Kick detection and well control in a closed wellbore". In: *The APPEA Journal* 51.1, pp. 109–118. DOI: 10.1071/AJ10006.

Orban, J J and K J Zanker (1988). "Accurate flow-out measurements for kick detection, actual response to controlled gas influxes". In: *SPE/IADC Drilling Conference, 28 February-2 March, Dallas, Texas*. Society of Petroleum Engineers. DOI: 10.2118/17229-MS.

Orban, J J, K J Zanner, and A E Orban (1987). "New flowmeters for kick and loss detection during drilling". In: *SPE Annual Technical Conference and Exhibition, 27-30 September, Dallas, Texas*. Society of Petroleum Engineers. DOI: 10.2118/16665-MS.

Orban, Jacques JH, Klaus J Zanker, and Andre E Orban (1988). *Method and apparatus for measurement of fluid flow in a drilling rig return line*. US Patent 4,754,641.

Patel, Bhavin, Todd Cooper, Will Billings, et al. (2013). "The application of advanced gas extraction and analysis system complements early kick detection & control capabilities of managed pressure drilling system with added HSE value". In: *SPE/IADC Drilling Conference*. Society of Petroleum Engineers. DOI: 10.2118/163498-MS.

Reitsma, Don et al. (2010). "A simplified and highly effective method to identify influx and losses during Managed Pressure Drilling without the use of a Coriolis flow meter." In: *SPE/IADC Managed Pressure Drilling and Underbalanced Operations Conference and Exhibition*. Society of Petroleum Engineers. DOI: 10.2118/130312-MS.

— (2011). "Development of an automated system for the rapid detection of drilling anomalies using standpipe and discharge pressure". In: *SPE/IADC Drilling Conference and Exhibition*. Society of Petroleum Engineers. DOI: 10.2118/140255-MS.

Schafer, D M et al. (1991). "An evaluation of flowmeters for the detection of kicks and lost circulation during drilling". In: *SPE/IADC Drilling Conference, 18-21 February, New Orleans, Louisiana*. DOI: 10.2118/23935-MS.

Song, Xingyong and Jason D Dykstra (2017). *Real-Time Downhole Drilling Mud Viscosity And Density Estimations*. US Patent App. 15/323,836.

Speers, J M and G F Gehrig (1987). "Delta flow: An accurate, reliable system for detecting kicks and loss of circulation during drilling". In: *SPE Drilling Engineering* 2.04, pp. 359–363. DOI: 10.2118/13496-PA.

Stokka, S I et al. (1993). "Gas kick warner-an early gas influx detection method". In: *SPE/IADC Drilling Conference*. Society of Petroleum Engineers. DOI: 10.2118/25713-MS.

Thapa, Jeevan et al. (2017). *Evaluation of radar based level measurements and the use of critical depth for flow estimation of drilling fluid*. Master Project, University College of Southeast Norway.

Tompkins, E (1974). *Capillary flow meter*. US Patent 3,838,598.

USYD (2005). *Integral Approach to the Control Volume analysis of Fluid Flow, Kinetic Energy Correction Factor*. URL: http://www-mdp.eng.cam.ac.uk/web/library/enginfo/aerothermal_dvd_only/aero/fprops/cvanalysis/node41.html.

Xsens (2018). *Flow Solutions*. URL: http://xsens.no/.

Yeung, Hoi (2007). "An examination of BS3680 4C (ISO/DIS 4369) on the measurement of liquid flow in open channels flumes". In: *Flow measurement and Instrumentation* 18.3, pp. 175–182. DOI: 10.1016/j.flowmeasinst.2007.01.002.

Part II

Scientific Articles

List of Publications

1. Khim Chhantyal, Håkon Viumdal, Saba Mylvaganam, and Geir Elseth (2016). "Ultrasonic level sensors for flowmetering of non-Newtonian fluids in open Venturi channels: Using data fusion based on Artificial Neural Network and Support Vector Machines". In: Sensors Applications Symposium (SAS), 2016 IEEE, Catania, Italy. DOI: 10.1109/SAS.2016.7479829.

   Short Overview

   Two mass flow based machine learning models (i.e., ANN and SVR models) are compared with the one-dimensional Saint-Venant equations. The comparison study shows that both ML models performs better than the mechanistic model in terms of accuracy and response time. The accuracy of the mechanistic model is acceptable with a response time of 3 seconds per sample.

2. Khim Chhantyal, Håkon Viumdal, Saba Mylvaganam, and Geir Elseth (2016). "Estimating viscosity of non-Newtonian fluids using support vector regression method: Rheological parameters of drilling fluids using data fusion". In: Sensors Applications Symposium (SAS), 2016 IEEE, Catania, Italy. DOI: 10.1109/SAS.2016.7479860.

   Short Overview

   A preliminary study on estimating viscosity of non-Newtonian fluids in a pipe flow using support vector regression method is presented. Laboratory rheometers are used to measure density, shear stress, shear rate and viscosity data of different test samples. These data are used to develop a SVR model using density and shear stress as inputs and viscosity as output. In the flow loop, density is measured using the Coriolis mass flow meter and shear stress is calculated using the differential pressure drop.

3. Khim Chhantyal, Håkon Viumdal, Saba Mylvaganam, and Minh Hoang (2016). "Flow rate Estimation using Dynamic Artificial Neural Networks with Ultrasonic Level Measurements". In: 2016 9th EUROSIM Congress on Modelling and Simulation, 2016, Oulu, Finland.

   Short Overview

   The drilling operation is a continuous process. The returning drilling fluid flow depends on the previous flow conditions. In this study, dynamic artificial neural networks (DANN) are used with previous input and output data along with a new inputs to estimate the current flow. Further, three different types of learning algorithms are tested with DANN.

4. Khim Chhantyal, Håkon Viumdal, and Saba Mylvaganam, (2017). "Online Drilling Fluid Flowmetering in Open Channels with Ultrasonic Level Sensors using Critical Depths". In: Linköping Electronic Conference Proceedings, 385-390, SIMS 2017, Reykjavik, Iceland. DOI: 10.3384/ecp17138385.

   Short Overview

A study on critical level based flow model is presented. Full paper is attached as Paper A.

5. Khim Chhantyal, Håkon Viumdal, and Saba Mylvaganam, (2017). "Ultrasonic level scanning for monitoring mass flow of complex fluids in open channels A novel sensor fusion approach using AI techniques". In: Sensors, 2017 IEEE, Glasgow, United Kingdom. DOI: 10.1109/ICSENS.2017.8234010.

   Short Overview

   The ML mass flow model based radial basis neural network (RBNN) is developed to estimate drilling fluid flow rate.

6. Khim Chhantyal, Håkon Viumdal, and Saba Mylvaganam, (2017). "Soft Sensing of Non-Newtonian Fluid Flow in Open Venturi Channel Using an Array of Ultrasonic Level SensorsAI Models and Their Validations". In: Sensors, 17 (11), 2458. DOI: 10.3390/s17112458.

   Short Overview

   Different mass flow ML flow models are presented. Full paper is attached as Paper B.

7. Khim Chhantyal, Morten Hansen Jondahl, Håkon Viumdal, and Saba Mylvaganam, (2018). "Upstream Ultrasonic Level Based Soft Sensing of Volumetric Flow of non-Newtonian Fluids in Open Venturi Channels". In: IEEE Sensors Journal, 18 (12), pp. 5002-5013. DOI: 10.1109/JSEN.2018.2831445.

   Short Overview

   Different volumetric flow ML flow models are presented. Full paper is attached as Paper C.

Paper A

Online Drilling Fluid Flowmetering in Open Channels with Ultrasonic Level Sensors using Critical Depths

Published in Linköping Electronic Conference Proceedings, The 58th International Conference of Scaninavian Simulation Society, SIMS 2017, pp. 385-390, 2017, doi:10.3384/ecp17138385.
Authors: Khim Chhantyal, Håkon Viumdal, and Saba Mylvaganam.

Online Drilling Fluid Flowmetering in Open Channels with Ultrasonic Level Sensors using Critical Depths

Khim Chhantyal Håkon Viumdal Saba Mylvaganam

Faculty of Technology, Natural Sciences, and Maritime Sciences, University College of Southeast Norway,
{khim.chhantyal,hakon.viumdal,saba.mylvaganam}@usn.no

Abstract

In drilling operations, non-Newtonian drilling fluid is continuously circulated in a closed loop. One of the ways to monitor and regulate drilling operations is by accurately measuring the flow rate of circulating drilling fluid before entering and after returning from the wellbore. The circulating fluid flows in an open channel on the return path from the wellbore. This work investigates the use of Venturi constriction to estimate the non-Newtonian fluid flow in an open channel. Based on the specific energy principle, a relation between volumetric flow rate and critical depth is developed, which is used to estimate the flow rate based on the measured critical depth. To measure a critical depth for a given flow rate, it is necessary to locate a critical depth position in the Venturi flume. In this study, the critical depth position is located using specific energy diagram (at a minimum specific energy within the Venturi constriction) and Froude Number approach (at a Froude Number equals to 1). Based on the identified critical depth, the flow conditions (subcritical, critical or supercritical) along the Venturi flume are observed. The location of the critical depth in the Venturi section is found by performing experiments at 350 [*kg/min*] flow rate of the fluid. Further, the developed critical depth flow model is tested for randomly varying flow rates (250-500 [*kg/min*]) with the identified critical depth location. The flow estimations of the model were within the acceptable limit. However, it is found that the estimates for 350 [*kg/min*] are comparatively more accurate, which proves that the critical depth and critical depth position depends on the flow rate and rheological properties.

Keywords: open channel Venturi flume, non-Newtonian flow, critical depth, ultrasonic scanning of open channel flow

1 Introduction

Open channel flow is a flow of fluid in conduct with a free surface. Examples of open channel flow are rivers, irrigation ditches, canals, storm and sanitary sewer systems, industrial waste applications, sewage treatment plants, transportation of non-Newtonian slurries, etc. In this work, a non-Newtonian drilling fluid flow in the open channel is studied.

The drilling fluids used in the oil & gas industries are non-Newtonian, which helps:

- to keep the bottom-hole pressure within a pressure window of acceptable margins to prevent kicks and their losses into down-hole environment,
- to lubricate the drill bit, and
- to remove swiftly the cuttings and debris from down-hole due to their high viscous nature.

In drilling operations, the drilling fluid is continuously pumped down to wellbore through the drill pipe and is circulated through the annulus back to the surface where the flow is conducted in an open channel.(Caenn et al., 2011)

One way of maintaining the stability of bottom-hole pressure is by monitoring and regulating the drilling fluid flow rate. An early indication of wellbore instability can be detected using delta flow method, which is based on the difference between inflow and outflow measurements of drilling fluid while circulating the fluid, (Maus et al., 1979; Speers and Gehrig, 1987; Orban et al., 1987; Orban and Zanker, 1988; Schafer et al., 1992; Lloyd et al., 1990). Therefore, it is important to measure inflow and outflow of drilling fluid accurately. It is convenient to measure inflow accurately, as drilling fluids flowing in have known rheological properties with negligible impurities. In literature (Orban et al., 1987; Orban and Zanker, 1988; Schafer et al., 1992), flow meters like conventional pump stroke counter, rotatory pump speed counter, magnetic flow meter, ultrasonic Doppler flow meter, and Coriolis mass flow meter can be used to measure the inflow. However, it is difficult to accurately measure the outflow as the returning fluid contains rock cuttings, formation gases, and formation liquids. In literature (Orban et al., 1987; Orban and Zanker, 1988; Schafer et al., 1992), flow meters like standard paddle meter, ultrasonic level meter, a prototype rolling float meter, magnetic flow meter, and Venturi flow meter can be used to measure the outflow. In recent years, Rainer Haldenwang and his research group has performed several open channel flow studies in different cross-sectional shapes, (Burger et al., 2010, 2014; Kabwe et al., 2017). Our study focuses on the use of Venturi flow meter in an open channel for drilling fluid flow measurement.

2 System Description

A flow loop is available at University College of Southeast Norway (USN), Porsgrunn Campus for the study of drilling fluid flow through an open channel Venturi flume. The flow loop consist of a trapezoidal cross-sectional open channel with Venturi constriction as shown in Figure 1 and Figure 2. The flume can be inclined upto 2 degrees angle to the horizontal. There are three adjustable ultrasonic level sensors above the flume for flow depth measurements at different section of the flume. Different model-drilling fluids are available for testing purposes. For this study, a water-based non-Newtonian shear thinning fluid with a density of 1153 kg/m^3 and viscosity of approximately 23 - 100 cP for corresponding shear rates of 500 - 1 s^{-1} is used. A centrifugal pump is used to circulate model-drilling fluids in the flow loop through the open channel.

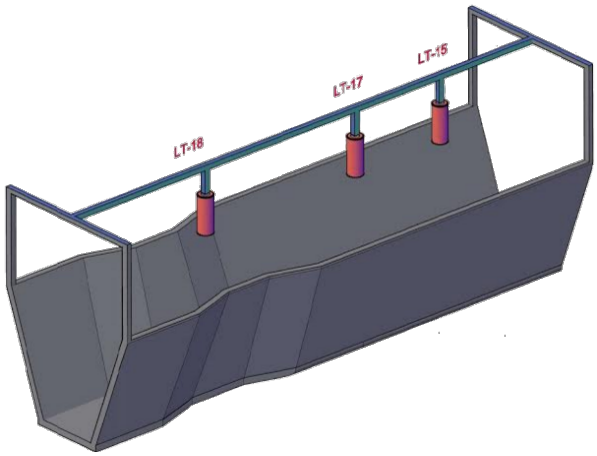

Figure 1. An open channel with Venturi constriction and three ultrasonic level sensors (LT-15, LT-17, and LT-18). (Chhantyal et al., 2016)

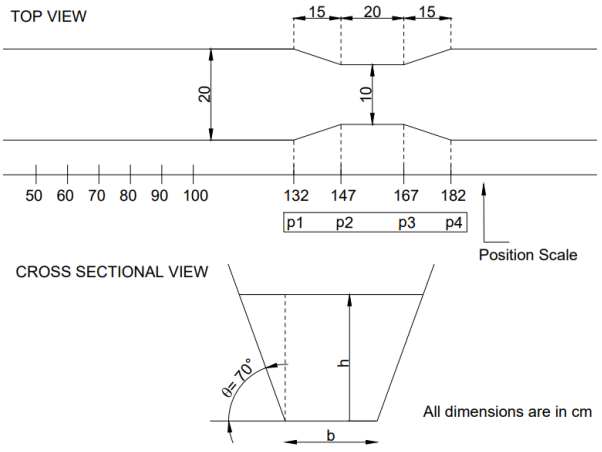

Figure 2. Top and cross sectional view of open channel Venturi flume with the position scale in centimetres. The Venturi constriction is shown in three sections with positions p1-p2 as converging section, positions p2-p3 as throat section, and p3-p4 as diverging section.

3 Methods

For a steady and incompressible fluid flow, the total energy remains constant along the horizontal flow conduct. The Bernoulli flow principle gives the energy equation of the flow as,

$$P+\rho gz+\frac{\rho v^2}{2}=constant \tag{1}$$

where P is applied pressure, ρ is fluid density, g is acceleration due to gravity, z is elevation, and v is average fluid velocity.

Dividing Equation 1 by specific weight ($\gamma=\rho g$) gives specific energy equation as in Equation 2.

$$E_s=h+z+\frac{v^2}{2g} \tag{2}$$

where h is fluid depth.

If the bottom surface of the conduct is considered as the datum, we can use $z=0$ and Equation 2 becomes,

$$E_s=h+\frac{v^2}{2g} \tag{3}$$

where E_s is the specific energy of fluid and is dependent on fluid depth and velocity of the fluid.

In open channel flow, the surface or profile of fluid flow is studied using Hydraulic Grade Line (HGL) and Energy Grade Line (EGL), which are defined by Equation 4 and Equation 5 respectively.

$$HGL=h \tag{4}$$

$$EGL=h+\frac{v^2}{2g} \tag{5}$$

Further using $Q=v\cdot A$, Equation 3 can be rewritten as,

$$E_s=h+\frac{(Q/A)^2}{2g} \tag{6}$$

where Q is volumetric flow rate, and A is the cross-sectional area. For a trapezoidal channel, the cross-sectional area is $A=h(b+hcot\theta)$ where b is the bottom width of the channel and θ is the slope angle of the channel walls shown in Figure 2. Hence, the Equation 6 becomes,

$$E_s=h+\frac{Q^2}{2gh^2(b+hcot\theta)^2} \tag{7}$$

Using Equation 7, a specific energy diagram showing the relation between specific energy (E_s) vs. flow depth (h) can be developed for a given flow rate. From the specific energy diagram, different flow conditions (subcritical, critical, or supercritical) can be identified. For every value of given flow rate, there is a corresponding associated critical depth, h_c. Flow with a depth greater than the critical depth is a subcritical flow and flow with a

depth less than the critical depth is a supercritical flow. In subcritical flow, the potential energy component is large and in supercritical flow, the kinetic energy component is large. Whereas, the critical depth is a position having the minimum specific energy for the given flow rate in the specific energy diagram. Hence, the critical depth can be identified by equating the first derivative of Equation 7 to zero.

$$\frac{dE_s}{dh} = 0, \; for \; h = h_c \tag{8}$$

Using Equation 7 and Equation 8 with several mathematical simplifications, the flow rate and the critical depth relation can be obtained as in Equation 9,

$$Q = \left[\frac{g h_c^3 (b + h_c cot\theta)^3}{b + 2h_c cot\theta} \right]^{1/2} \tag{9}$$

In addition, Froude Number can be used to identify the critical depth. The dimensionless Froude Number for shallow fluid flow is given as the ratio of flow inertia to the wave velocity as in Equation 10,

$$Fr = \frac{v}{\sqrt{g(A/B)}} \tag{10}$$

where Fr is Froude Number and B is the free surface width. For Fr<1 flow is subcritical flow, Fr>1 flow is supercritical flow, and for $Fr \approx 1$ flow is critical flow.

For detail study on open channel flow energy principles, refer to (Featherstone and Nalluri, 1982; Chaudhry, 2007).

4 Results

To study the flow profile and identify the critical depth, the model-drilling fluid is circulated at five different flow rates (Q = 275, 300, 350, 400, 450 [*kg/min*]) in 12 different experimental set-ups. In each experimental set-up, the three ultrasonic level measurements are uniquely positioned along the Venturi-flume. As a result, 36 different flow depths are logged for each flow rate. These flow depths are used to locate critical depth along the Venturi constriction. Finally, the randomly varying flow rates are estimated using the critical depth.

4.1 Flow Profile Study

To study the flow profile, 36 different flow depths at the flow rate of 350 [*kg/min*] are fitted using an Artificial Neural Network (ANN) based polynomial. Thus obtained ANN based polynomial model for flow depth along the Venturi flume is further used to plot Hydraulic Grade Line (HGL) and Energy Grade Line (EGL) as shown in Figure 3. The HGL shows the steady upstream depth and is gradually reducing as the fluid flows through the constriction. EGL represents the total energy head available for the fluid at given flow rate. Within the constriction, EGL has a convex shape with a minimum specific energy, which represents the critical depth.

4.2 Specific Energy Diagram

Figure 4a shows a specific energy diagram within the Venturi constriction for the flow rate of 350 [*kg/min*]. Locating the minimum specific energy in the specific energy diagram, critical fluid depth is identified for the given flow rate. Any flow with flow depth greater than identified critical depth is subcritical flow and flow with a depth less than the critical depth is supercritical flow as shown in Figure 4a.

To identify the position of critical depth along the Venturi throat section, specific energy vs. position is plotted as shown in Figure 4b. The minimum specific energy is obtained around 156 [*cm*] position, which lies within the throat section of the Venturi constriction.

4.3 Froude Number Study

Froude Number is used to identify different flow conditions and the position of critical depth as shown in Figure 5. The flow is subcritical with Fr<1, critical with Fr=1, and supercritical with Fr>1 as indicated in Figure 5. Tracking the corresponding position for Fr=1, the critical depth is around 156 [*cm*] position in the throat section of the Venturi constriction.

4.4 Critical Depth Flow Model

The volumetric fluid flow can be estimated based on the critical depth using the Equation 9. In the context of this study, the flow rate is randomly varied and the critical depth is measured at 156 [*cm*] position using an ultrasonic level sensor. Figure 6 shows the comparison of estimates of critical depth flow model against the randomly varying mass flow rate setpoints. The original ultrasonic level measurements are very noisy. So, the moving average filter with last 10 samples is used to filter the noise to some extent. Both of the flow estimates with and without filtering are presented in Figure 6. The filtered estimates seem to be less noisy compared to the unfiltered estimates. However, the Mean Absolute Percentage Error (MAPE) is slightly better for unfiltered estimates.

In Figure 6, it can be seen that the estimates are comparatively much accurate for the flow rate of 350 [*kg/min*]. It is because the position of critical depth measurement is chosen based on the critical depth position of 350 [*kg/min*] flow rate. The critical depth and position of critical depth are dependent on the flow rate and rheological properties of the fluid.

Figure 7a shows the specific energy diagram of fluid flow along the Venturi constriction at different flow rates. It can be observed that with the increase in fluid flow rate, the specific energy and critical depth of the fluid increases. The primary reason for this is the increases in fluid volume. The possible secondary reason is the reduction in the viscosity of the fluid as flow rate increases for the shear thinning model-drilling fluid.

Figure 7b shows the specific energy vs. position plot in the throat section of Venturi constriction. It can be observed that the minimum specific energy point is

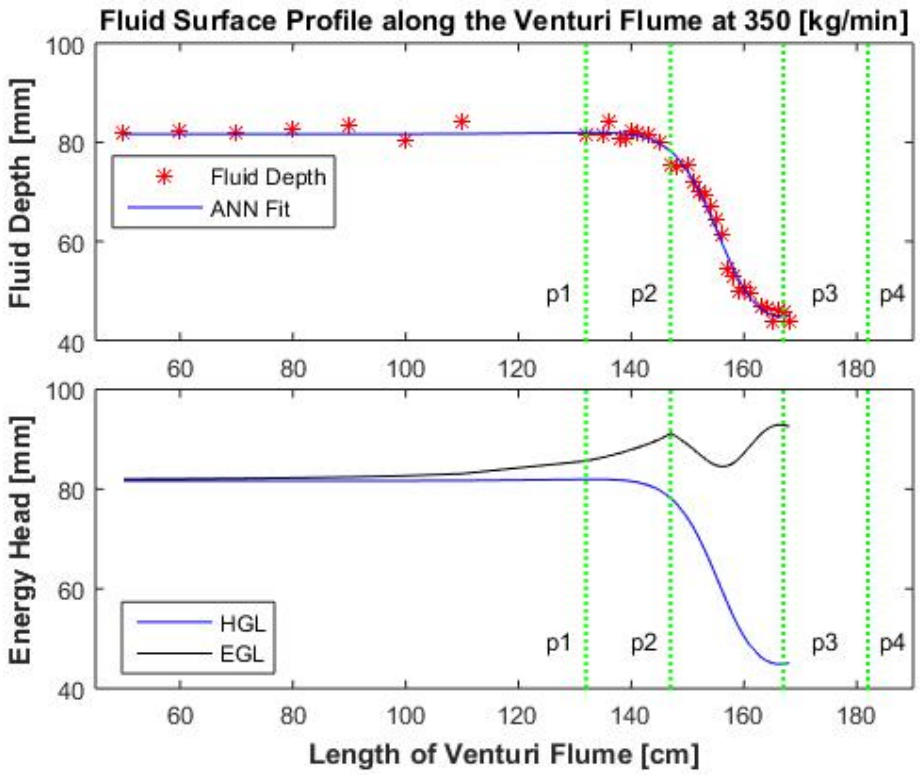

Figure 3. a) Experimental ultrasonic flow depth measurements with an Artificial Neural Network based polynomial fit. b) The Hydraulic Grade Line and Engery Grade Line along the Venturi flume at the flow rate of 350 [*kg/min*]. The green dotted lines indicate the different sections of Venturi constriction according to Figure 2.

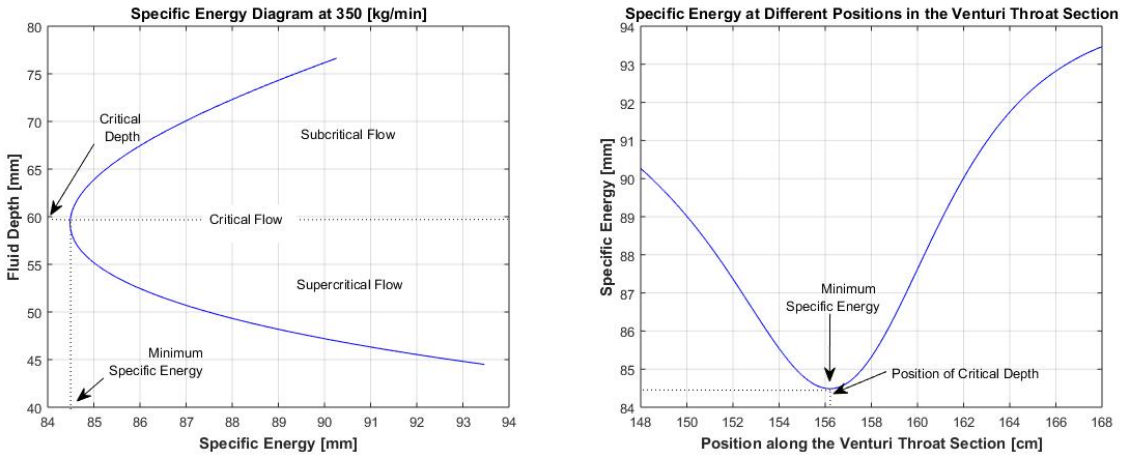

Figure 4. a) Specific energy diagram at the flow rate of 350 [*kg/min*] showing critical depth (at minimum specific energy point) and different flow conditions. b) Specific energy vs. position diagram showing the exact critical depth position in the Venturi constriction.

slightly shifting towards the end of the throat as the flow rate increases, giving different critical depth position for different flow rates. It is due to the momentum of the fluid flowing through the Venturi constriction. The higher flow rate fluid will flow faster within the fixed cross-section of Venturi flume, providing extra momentum as the flow rate increases.

5 Conclusion

In this work, one of the applications of open channel flow in the field of drilling operations is investigated. In drilling operations, non-Newtonian fluid is circulated in a closed loop from the mud tank, into the bottom-hole and back to the mud tank. The return flow is an open channel flow

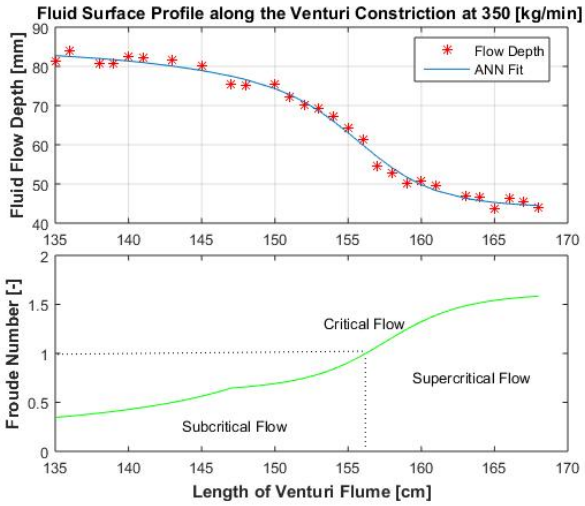

Figure 5. a) Experimental ultrasonic flow depth measurements with an Artificial Neural Network based polynomial fit. b) Froude number along the Venturi constriction showing critical depth position and different flow conditions at the flow rate of 350 [*kg/min*].

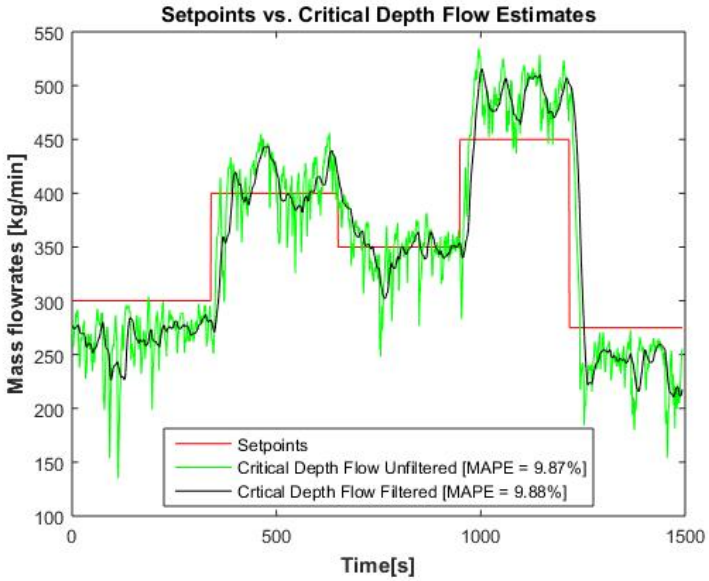

Figure 6. The comparison of estimated flow rates using critical depth (with or without filter) against the randomly varying setpoints based on Mean Absolute Percentage Error (MAPE).

and there is a need for accurate return flow for safe and efficient drilling operations. The study investigates the use of Venturi constriction in the return flow to estimate the flow rates based on the critical depth measurements using the test flow loop available at USN.

For the measurement of critical depths, specific energy diagram and Froude Number approaches are used to locate the critical depth position along the Venturi constriction. Using specific energy diagram, critical depth and critical depth position for a given flow rate are identified at the location of minimum specific energy. Using Froude Number, critical depth position is identified for the *Fr* value equal to 1. In both approaches, different flow conditions: subcritical flow, critical flow, and supercritical flow along the Venturi flume are observed with respect to the critical depth. Further, a critical depth flow model is derived from specific energy equation, which can estimate flow rate for measured critical depth.

The detailed study is performed for 350 [*kg/min*] flow rate with the critical depth at 156 [*cm*] position in the throat section of Venturi constriction. For randomly varying flow rates, the estimates of critical depth flow model with critical depth position at 156 [*cm*] are compared with the setpoints. The comparison result shows that the estimates are within the acceptable limits. However, the estimates are more accurate for 350 [*kg/min*] flow as the critical depth position for 350 [*kg/min*] is chosen for critical depth measurement.

To investigate the effect of flow rates on critical depth, specific diagram for different flow rates are studied.

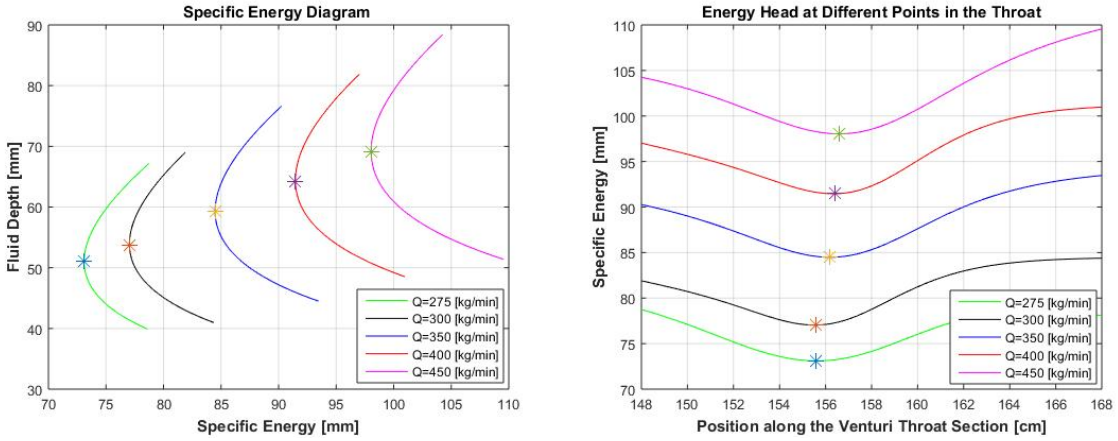

Figure 7. a) Specific energy diagram at different flow rates. b) Specific energy vs. position diagram at different flow rates. The asterisk signs with different colors indicate the point of minimum specific energy at different flow rates.

The study shows that as the flow rate increases the specific energy increases, critical depth increases, and the critical depth position shifts towards the end of the throat section. The changes are due to the increase in fluid flow momentum and change in rheological properties.

We foresee the future efforts in comparing and investigating specific energy diagrams of different model-drilling fluids at different flow rates to analyse the relation between critical depth and rheological properties.

Acknowledgement

The Ministry of Education and Research of the Norwegian Government is funding Khim Chhantyal's Ph.D. studies at USN. We acknowledge the collaboration with and support from STATOIL for providing open channel Venturi rig dedicated for flow studies of different Newtonian and non-Newtonian fluids.

References

JH Burger, R Haldenwang, and NJ Alderman. Laminar and turbulent flow of non-newtonian fluids in open channels for different cross-sectional shapes. *Journal of Hydraulic Engineering*, 141(4):04014084, 2014.

Johan Burger, Rainer Haldenwang, and Neil Alderman. Laminar non-newtonian open channel flow: investigating velocity, wall shear stress and fluid depth. BHR Group, 2010.

Ryen Caenn, Henry CH Darley, and George R Gray. Composition and properties of drilling and completion fluids. chapter 1, pages 7–16. Gulf professional publishing,Waltham, USA, 2011.

M Hanif Chaudhry. *Open-channel flow*. Springer Science & Business Media, 2007.

Khim Chhantyal, Håkon Viumdal, Saba Mylvaganam, and Minh Hoang. Flow rate estimation using dynamic artificial neural network with ultrasonic level measurements. In *The 9th Eurosim congress on modelling and simulation, Oulu, Finland*. Eurosim, 2016.

RE Featherstone and Chandra Nalluri. Civil engineering hydraulics: essential theory with worked examples. chapter 8, pages 185–248. Collins, 1982.

Christine Kabwe, Rainer Haldenwang, Veruscha Fester, and Raj Chhabra. Transitional flow of non-newtonian fluids in open channels of different cross-sectional shapes. *Journal of the Brazilian Society of Mechanical Sciences and Engineering*, pages 1–19, 2017.

GM Lloyd, DJ Bode, HV Nickens, SG Varnado, et al. Practical application of real-time expert system for automatic well control. In *SPE/IADC Drilling Conference*. Society of Petroleum Engineers, 1990.

LD Maus, JD Tannich, and WT Ilfrey. Instrumentation requirements for kick detection in deep water. *Journal of Petroleum Technology*, 31(08):1–029, 1979. doi:doi.org/10.2118/7238-PA.

JJ Orban and KJ Zanker. Accurate flow-out measurements for kick detection, actual response to controlled gas influxes. In *SPE/IADC Drilling Conference*. Society of Petroleum Engineers, 1988. doi:10.2118/17229-MS.

JJ Orban, KJ Zanner, and AE Orban. New flowmeters for kick and loss detection during drilling. In *SPE Annual Technical Conference and Exhibition*. Society of Petroleum Engineers, 1987. doi:10.2118/16665-MS.

DM Schafer, GE Loeppke, DA Glowka, DD Scott, and EK Wright. An evaluation of flowmeters for the detection of kicks and lost circulation during drilling. In *SPE/IADC Drilling Conference*. Society of Petroleum Engineers, 1992. doi:10.2118/23935-MS.

JM Speers and GF Gehrig. Delta flow: An accurate, reliable system for detecting kicks and loss of circulation during drilling. *SPE Drilling Engineering*, 2(04):359–363, 1987. doi:10.2118/13496-PA.

Paper B

Soft Sensing of Non-Newtonian Fluid Flow in Open Venturi Channel Using an Array of Ultrasonic Level Sensors - AI Models and Their Validations

Published in Sensors Journal, Volume 17, Number 1, pp. 2458, 2017, doi:10.3390/s17112458.
Authors: Khim Chhantyal, Håkon Viumdal, and Saba Mylvaganam.

sensors

MDPI

Article

Soft Sensing of Non-Newtonian Fluid Flow in Open Venturi Channel Using an Array of Ultrasonic Level Sensors—AI Models and Their Validations

Khim Chhantyal *, Håkon Viumdal † and Saba Mylvaganam †

Faculty of Technology, Natural Sciences, and Maritime Sciences, University College of Southeast Norway, Kjølnes Ring 56, 3918 Porsgrunn, Norway; hakon.viumdal@usn.no (H.V.); saba.mylvaganam@usn.no (S.M.)

* Correspondence: khim.chhantyal@usn.no; Tel.: +47-9395-0662

† These authors contributed equally to this work.

Received: 27 September 2017; Accepted: 23 October 2017; Published: 26 October 2017

Abstract: In oil and gas and geothermal installations, open channels followed by sieves for removal of drill cuttings, are used to monitor the quality and quantity of the drilling fluids. Drilling fluid flow rate is difficult to measure due to the varying flow conditions (e.g., wavy, turbulent and irregular) and the presence of drilling cuttings and gas bubbles. Inclusion of a Venturi section in the open channel and an array of ultrasonic level sensors above it at locations in the vicinity of and above the Venturi constriction gives the varying levels of the drilling fluid in the channel. The time series of the levels from this array of ultrasonic level sensors are used to estimate the drilling fluid flow rate, which is compared with Coriolis meter measurements. Fuzzy logic, neural networks and support vector regression algorithms applied to the data from temporal and spatial ultrasonic level measurements of the drilling fluid in the open channel give estimates of its flow rate with sufficient reliability, repeatability and uncertainty, providing a novel soft sensing of an important process variable. Simulations, cross-validations and experimental results show that feedforward neural networks with the Bayesian regularization learning algorithm provide the best flow rate estimates. Finally, the benefits of using this soft sensing technique combined with Venturi constriction in open channels are discussed.

Keywords: soft sensing in open channels; non-Newtonian flow; ultrasonic scanning of open channel flow; neural networks; Bayesian regularization learning; fuzzy logic; support vector regression

1. Introduction

One of the important phases in extracting oil and gas is drilling from the surface down to the reservoir. Due to high temperature and pressure conditions in the bottom-hole, there is a high risk of failure while drilling. Drilling fluid circulation plays a vital role in safe and efficient drilling operations. The drilling fluid can be water-based or oil-based depending on the type of reservoir. While drilling, the drilling fluid is continuously pumped down into the wellbore through the drill pipe. The circulating drilling fluid returns to the surface through the annulus, i.e., the space between the drill pipe and the wellbore. The drilling fluid circulation continues until the desired depth is reached. The primary functions of drilling fluid circulation are stabilizing the wellbore, the cleaning borehole and transporting rock cuttings. These functions are dependent on the properties of drilling fluid, among which density, viscosity and flow rate are the most important ones. The viscosity and other rheological properties of circulating fluid regulate the hole cleaning and transportation of rock cuttings [1].

In the context of this paper, variations of viscosity are not taken into account. The drilling fluid density is responsible for wellbore stability. For any reservoir, there exists a certain pressure window

where the drilling operation can be performed safely. The pressure window extends from formation pressure (P_f) to formation fracture pressure (P_{ff}). The wellbore pressure must be maintained within this pressure window ($P_{ff} - P_f$) for safe drilling. In the case of reservoir failure, two main problems might occur. If the wellbore or bottom-hole pressure (P_b) is greater than formation pressure (P_f), the high-pressure drilling fluid displaces the formation fluids and enters into the formation pores, causing a fluid loss. If the drilling fluid pressure is greater than formation fracture pressure (P_{ff}), it fractures the formation, and the fluid loss further increases, which is a state of lost circulation while drilling. Alternatively, if ($P_b < P_f$), the high-pressure formation fluids and gasses displace the drilling fluid, which is the state of kick while drilling. The kick should be detected as early as possible, as it can initially lead to wellbore stability problems, and in the extreme case, it might result in the blowout of the whole rig, e.g., the Deepwater Horizon explosion [2]. The bottom-hole pressure depends on the hydrostatic pressure exerted by the circulating drilling fluid, choke pressure and frictional pressure. The hydrostatic pressure is mainly responsible for bottom-hole pressure, which is dependent on the density of drilling fluid or drilling fluid weight. In this way, by monitoring the density of circulating drilling fluid, the wellbore pressure can be maintained within the acceptable pressure window [1].

Loss of the drilling fluid, kick, unexpected changes in surge pressure and any uncontrolled high flow rates of drilling fluid should be indicated to the operator (human or autonomous) by a timely and preventive alarm, so that the operator takes the necessary actions to limit material damages and hazards to personnel. The early detection of these problems can lead to less fluid loss, less formation damage, lower drilling costs and, above all, increased safety with minimized maintenance costs. One of the simplest methods for early detection is the so-called delta flow method, which utilize the difference between inflow and outflow measurements in a circulation loop. To implement the delta flow method, two flow measurements for drilling fluid entering the well (inflow) and drilling fluid returning from the well (outflow) are needed. When the inflow exceeds outflow, lost circulation in the loop is a possibility. On the other hand, for inflow less than outflow, the possible occurrence of kick is indicated. Other different methods for kick and lost circulation detection are discussed in [3–6].

Therefore, the aim is to accurately determine the delta flow in the circulation loop. There are different types of flow measurement systems for delta flow measurement in the literature [7–11]. To point out some of them, the conventional pump strokes counter, rotatory pump speed counter and Coriolis mass flowmeter can be used for inflow measurement and the standard paddle meter, ultrasonic level meter, a prototype rolling float meter and open channel Venturi flow meter can be used for outflow measurements. With some adjustments, the magnetic flow meter and Doppler ultrasonic flow meter can be used for both inflow and outflow measurements, although due to high attenuation of ultrasonic signals in drilling fluids, this might not be a suitable option. The Coriolis mass flowmeter delivers one of the smallest uncertainties in flow metering. It has a very high accuracy with both Newtonian and non-Newtonian fluids. However, bubbles and mechanical vibrations affect the Coriolis measurement [12]. Therefore, it is not appropriate to use for outflow measurement, where the returning fluid contains rock cuttings, formation gasses and formation liquids. In addition, the Coriolis meter is an expensive option. Different flowmeters based on reliability and accuracy are discussed in [11]. The analysis concludes that the magnetic flowmeter or Doppler ultrasonic flowmeter can be used for inflow measurement, and prototype rolling float meters can be used for outflow measurement. Speers and Gerhrig [8] have presented the usage of magnetic flowmeters for delta flow measurement. However, magnetic flowmeters are limited to water-based or conductive drilling fluids. Another problem with magnetic flowmeters is the the requirement of a U-tube designed pipe to ensure a complete filled pipe. With this desgin, there will be a settlement of rock cuttings in the U-tube when the flow velocity is low. In this paper, the usage of an open channel with Venturi constriction is presented where the limitations using the magnetic flowmeter no longer exist [9,10].

In an open channel with Venturi constriction, the upstream pressure relative to the level in the control section is used to estimate the flow rate of the fluid [13]. Fluids flow from the subcritical to supercritical flow condition due to the Venturi effect [14]. The critical depth is determined within the

control section, and the level of the fluid in the upstream is measured. Ultrasonic or radar sensors can be used for level measurement, which can be used to estimate the flow of the fluid through the open channel [15].

To study the possibility of using Venturi constriction in an open channel for flow measurement, a flow loop is available at University College of Southeast Norway (USN), Campus Kjølnes, Norway. As a part of this study, the Computational Fluid Dynamics (CFD) simulation study is investigated in [16,17]. The possibility of using the Saint Venant equation for non-Newtonian fluid through the open channel is presented in [18]. The usage of the Ensemble Kalman Filter (EnKF) for estimating non-Newtonian fluid flow in an open channel is studied in [19]. This mathematical approach presented in [18,19] is computationally demanding and is only applicable to a slow system with a large sampling time. These considerations indicate that for real-time monitoring and controlling purposes, these approaches are not suitable. In [20], static Artificial Neural Network (ANN) and Support Vector Regression (SVR) techniques are implemented for flow measurement in an open channel. The simulation-based study shows that both static ANN and SVR models have more than a 100-times faster response time as compared to the mechanistic model presented in [18,19]. With an assumption of delta flow measurement as a dynamic problem, dynamic ANN with different learning algorithms is investigated in [21]. Further, the Bernoulli equation can be implemented for the flow rate estimation. The fundamental Bernoulli equation for the flow of an incompressible fluid in an inclined channel takes the following form:

$$\frac{P_1}{\rho g} + \frac{u_1^2}{2g} + z_1 = \frac{P_2}{\rho g} + \frac{u_2^2}{2g} + z_2 \tag{1}$$

where P, u, z, ρ and g are fluid pressure, fluid velocity, elevation of the channel relative to the datum, fluid density and acceleration due to gravity, respectively, with the subscripts indicating two distinct positions in the inclined channel. The further simplification of Equation (1) along with continuity equation, $u_1 \times A_1 = u_2 \times A_2$ gives Equation (2),

$$Q_v = A_1 A_2 \left[2g \left\{ \frac{(h_2 - h_1) + (z_2 - z_1)}{A_2^2 - A_1^2} \right\} \right]^{1/2} \tag{2}$$

where Q_v, h_1, h_2, A_1 and A_2 are volumetric flow rate, upstream level measurement, level measurement at the throat, area before the constriction and area at the constriction, respectively. The mass flow rate (Q_m) of the fluid can be calculated as $Q_m = Q_v \times \rho$.

In theory, the simplified equation (Equation (2)) can be used to estimate the flow rate using a set of spatial samplings of the open surface of the fluid in the Venturi channel, leading to a set of level measurements. However, due to non-ideal conditions (for example: compressible fluid, sediments leading to variations of the cross-sections, fluctuations of the open surface of the non-Newtonian fluid, varying velocity profile in the cross-section of the channel, etc.) and uncertainties in the geometrical parameters (for example: cross-sectional area of the fluid in the channel, channel elevation, etc.), we are resorting to a soft sensor approach using non-invasive measurements in this work. Hence, the present paper focuses on using different empirical methods such as fuzzy logic, ANN and Support Vector Machine (SVM) with both simulation and experimental results.

The system description is presented in Section 3, and different proposed methods are described in Section 4. Finally, the results from simulations and experimental studies are presented in Section 5 and Section 6, respectively.

2. Requirements for a Drilling Fluid Flowmeter

In an earlier paper [9], addressing the need for reliable and accurate flow measurement of non-Newtonian fluids, the following features are expected from a suitable flowmeter:

- Over the full range of flow, the reliability and accuracy of measurements are guaranteed.

- In the common drilling operational environment, an accuracy of 1.5–3 L/s for flow rates up to 75 L/s.
- For any type of drilling fluids (water and oil based) in the viscosity range 1–200 cP and density range of 1000–2160 kg/m^3, the accuracy should be maintained.

The methods presented here may be used for non-intrusive measurements of drilling fluids in many sectors satisfying all these requirements. Although some changes in these expected features may be seen in the practices of different operators, these can be used as design guidelines.

3. System Description

Figure 1 shows a flow loop available at USN consisting of a mud tank and a blender for mixing. Different model-drilling fluids are available for testing purposes. The centrifugal pump is used to pump the model-drilling fluid from the mud tank through the pipelines to the open channel with Venturi constriction as shown in Figure 1b. The pumped fluid flows through the open channel and down to the mud tank forming a complete flow loop. The flow loop includes different types of measurement systems like the pressure transmitter, temperature transmitter, Coriolis mass flowmeters, Gamma sensor dedicated for density measurement, differential pressure sensor, an open channel with Venturi constriction, an inclination sensor and different ultrasonic level sensors.

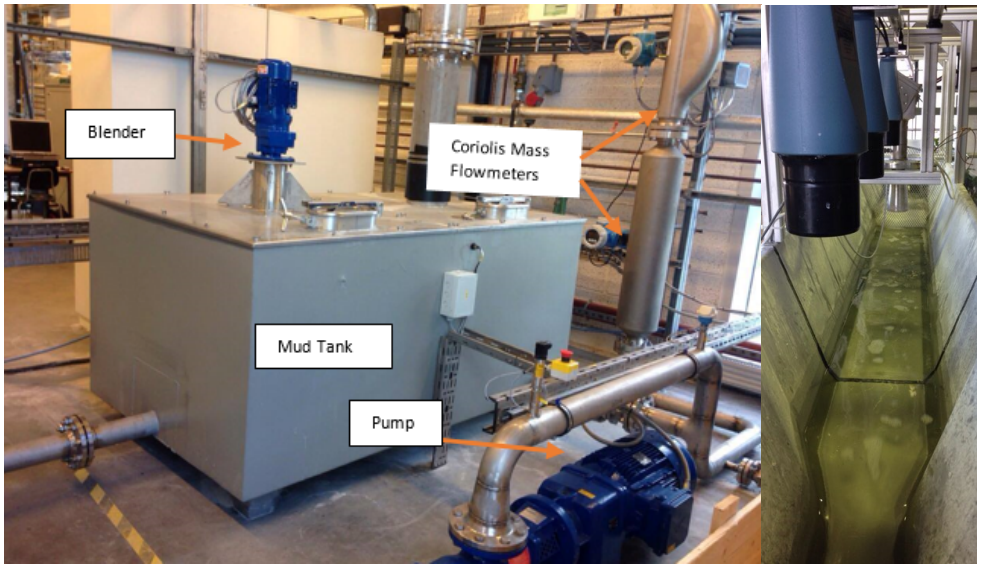

(**a**) (**b**)

Figure 1. (**a**) Test flow loop at University College of Southeast Norway, Kjølnes Campus, showing mud tank, blender, pump and Coriolis flowmeters. (**b**) Open Venturi channel with ultrasonic level sensors.

In this study, an accurate Coriolis mass flowmeter is used as a reference meter for all comparisons of results from empirical models. The open channel has a trapezoidal cross-section with Venturi constriction. The upstream length is long enough to ensure fully developed flow before entering the constriction. Further, the channel can be inclined to the horizontal at different angles to analyze different flow conditions. Three different ultrasonic level sensors are installed over the open channel, giving levels of fluid in the channel, which will be used for flow measurements, as discussed in the following sections. Figure 2a shows the 3D view of open channel with Venturi constriction and three ultrasonic level sensors. The schematic of the system is given in Figure 2b.

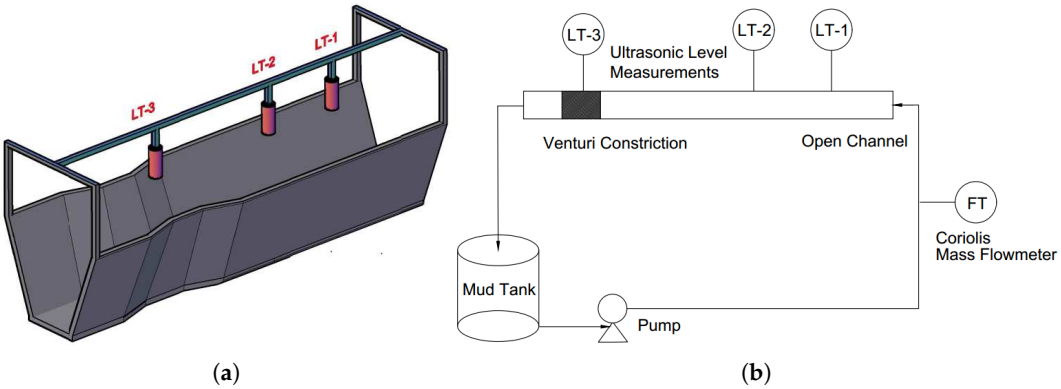

Figure 2. (**a**) An open channel with Venturi constriction and three ultrasonic level sensors (LT-1, LT-2, and LT-3). (**b**) Extremely simplified P&IDfor the flow loop with the measurands used in the study. The schematic shows the "hard sensors" in the system under study. The focus is on drilling fluid (also called "mud") mass balance based on flow measurements [21].

For the current study, a model-drilling fluid consisting of potassium carbonate (as the densifier) and xanthan gum (as the viscosifier) is used. The fluid is viscoplastic in nature with a density of 1153 kg/m^3, and its viscosity values are within 23–180 cP for corresponding shear rates within 500–1 s^{-1}.

This water-based non-Newtonian fluid with the properties given above is used in assessing the performance of a method of estimating its volumetric flow by sampling the levels of the open surface of the fluid flowing in the Venturi channel with an array of non-invasive ultrasonic level sensors. The performance of this soft sensing of the flow rate should satisfy the criteria outlined in Section 2.

The first step in conceiving of a suitable empirical model is the identification of suitable input feature space for estimating the mass flow rate of a drilling fluid. The Partial Least Square (PLS) method used in steady state conditions from earlier studies [20] shows that two upstream level measurements, LT-1 and LT-2, and the level measurement at the throat, LT-3, are highly correlated with Coriolis mass flow measurement, as shown in the loading weights plot in Figure 3. The list of different measurement devices with the respective technical specifications considered for the identification of input and output features for empirical models is presented in Table 1.

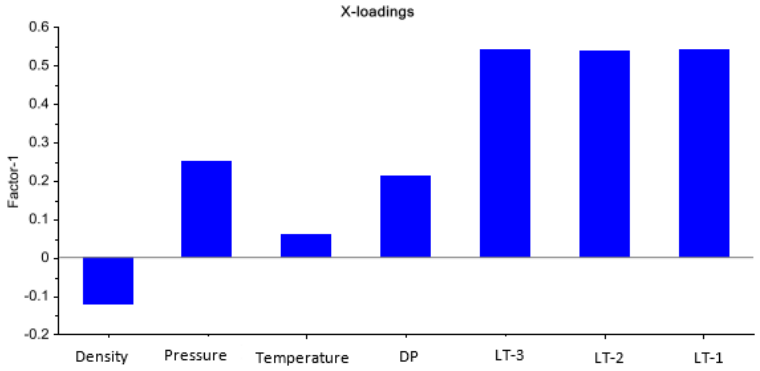

Figure 3. Loading weight plot using the Partial Least Square (PLS) method to identify the most important variables correlated with mass flow measurements. The three level measurements show obviously high PLS scoring [20].

Table 1. Technical specifications of different measurement devices considered for initial identification of input and output features for empirical models. Based on information from the vendors.

Measurement Devices	Vendor	Model	Range	Uncertainty
Coriolis meter (flow rate)	Endress + Hauser	Promass 63F	0–1000 (L/min)	±0.10%
Coriolis meter (density)	Endress + Hauser	Promass 63F	0.8–1.8 (g/cc)	±0.001
Temperature transmitter	Endress + Hauser	TI00110REN14	−50–200 (°C)	±0.19
Ultrasonic level sensor	Rosemount	3107	0.3–12 (m)	±0.25%
Pressure transmitter	Aplisens	PCE-28 Smart	0–7 (bar)	±0.10%
Differential pressure	Aplisens	APRE-2000	0–250 (mbar)	±0.10%

For developing models, about 1800 data samples are used for each of the three input variables (ultrasonic levels) and the single output variable (Coriolis flow rate). The samples are obtained at the data sampling rate of one sample per second using compactDAQ in the LabVIEW environment. The ranges, units and input/output types of each variable considered for modeling are tabulated in Table 2. The simultaneous inputs and output measurements are shown in Figure 4. In Figure 4a, the level measurements LT-1 and LT-2 are measuring almost the same upstream levels. LT-1 measures comparatively lower levels, which is due to the energy losses during the backward flow of the fluid initiated by the hydraulic jump near the constriction. The level measurements are noisy due to the presence of foams in the flowing fluid and due to random uncertainties in ultrasonic measurements. The data samples are normalized in the range of 0–1. From the 1800 normalized data samples, 75%, 12.5% and 12.5% of the data are used for training, validation and testing purposes, respectively.

Table 2. Input and output variables used in flow rate models with the units, ranges and variable types.

Variables	Range	Units	Type
LT-1	37.2–107.5	mm	Input
LT-2	28.9–78.3	mm	Input
LT-3	44.3–106.6	mm	Input
Coriolis mass flow rate	250–500	kg/min	Output

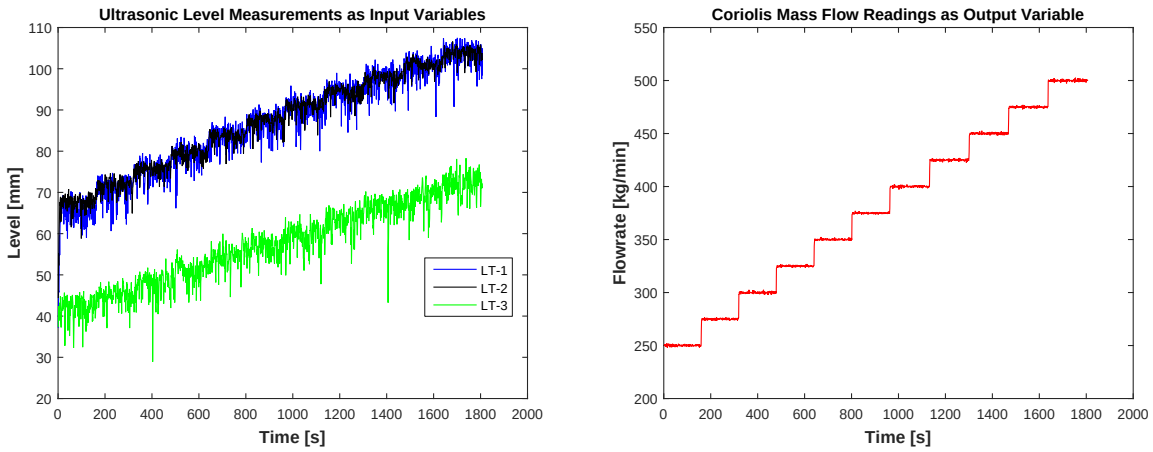

(**a**) (**b**)

Figure 4. Input and output variables used in flow rate models. (**a**) Three ultrasonic level measurements, namely LT-1, LT-2, and LT-3, as inputs. (**b**) Flow measurement using the Coriolis mass flowmeter as the reference output [21].

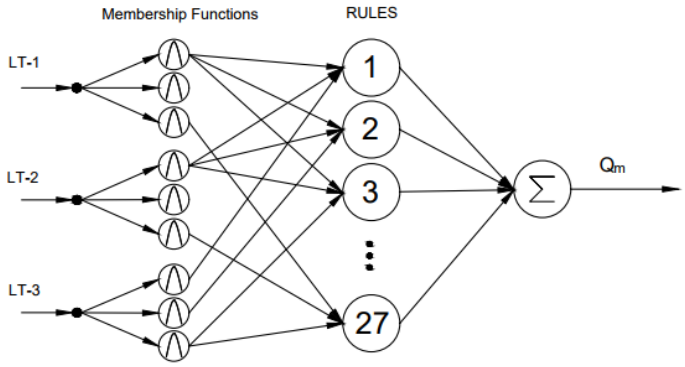

Figure 5. A Sugeno-type Fuzzy Logic architecture with outputs from "hard" sensors LT-1, LT-2 and LT-3 as crisp inputs and drilling fluid outflow as the crisp soft sensor output. Adapted from [22] and modified.

4. Methods Used with Selected Algorithms

In this work, different Artificial Intelligence (AI) methods are used to estimate the flow rate of the non-Newtonian fluid. Under this section, AI methods like Fuzzy Logic (FL), feedforward and feedback ANN and Support Vector Regression (SVR) are briefly discussed.

4.1. Fuzzy Logic Approach

Fuzzy Logic (FL) is an approach where the computing is based on degrees of truth rather than crisp true or false values. The FL tool can be considered as a function that receives inputs and gives an output based on the defined rules and membership functions. Analysis of the literature [23–26] shows that the fuzzy logic approach can be successfully applied for learning, predicting and controlling. Figure 5 shows the architecture of the Sugeno-type fuzzy logic with ANFIS used in predicting mass flow rates based on three ultrasonic level measurements. In this work, the Sugeno-type fuzzy logic with the Adaptive Neuro-Fuzzy Inference System (ANFIS) is used.

4.2. Feedforward Artificial Neural Network

ANN is a kind of non-linear mapping system suitable for pattern recognition, regression problems, image compression, etc. [27–33]. In the network, the bias of the neuron and weights between the neurons are the model parameters. These model parameters are tuned based on a certain cost function using a suitable learning algorithm [27,28]. A feedforward ANN is a static ANN that uses current inputs to estimate current outputs. The architecture of the feedforward ANN always moves in one direction as shown in Figure 6.

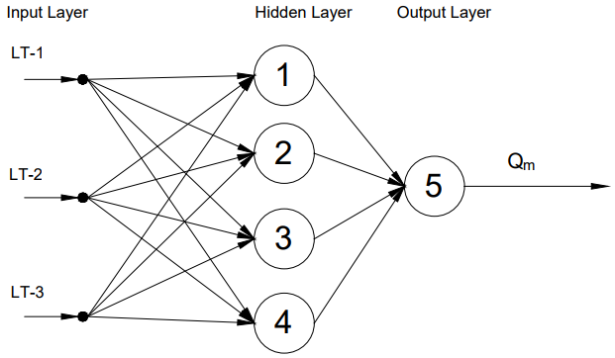

Figure 6. A feedforward artificial neural network architecture with an input layer, hidden layer and an output layer. Three ultrasonic level measurements, LT-1, LT-2 and LT-3, are inputs to the network and drilling fluid outflow as the soft sensor output from the network [20].

In this paper, feedforward ANN with three different learning algorithms, Levenberg–Marquardt (LM) learning, Bayesian Regularization (BR) learning and Scaled Conjugate Gradient (SCG) learning, are investigated. The cost function for LM learning and SCG learning algorithms is the mean squared error defined by Equation (3), and the generalization is performed using the early stop technique. Both of these algorithms are faster in learning. However, regarding memory, LM learning takes more memory compared to SCG learning [34]; whereas, the BR learning algorithm involves the minimization of mean squared error and weight parameters of a network. The cost function for BR learning is defined by Equation (4), and the generalization is performed using regularization [34].

$$J(w,b) = \frac{1}{2n}\sum_{i=1}^{n}(\|p_i - T_i\|)^2 \quad (3)$$

$$J(w,b,\lambda) = \frac{1}{2n}\sum_{i=1}^{n}\left\{(\|p_i - T_i\|)^2 + \lambda W^2\right\} \quad (4)$$

where J represents the cost function, which is a function of weights (w) and bias (b). Parameters n, p and T represent the number of samples, model prediction and target value, respectively. W is the weight parameter vector and λ the regularization parameter or weight decaying factor.

4.3. Feedback Artificial Neural Network

A feedback ANN is a dynamic ANN that uses previous inputs and outputs to estimate current outputs. The architecture of a fully-connected feedback ANN consisting of feedback loops and self-feedback loops is shown in Figure 7.

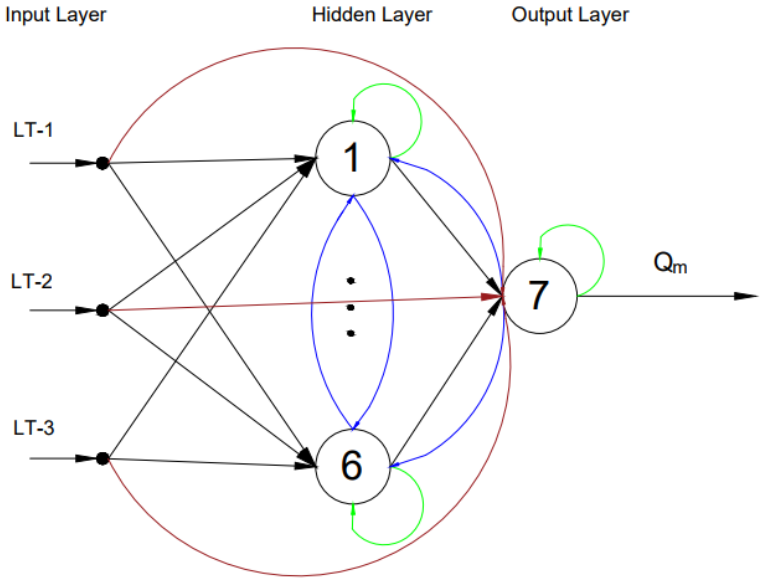

Figure 7. The architecture for feedback ANN with self-feedback (denoted by green connections), feedback loops (denoted by blue connections) and direct connections from inputs to the output neuron (denoted by brown connections). Ultrasonic level measurements as input vectors to the network and the drilling fluid flow rate as the output from the network [21].

In this paper, feedback ANN with three different learning algorithms, Back Propagation Through Time (BPTT), Real-Time Recurrent Learning (RTRL) and Extended Kalman Filter Learning (EKF), is studied. BPTT is an extension of the classical gradient-based back-propagation algorithm where the feedback ANN architecture is unfolded into feedforward ANN with a different number of folds [35–38]. It converges faster, but it is an offline learning algorithm [35–38]. On the other hand, both RTRL and EKF are online learning algorithm. RTRL is simple and the slowest converging algorithm, whereas

EKF is complex and the fastest learning algorithm [35–38]. Mean squared error defined by Equation (3) is used as a cost function in all three feedback learning algorithms.

4.4. Support Vector Regression

The Support Vector Machine (SVM) technique is applied in applications like classification problems, pattern recognition, time series predictions and regression problems [39–42]. The basic idea of the SVM technique is to perform a mapping of original data in the input space into the higher dimensional feature space through non-linear mapping functions. In this paper, SVM is used in its regression form, defined by (Equation (5)) as Support Vector Regression (SVR) [39].

$$y = \sum_{i=1}^{N_{SV}} (w_i \cdot \phi_i(x)) + b \tag{5}$$

where $\phi(x)$ (also represented as $k(x, x_i)$, k representing the kernel function) is the mapping function from the input space to the feature space, b is the bias term, x represents the input, y represents the output and N_{SV} is the number of support vectors. The architecture of SVR used in this paper is shown in Figure 8. Three ultrasonic level measurements (X) are transformed into higher dimensional feature space using the Radial Basis Function (RBF) kernel. Thus, the obtained higher dimensional feature is mapped with mass flow rate to develop a regression model.

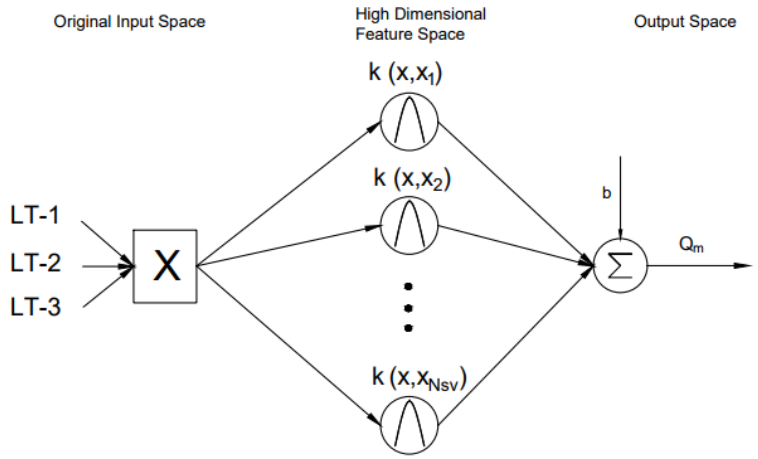

Figure 8. An architecture of Support Vector Regression (SVR) showing a mapping from input space to high dimensional feature space using the radial basis kernel function. Ultrasonic level measurements as input vectors and the drilling fluid flow rate as the output [20].

4.5. Building AI Models

Different AI models are developed using the data from three ultrasonic level measurements LT-1, LT-2 and LT-3 as inputs and Coriolis mass flow readings as the output. The dataset is normalized and divided into three sets for training, validation and testing. Different empirical relations (hypothesis) between inputs and output are developed using the training dataset. The empirical models developed are then validated leading to the final hypothesis with associated optimal model parameters. Finally, the eight models are tested for their performance. The flowchart for training, validating and testing all the AI models is shown in Figure 9. A pseudocode for training, validating and testing different AI models is presented below.

(a) % Get and normalize dataset
$dataSet = GetDataSet()$
$data = Normalize(dataSet)$

(b) % Divide dataset into training, validation and testing sets
$trainingData = FindTrainingSet(data)$
$validationData = FindValidationSet(data)$
$testData = FindTestSet(data)$
(c) % Construct two arrays of different AI techniques and corresponding learning algorithms
$artificialIntelligenceTechniques = \{'fuzzyLogicAlgorithm', 'feedforwardLMAlgorithm',$
$'feedforwardBRAlgorithm', 'feedforwardSCGAlgorithm', 'feedbackBPTTAlgorithm',$
$'feedbackRTRLAlgorithm', 'feedbackEKFAlgorithm', 'svrAlgorithm'\}$
$LearningAlgorithms = \{'ANFISLearningAlgorithm', 'LMLearningAlgorithm',$
$'BRLearningAlgorithm', 'SCGLearningAlgorithm', 'BPTTLearningAlgorithm',$
$'RTRLLearningAlgorithm', 'EKFLearningAlgorithm', 'SVRLearningAlgorithm'\}$
(d) % Train different AI techniques using training data set
$FOR\ algorithm = 1–8$
$artificialIntelligenceTechniques\{algorithm\} = LearningAlgorithms\{algorithm\}(trainingData)$
$ENDFOR$
(e) % Validate all the AI techniques using the validation dataset
$FOR\ algorithm = 1–8$
$Validate(artificialIntelligenceTechniques\{algorithm\}, validationData)$
$ENDFOR$
(f) % Test all the AI techniques using test set
$FOR\ algorithm = 1–8$
$Test(artificialIntelligenceTechniques\{algorithm\}, testData)$
$ENDFOR$

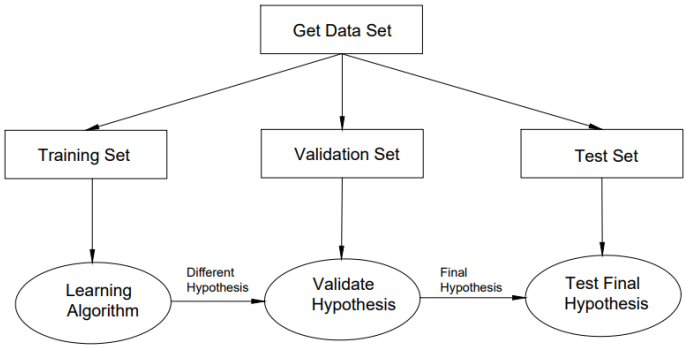

Figure 9. A flowchart for training, validating and testing different AI techniques.

4.6. Cross-Validation for Model Selection

In this work, the cross-validation technique is used for model selection. For the purpose of model selection, the dataset is divided into k number of folds ($k = 10$, in our case). Out of k subsets, the $(k-1)$ set is used for training or calibrating the model, and remaining subsets are used for validating or testing the model. The process is repeated by changing the validation subset, and then, the average cross-validation error is calculated. The model with the lowest cross-validation error is considered to be the best model using this technique [43,44].

Further, Table 3 shows the pros and cons of different AI methods used in this study. The selection of a suitable model is application dependent.

Table 3. Pros and cons of different AI methods used in this study.

AI Methods	Pros	Cons
Fuzzy Logic	Simple to implement and can be a good alternative for solving complex problems.	The performance depends on the model parameters and rules. Insufficient knowledge about the system can degrade the performance.
Artificial Neural Network	Suitable for modeling non-linear problems and one of the best choices for a large number of input features.	Training is computationally expensive.
Support Vector Regression	Works very well with non-linear problems and is not biased by outliers.	The algorithm is more complex and is not the best method for a large number of features.

5. Simulation Study

Based on the setup discussed in Section 3, the results of the simulation study are presented under this section. As discussed in Section 3, we have measurements from three level measurements from ultrasonic sensors LT-1, LT-2 and LT-3 and the Coriolis mass flowmeter. All the models are evaluated using Mean Absolute Percentage Error (MAPE) and coefficient of determination R^2. The low value of MAPE represents the better performance of the model, as it gives the error percentage value. On the other hand, the value of R^2 closer to 1.0 indicates that the model predictions and target values are highly correlated. The parameter tuning of models is one of the most important steps in empirical modeling. In this paper, the parameters of ANN models are tuned based on the grid search method followed by some adjustment using trial and error. Most of the parameters of the Sugeno-type fuzzy logic model are tuned automatically, and the rest of the parameters are based on trial and error. Optimal selection of SVR model parameters is made using the process described in [45]. Table 4 shows the optimal parameters used in all the models. All the symbols used in Table 4 are given in Appendix A.

Table 4. The optimal parameters used in all the proposed models for estimating the flow rate of the non-Newtonian fluid. All models implemented off-line using MATLAB. Model parameters, mostly software specific, are described in the nomenclature.

Methods	Optimal Parameters
Sugeno-type fuzzy logic	$N_m = 3$, $N_r = 27$ M_m = Gaussian-type, output = linear-type
Feedforward ANN with LM learning	$N_h = 1$, $N_n = 4$, $\alpha = 0.1$, $Epoch = 1000$
Feedforward ANN with BR learning	$N_h = 1$, $N_n = 4$, $\alpha = 0.1$, $Epoch = 1000$
Feedforward ANN with SCG learning	$N_h = 1$, $N_n = 4$, $\alpha = 0.1$, $Epoch = 1000$
Feedback ANN with BPTT learning	$N_n = 7$, $\alpha = 0.1$, $N_f = 7$, $Epoch = 200$, $N_i = 1$, $N_o = 3$
Feedback ANN with RTRL learning	$N_n = 7$, $\alpha = 0.1$, $Epoch = 200$, $N_i = 4$, $N_o = 4$
Feedback ANN with EKF learning	$N_n = 7$, $\alpha = 0.1$, $Epoch = 200$, $N_i = 4$, $N_o = 4$
Support vector regression with RBF	$C = 500$, $\epsilon = 0.01$, $\sigma = 0.1$

Figure 10 shows the flow rate estimations of non-Newtonian fluid using all the proposed empirical models compared to the Coriolis mass flow measurements. From these simulation studies, it can be seen that all the proposed models can track the changes in flow rates with high accuracy and are capable of describing both the steady state and dynamic behaviors of the fluid flow.

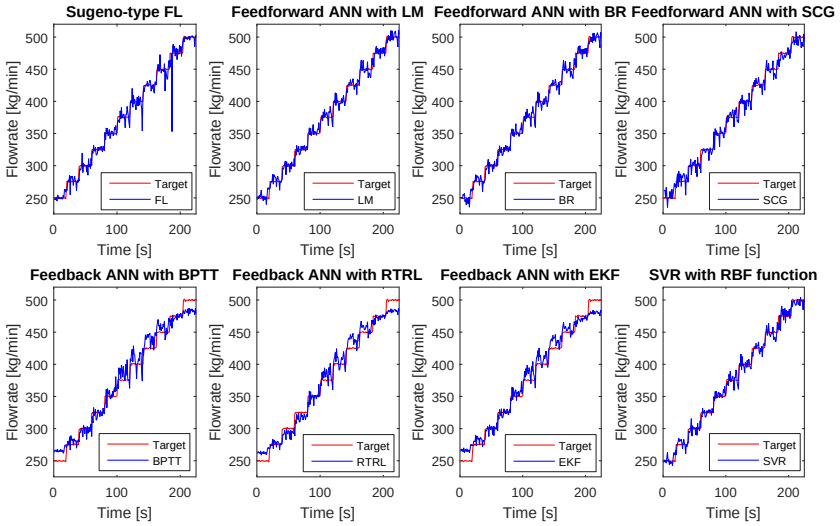

Figure 10. The flow rate estimates of non-Newtonian fluid based on simulations compared to the flow rate using from Coriolis meter. Both in static and dynamic conditions, simulation results and Coriolis meter readings tally very well.

Table 5 shows the comparison of the results from different proposed models based on MAPE and R^2. Based on these performance criteria, feedforward ANN with Bayesian Regularization and Levenberg–Marquardt learning algorithms are the best models to be implemented with the lowest percentage error and highest correlation with target values. However, other proposed models also have very accurate predictions.

Table 5. The comparison of the simulation performance in estimating output flow; all the proposed models are based on MAPE or R^2. Selected methods (represented by bold numbers) are considered in cross-validation for model selection.

Methods	MAPE (%)	R^2
Sugeno-type fuzzy logic	**1.74**	**0.98**
Feedforward ANN with LM learning	1.58	0.99
Feedforward ANN with BR learning	**1.58**	**0.99**
Feedforward ANN with SCG learning	1.97	0.99
Feedback ANN with BPTT learning	2.89	0.97
Feedback ANN with RTRL learning	**2.57**	**0.98**
Feedback ANN with EKF learning	2.71	0.98
Support vector regression with RBF	**1.61**	**0.99**

For further analysis, four different types of models are selected, one from each method. The cross-validation technique with 10-folds is implemented in each of the selected models. Table 6 shows the selected models with corresponding cross-validation error. Based on the cross-validation check, the best model for flow rate estimation is feedforward ANN with the Bayesian regularization model, which has the lowest cross-validation error. It is due to the fact that the BR learning algorithm uses regularization for the generalization of a model. The regularization parameter prevents the model from being over-fit by minimizing the connection weights.

Table 6. The model selection using the cross-validation technique.

Methods	Cross-Validation Error (%)
Sugeno-type fuzzy logic	1.89
Feedforward ANN with BR learning	1.59
Feedback ANN with RTRL learning	2.70
Support vector regression with RBF	1.75

6. Experimental Study

Based on the simulation study, four different models, the Sugeno-type fuzzy logic model, feedforward ANN with BR learning model, feedback ANN with RTRL learning and SVR with RBF kernel model, are implemented in the flow loop. Figure 11 shows the experimental results obtained with non-Newtonian fluid using these models. During the experiments, the set point is randomly varied between 250 and 475 kg/min. In response, all the models can track the varying references with good accuracy. Table 7 shows the comparison of the experimental performance of different models based on MAPE, R^2 and Root Mean Squared Error (RMSE). From the performance table, it can be seen that the feedforward ANN with BR learning model having the lowest MAPE and RMSE of 3.28% and 0.3 L/s respectively, and the highest R^2 of 94% is the best generalized model for estimating the flow rate of the non-Newtonian fluid. However, all these models give much smaller RMSE with acceptable uncertainties for a flowmeter needed for the current application.

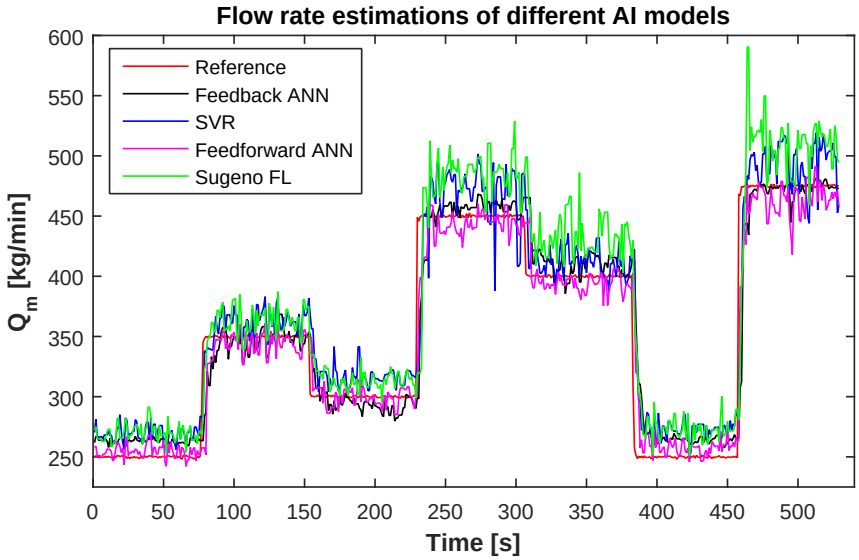

Figure 11. The flow rate estimates using feedback ANN with the RTRL learning algorithm, SVR with the RBF kernel function, feedforward ANN with the Bayesian regularization learning algorithm and Sugeno-type FL compared to the Coriolis meter readings.

Table 7. The comparison of the experimental performance of different models used for estimating flow based on MAPE, R^2 and RMSE.

Methods	MAPE (%)	R^2	RMSE (kg/min)	RMSE (L/s)
Sugeno-type fuzzy logic	7.72	0.83	34.94	0.51
Feedforward ANN with BR learning	3.28	0.94	20.90	0.30
Feedback ANN with RTRL learning	4.25	0.91	25.02	0.36
Support vector regression with RBF	6.43	0.89	28.30	0.41

Figure 12 shows box plots for Coriolis flowmeter readings and feedforward ANN estimates at different flow rates. As a reference, a varying setpoint is also included in the plots. In the box plot, a blue box is an Interquartile Range (IQR), and the central red line is a median of measurements/estimates. Two whiskers above and below the box are 1.5 × IQR from the edge of the box, which corresponds to the 99.3% confidence interval for a normal distribution. Hence, the size of a box represents the spread or variance of measurements/estimates. Figure 12a shows that the sizes of boxes for Coriolis readings are very small, and the medians are very close to the reference line. This represents the high accuracy of the Coriolis flowmeter; whereas, the size of boxes for the estimates of feedforward ANN are comparatively larger, as shown in Figure 12b. The sizes of boxes are small at low flow rates and large at high flow rates, representing low and high variances, respectively. In addition, the medians for feedforward ANN are slightly displaced from the reference line showing some limited accuracy in estimations.

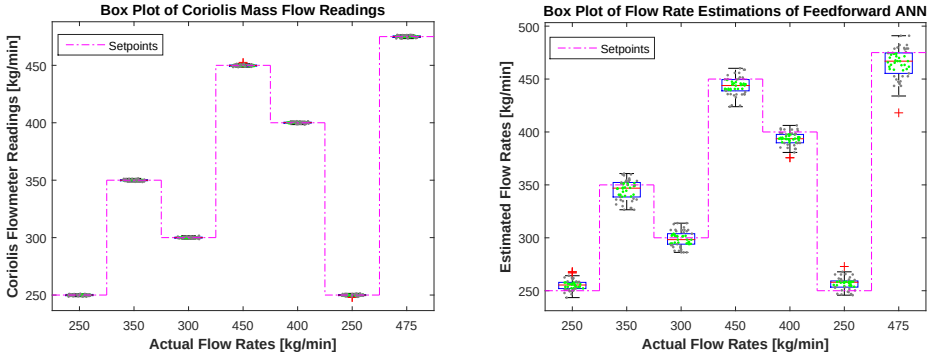

(**a**) (**b**)

Figure 12. Box plots showing the spread of the sensor measurements and model-based estimates at different flow rates. Green dots, black dots and the red plus sign represent measurements/estimates within the Interquartile Range (IQR), within the upper and lower bounds, but out of IQR, and outliers, respectively. (**a**) Box plots for Coriolis mass flow meter readings. (**b**) Box plots for flow rate estimations of feedforward ANN.

Further, feedforward ANN is considered under the repeatability test as shown in Figure 13. Under similar conditions, three experiments are performed, and the estimates of feedforward ANN are compared. For the comparison, only the steady state measurements are considered. Table 8 shows the results of the repeatability test. The calculated MAPE and R^2 show that the estimates of feedforward ANN are highly repeatable.

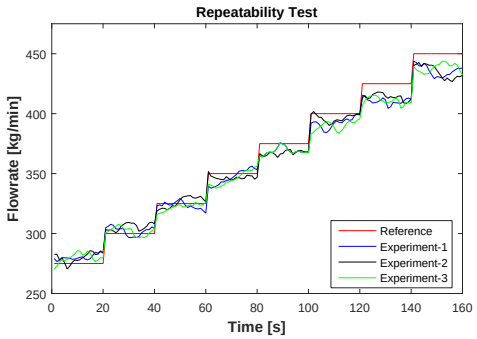

Figure 13. Repeatability test conducted on three different experiments under the same conditions. The estimated flow rates using feedforward ANN in different experiments are compared against the reference setpoints.

Table 8. Repeatability test performed with three experiments under the same conditions. The results are evaluated based on MAPE and R^2.

Experiments	MAPE (%)	R^2
1	1.97	0.975
2	1.90	0.977
3	2.01	0.975

The simulation and experimental study is summarized in Figure 14.

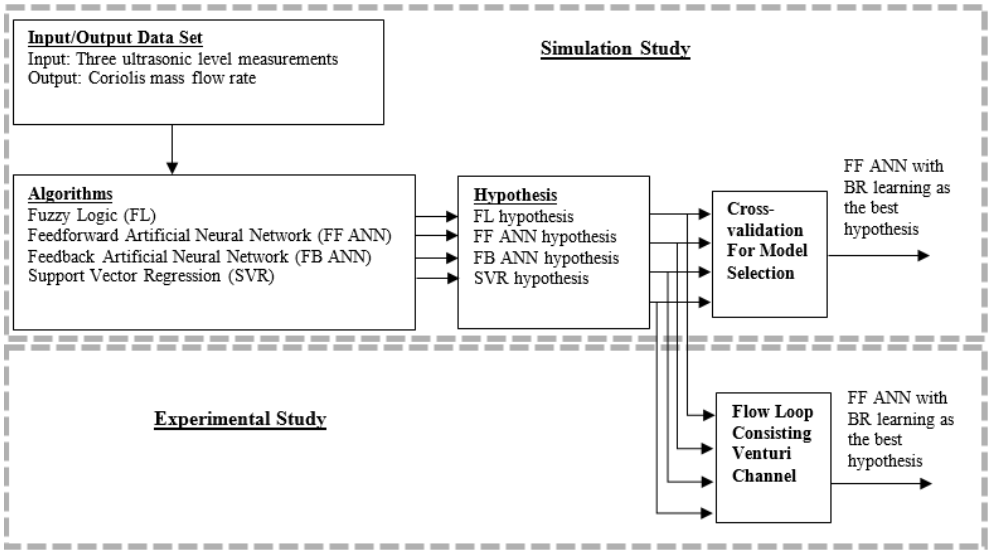

Figure 14. Overview of the strategies used during the simulation and experimental studies. Feedforward with Bayesian Regularization (BR) learning comes out as the best approach for soft sensing of the flow rate.

7. Conclusions

The drilling operation is one of the main phases of extracting oil and gas from the reservoir in oil and gas industries. In the context of geothermal applications, it helps to reach the necessary depth for achieving the high-temperature environment for heat transfer. In the context of oil and gas boring operations, due to extreme conditions in the bottom-hole, there is a high risk of failure while drilling. In unusual cases, there might be two problems while drilling: the influx of formation fluid (i.e., kick) and loss of circulation fluid. One of the best ways to detect these problems is the delta flow method, which utilizes the difference in inflow and outflow measurements of drilling fluid in a flow loop. There are different methods to perform accurate inflow measurements discussed in the literature. However, it is complicated to measure the outflow measurement accurately, particularly so for non-Newtonian fluids. In this paper, we introduce different empirical models and present both simulation and experimental results based on the comparison to readings from the Coriolis mass flowmeter. The starting point for this particular investigation is the set of three ultrasonic height measurements. The question is whether we can estimate the bulk flow velocity based only on these three parameters using non-invasive techniques. This is where soft sensor models come into play. The results from extensive experiments with non-Newtonian model-drilling fluids in the research laboratory of Statoil and in the flow loop at USN are used to develop the soft sensor models presented in this paper.

Different empirical models presented in this work are: the Sugeno-type fuzzy logic model, feedforward ANN models with three learning algorithms (Levenberg–Marquardt learning, Bayesian regularization learning and scaled conjugate gradient learning), feedback ANN models with

three learning algorithms (back propagation through time, real-time recurrent learning and extended Kalman filter learning) and support vector regression model with the radial basis function as the kernel function. For these models, the partial least square method is used to identify the inputs and output variables. In the simulation study, feedforward ANN with LM learning and BR learning are found to be the best models based on the MAPE and R^2. Further, some of the models are considered under the 10-fold cross-validation technique for suitable model selection. In this study, feedforward ANN with BR learning is selected to be the best generalized model with the lowest cross-validation error. Similar to simulation results, the flow rate estimates using feedforward ANN with BR learning are close to the results from the experiments. However, all the presented models are capable of tracking both the static and dynamic behavior of time-varying non-Newtonian fluid flow. The results presented here along with the measurements based on the array of ultrasonic transducers confirm that the flow rate of the drilling fluids could be measured satisfying the requirements specified in [9].

For future work, the quality and quantity of the training and validating datasets can be improved. As the proposed modeling is mainly dependent on the type of data, we believe that improvement in data measurement and extraction will improve the performance of the models. For this purpose, the first step will be filtering the noise from the data and performing other signal processing techniques to improve the signal information.

The technique presented here paves the way for realizing a simple and effective soft sensing system for monitoring a commonly-occurring module in the fossil fuel and renewable industries, viz. the operational unit for transport, cleaning recovery and mass balance budgeting of a costly and environmentally-hazardous drilling fluid, which is non-Newtonian. The soft sensing of the fluid flow rate using an array of non-intrusive and non-invasive ultrasonic transducers could spare the operators expensive maintenance costs and improve autonomous operation of plants in conventional fossil fuel and emerging renewable energy industries. For interested researchers, the data used in this study are made available in the web portal of this journal.

Supplementary Materials: The Supplementary Materials are available online at http://www.mdpi.com/1424-8220/17/11/2458/s1.

Acknowledgments: The Ministry of Education and Research of the Norwegian Government is funding Khim Chhantyal's Ph.D. studies at USN. We acknowledge the collaboration with and support from STATOILfor providing and commissioning the open channel Venturi rig with various types of sensors and control systems dedicated to flow studies of different Newtonian and non-Newtonian fluids. We appreciate the expert advice on drilling operations by Geir Elseth of STATOIL. We acknowledge all the practical work done by various groups of bachelor and master students of USN in conjunction with this work.

Author Contributions: All the authors in collaboration with STATOIL have conceived of and designed the experiments. Khim Chhantyal with some assistance from the workshop and lab engineers has performed the experiments. Mainly Khim Chhantyal in collaboration with the co-authors has analyzed the data and developed different AI models. Khim Chhantyal and Saba Mylvaganam with inputs from Håkon Viumdal wrote the paper.

Conflicts of Interest: The authors declare no conflict of interest.

Appendix A. List of Symbols and Abbreviations

Appendix A consist of a list of symbols and abbreviations used in this work.

Symbols		**Abbreviations**	
b	Bias term	AI	Artificial Intelligence
C	Punishing factor	ANFIS	Adaptive Neuro-Fuzzy Inference System
$Epoch$	Maximum epochs for learning	ANN	Artificial Neural Network
g	Acceleration of gravity	BPTT	Back Propagation Through Time
h	Fluid level	BR	Bayesian Regularization
J	Cost function	CFD	Computational Fluid Dynamics
M_m	Type of membership function	DP	Differential Pressure
n	Number of samples	EKF	Extended Kalman Filter
N_f	Number of folding	FB	Feedback

N_h	Number of hidden layers	FF	Feedforward
N_i	Number of previous inputs	FL	Fuzzy Logic
N_m	Number of membership function	IQR	Interquartile Range
N_n	Number of hidden neurons	LM	Levenberg–Marquardt
N_o	Number of previous outputs	LT	Level Transmitter
N_r	Number of rules	MAPE	Mean Absolute Percentage Error
N_{sv}	Number of support vectors	PLS	Partial Least Square
p	Model predictions	RBF	Radial Basis Function
P	Fluid pressure	RMSE	Root Mean Squared Error
P_b	Formation pressure	RTRL	Real-Time Recurrent Learning
P_{ff}	Formation fracture pressure	SCG	Scaled Conjugate Gradient
Q_m	Mass flow rate	SVM	Support Vector Machine
Q_v	Volumetric flow rate	SVR	Support Vector Regression
R^2	Coefficient of determination	USN	University College of Southeast Norway
T	Target		
u	Fluid velocity		
w	Weight		
W	Weight parameter vector		
X	Input matrix		
Y	Outputs		
z	Elevation relative to a datum		
α	Learning rate		
ϵ	Tolerance zone		
ρ	Fluid density		
σ	Width of RBF function		
λ	Regularization parameter		
$\phi(\cdot)$	Mapping function		

References

1. Caenn, R.; Darley, H.C.; Gray, G.R. Introduction to drilling fluids. In *Composition and Properties of Drilling and Completion Fluids*, 6th ed.; Gulf Professional Publishing: Waltham, MA, USA; Kidlington, Oxford, UK, 2011; pp. 7–16, ISBN 978-0-12-383858-2.
2. Hauge, S.; Øien, K. Deepwater horizon: Lessons learned for the norwegian petroleum industry with focus on technical aspects. *Chem. Eng.* **2012**, *26*, 888–896, doi:10.3303/CET1226104.
3. Kamyab, M.; Shadizadeh, S.R.; Jazayeri-rad, H.; Dinarvand, N. Early kick detection using real time data analysis with dynamic neural network: A case study in iranian oil fields. In Proceedings of the Nigeria Annual International Conference and Exhibition, Calabar, Nigeria, 31 July–7 August 2010; Society of Petroleum Engineers: Richardson, TX, USA, 2010, doi:10.2118/136995-MS.
4. Mills, I.; Reitsma, D.; Hardt, Z.; Tarique, Z. Simulator and the first field test results of an automated early kick detection system that uses standpipe pressure and annular discharge pressure. In Proceedings of the SPE/IADC Managed Pressure Drilling and Underbalanced Operations Conference and Exhibition, Milan, Italy, 20–21 March 2012; Society of Petroleum Engineers: Richardson, TX, USA, 2012, doi:10.2118/156902-MS.
5. Ali, T.H.; Haberer, S.M.; Says, I.P.; Ubaru, C.C.; Laing, M.L.; Helgesen, M.; Liang, M.; Bjelland, B. Automated alarms for smart flowback fingerprinting and early kick detection. In Proceedings of the SPE/IADC Drilling Conference, Amsterdam, The Netherlands, 5–7 March 2013; Society of Petroleum Engineers: Richardson, TX, USA, 2013, doi:10.2118/163474-MS.
6. Patel, B.; Cooper, T.; Billings, W. The application of advanced gas extraction and analysis system complements early kick detection & control capabilities of managed pressure drilling system with added HSE value. In Proceedings of the SPE/IADC Drilling Conference, Amsterdam, The Netherlands, 5–7 March 2013; Society of Petroleum Engineers: Richardson, TX, USA, 2013, doi:10.2118/163498-MS.
7. Maus, L.; Tannich, J.; Ilfrey, W. Instrumentation requirements for kick detection in deep water. *J. Pet. Technol.* **1979**, *31*, 1–29, doi:10.2118/7238-PA.

8. Speers, J.; Gehrig, G. Delta flow: An accurate, reliable system for detecting kicks and loss of circulation during drilling. *SPE Drill. Eng.* **1987**, *2*, 359–363, doi:10.2118/13496-PA.
9. Orban, J.; Zanner, K.; Orban, A. New flowmeters for kick and loss detection during drilling. In Proceedings of the SPE Annual Technical Conference and Exhibition, Dallas, TX, USA, 27–30 September 1987; Society of Petroleum Engineers: Richardson, TX, USA, 1987, doi:10.2118/16665-MS.
10. Orban, J.; Zanner, K. Accurate flow-out measurements for kick detection, actual response to controlled gas influxes. In Proceedings of the SPE/IADC Drilling Conference, Dallas, TX, USA, 28 February–2 March 1988; Society of Petroleum Engineers: Richardson, TX, USA, 1988, doi:10.2118/17229-MS.
11. Schafer, D.; Loeppke, G.; Glowka, D.; Scott, D.; Wright, E. An evaluation of owmeters for the detection of kicks and lost circulation during drilling. In Proceedings of the SPE/IADC Drilling Conference, New Orleans, LA, USA, 18–21 February 1992; Society of Petroleum Engineers: Richardson, TX, USA, 1992, doi:10.2118/23935-MS.
12. Endress and Hauser and U.S. Meter Maintenance & Controls Inc., Coriolis Mass Flow Measurement System Promass 63. Available online: http://www.pandtec.com/files/documents/Endress+Hauser%20promass%2063.pdf (accessed on 25 October 2017).
13. White, F.M. Open-Channel Flow. In *Fluid Mechanics*, 7th ed.; McGraw-Hill: New York, NY, USA, 2009; pp. 701–758, ISBN 978-0-07-352934-9.
14. Frenzel, F.; Grothey, H.; Habersetzer, C.; Hiatt, M.; Hogrefe, W.; Kirchner, M.; Lütkepohl, G.; Marchewka, W.; Mecke, U.; Ohm, M.; et al. *Industrial Flow Measurement Basics and Practice*; ABB Automation Products GmbH: Ladenburg, Germany, 2011.
15. Gerätebau. *Equipment for Engineering Education, Instruction Manual HM 162.51 Venturi Flume*; G.U.N.T. GmbH: Barsbüttel, Germany, 2004.
16. Berg, C.; Malagalage, A.; Agu, C.; Chhantyal, K.; Mohammadi, F. *Simulation of Open Channel Flow for Mass Flow Measurement*; University of South East Norway: Porsgrunn, Norway, 2013.
17. Berg, C.; Malagalage, A.; Agu, C.; Kaasa, G.O.; Vaagsaether, K.; Lie, B. Model-based drilling fluid flow rate estimation using Venturi flume. *IFAC-PapersOnline* **2015**, *48*, 171–176, doi:10.1016/j.ifacol.2015.08.027.
18. Agu, C.; Lie, B. Numerical Solution of The Saint Vernant Equation for Non-Newtonian Fluid. In Proceedings of the 55th Conference on Simulation and Modelling (SIMS 55), Modelling, Simulation and Optimization, Aalborg, Denmark, 21–22 October 2014; pp. 218–228.
19. Agu, C.; Lie, B. Smart sensors for measuring fluid flow using a venturi channel. In Proceedings of the 55th Conference on Simulation and Modelling (SIMS 55), Modelling, Simulation and Optimization, Aalborg, Denmark, 21–22 October 2014; pp. 229–240.
20. Chhantyal, K.; Viumdal, H.; Mylvaganam, S.; Elseth, G. Ultrasonic level sensors for flowmetering of non-Newtonian fluids in open Venturi channels: Using data fusion based on Artificial Neural Network and Support Vector Machines. In Proceedings of the IEEE Sensors Applications Symposium (SAS), Catania, Italy, 20–22 April 2016, doi:10.1109/SAS.2016.7479829.
21. Chhantyal, K.; Viumdal, H.; Mylvaganam, S.; Hoang, M. Flow rate estimation using dynamic Artificial Neural Network with ultrasonic level measurements. In Proceedings of the 9th Eurosim Congress on Modelling and Simulation, Oulu, Finland, 12–16 September 2016.
22. Siddique, N.; Adeli, H. Introduction to Fuzzy Logic. In *Computational Intelligence: Synergies of Fuzzy Logic, Neural Networks and Evolutionary Computing*; John Wiley & Sons: Chichester, UK, 2013; pp. 19–64, ISBN 9781118337844.
23. Oleiwi, B.K.; Al-Jarrah, R.; Roth, H.; Kazem, B.I. Multi Objective Optimization of Trajectory Planning of Non-holonomic Mobile Robot in Dynamic Environment Using Enhanced GA by Fuzzy Motion Control and A*. *J. Commun. Comput. Inf. Sci.* **2014**, *440*, 34–49.
24. Al-Jarrah, R.; Roth, H. Visual fuzzy control for blimp robot to follow 3D aerial object. In Proceedings of the International Conference on Neural Networks and Artificial Intelligence, Brest, Belarus, 3–6 June 2014; pp. 98–111.
25. Izadi, D.; Abawajy, J.H.; Ghanavati, S.; Herawan, T. A data fusion method in wireless sensor networks. *Sensors* **2015**, *15*, 2964–2979.
26. Li, N.; Martínez, J.-F.; Díaz, V.H. The balanced cross-layer design routing algorithm in wireless sensor networks using fuzzy logic. *Sensors* **2015**, *15*, 19541–19559.
27. Haykin, S. Multilayer Perceptrons. In *Neural Networks and Learning Machines*; Pearson: Upper Saddle River, NJ, USA, 2009; pp. 122–217, ISBN 978-0-13-147139-9.

28. Siddique, N.; Adeli, H. Neural Networks. In *Computational Intelligence: Synergies of Fuzzy Logic, Neural Networks and Evolutionary Computing*; John Wiley & Sons: Chichester, UK, 2013; pp. 117–171, ISBN 9781118337844.
29. Zhang, G.P. Time series forecasting using a hybrid ARIMA and neural network model. *J. Neuro. Comput.* **2003**, *50*, 159–175, doi:10.1016/S0925-2312(01)00702-0.
30. Vaddella, V.R.P.; Rama, K. Artificial neural networks for compression of digital images: A review. *Int. J. Rev. Comput.* **2010**, *3*, 75–82, doi:10.1.1.187.5203.
31. Manoonpong, P.; Pasemann, F.; Roth, H. A modular neurocontroller for a sensor-driven reactive behavior of biologically inspired walking machines. *Int. J. Comput.* **2014**, *5*, 75–86.
32. Mestre, G.; Ruano, A.; Duarte, H.; Silva, S.; Khosravani, H.; Pesteh, S.; Ferreira, P.M.; Horta, R. An intelligent weather station. *Sensors* **2015**, *15*, 31005–31022.
33. Saad, S.M.; Andrew, A.M.; Shakaff, A.Y.M.; Saad, A.R.M.; Kamarudin, A.M.Y.; Zakaria, A. Classifying sources influencing indoor air quality (IAQ) using artificial neural network (ANN). *Sensors* **2015**, *15*, 11665–11684.
34. Syed, M.A.B.; Tahseen, A.J.; Cemal, A. A Comparison of First and Second Order Training Algorithms for Artificial Neural Networks. *Int. J. Comput. Electr. Autom. Control Inf. Eng.* **2007**, *1*, 145–151.
35. Schmidhuber, J. Deep learning in neural networks: An overview. *Neural Netw.* **2015**, *61*, 85–117, doi:10.1016/j.neunet.2014.09.003.
36. Dijk, E.O. *Analysis of Recurrent Neural Networks with Application to Speaker Independent Phoneme Recognition*; University Twente: Enschede, The Netherlands, 1999.
37. Bodén, M. *A Guide to Recurrent Neural Networks and Backpropagation*; Department of Computer Science, University of Skövde: Skövde, Sweden, 2001.
38. Williams, R.J. *Some Observations on the Use of the Extended Kalman Filter as a Recurrent Network Learning Algorithm*; College of Computer Science, Northeastern University: Boston, MA, USA, 1992.
39. Schölkopf, B.; Smola, A. Support Vector Machines and Kernel Algorithms. *Encyclopedia Biostat.* **2005**, *8*, 5328–5335.
40. Kazem, A.; Sharifi, E.; Hussain, F.K.; Saberi, M.; Hussain, O.K. Support vector regression with chaos-based firefly algorithm for stock market price forecasting. *Appl. Soft Comput.* **2013**, *13*, 947–958, doi:10.1016/j.asoc.2012.09.024.
41. Qi, Z.; Tian, Y.; Shi, Y. Robust twin support vector machine for pattern classification. *Pattren Recognit.* **2013**, *46*, 305–316, doi:10.1016/j.patcog.2012.06.019.
42. Yoo, J.; Kim, H.J. Target localization in wireless sensor networks using online semi-supervised support vector regression. *Sensors* **2015**, *15*, 12539–12559.
43. Arlot, S.; Celisse, A. A survey of cross-validation procedures for model selection. *Stat. Surv.* **2010**, *4*, 40–79, doi:10.1214/09-SS054.
44. Zhang, P. Model selection via multifold cross validation. *Ann. Stat.* **1993**, *21*, 299–313, doi:10.1214/aos/1176349027.
45. Cherkassky, V.; Ma, Y. Practical selection of SVM parameters and noise estimation for SVM regression. *Neural Netw.* **2004**, *17*, 113–126, doi:10.1016/S0893-6080(03)00169-2.

Doctoral dissertation no. 10
2018

—

Sensor Data Fusion based Modelling of Drilling Fluid Return Flow through Open Channels

Dissertation for the degree of Ph.D

—

Khim Chhantyal

—

ISBN: 978-82-7206-483-8 (print)
ISBN: 978-82-7206-484-5 (online)

usn.no